CHAPTER III

RESULTS

3.1 Surface characteristics of embryos as revealed by SEM

In order to observe the surface of embryos in SEM, the zona pellucida (ZP) was removed with a brief trypsin treatment (1 minute), so that no injury was done to the surface of underlying embryos.

One-cell embryos

The cell surface of a one-cell embryo was characterized by the presence of carpet-like consisting of rod-shaped microvilli (Figure 1: A, B), which were similar in size and uniformly distributed throughout the surface of the embryos. The diameter of one-cell embryo was approximately 48 μm and each microvillus was about 0.83 - 1.16 μm in length and 0.08 μm in diameter.

Two-cell embryos

After the first cleavage the diameter of each embryonic cell was reduced approximately to 27 μm. In general, the surface of these embryonic cells were not different from one-cell stage (Figure 1 : C,D). However, a loosely packed material was observed between the two blastomeres. This might be residual material arising from cell division, and that it might play role in the adhesion between the two blastomeres (Figure 1 : E). There were also interdigitations among contiguous microvilli between the two blastomeres which may help to interlock the two blastomeres together (Figure 1 : E, F, G). Small flat plate projections that protrude from the embryonic surface membrane

(Figure 1 : F, G) among microvilli were also observed in this stage. These projections will be described as microridges.

Four-cell embryos

There was a reduction in the number and length of rod-shaped microvilli on the surface of each blastomere, while the number of microridges increased (Figure 2 : A-E).

Eight-cell embryos

Blastomeres were loosely packed and remained attached to each other only in the central region. On the surface of each blastomere a further reduction in the number and length of microvilli was more apparent than in 4-cell embryos. In some embryos, disc-shaped projections or blebs were observed (Figure 2 : F, G, H).

Morulae

The blastomeres were packed together and the borders of cells on the periphery became quite obscure. Some blastomeres on the periphery began to flatten instead of having a round shape (Figure 12 : A). Close interdigitations of microvilli among blastomeres were clearly seen (Figure 3 : A, B). A dramatic reduction of rod-shaped microvilli was observed on the surface of each blastomere. Most of the remaining projections were flat microridges that interspersed with few remaining rod-shaped microvilli which had become shorter.

Blastocysts

At early stage, the outer flattened cells, called trophectoderm of the blastocyst (Figure 3 : D), were connected by interdigitation of microridges and short rod-shaped microvilli. Microridges were still present on the entire surface of trophectoderms.

Figure 1 Scanning electron micrograph of 1- and 2-cell embryos

A : The surface of 1-cell embryo, showing numerous rod-shaped microvilli

B : High magnification of numerous rod-shaped microvilli on the surface

C,D : The surface of 2-cell embryo, showing similar microvilli

E,F,G : High magnifications of 2-cell embryo at the zone between two blastomeres. Notice the two cells are interlocked by interdigitation of rod-shaped microvilli. Piece of residual membrane (RM) was also found in this gap. Disc-shaped projections (arrow heads) were found between the rod-shaped microvilli as well.

Figure 1

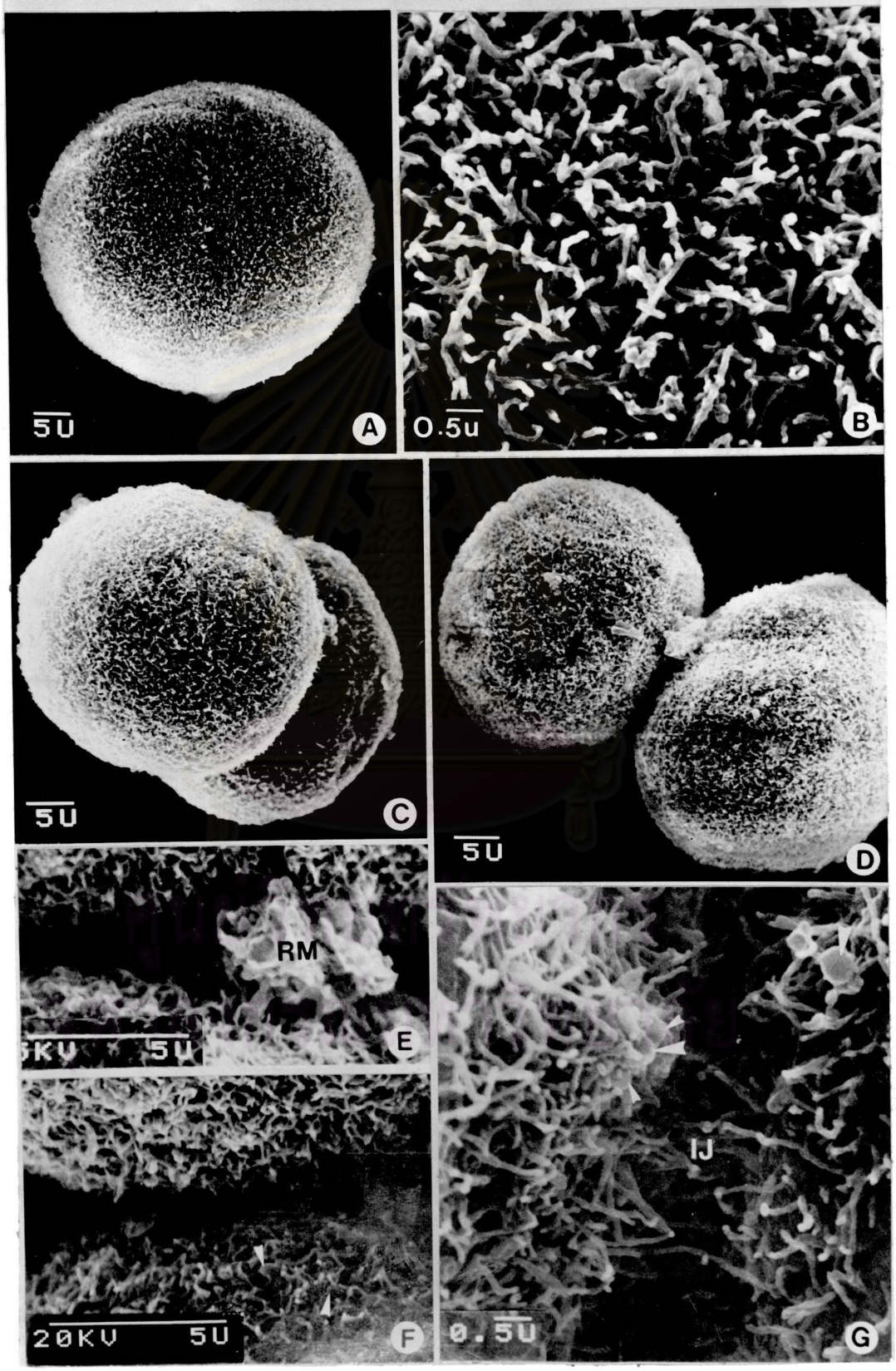

Figure 2 Scanning electron micrograph of 4- and 8-cell embryos

A,B : The surface of 4-cell embryos, showing still quite numerous rod-shaped microvilli

C,D,E : High mignifications, showing increasing number of disc-shaped projections (arrow heads) and decreasing number of rod-shaped microvilli

F,G : The surface of 8-cell embryos. Notice the reduction of rod-shaped microvilli on the entire surface of each blastomere. Disc-shaped projections were increased in number on the surface of each blastomere (arrow-G)

H : High magnification of the surface blastomere, showing sparse rod-shaped microvilli.

Figure 2

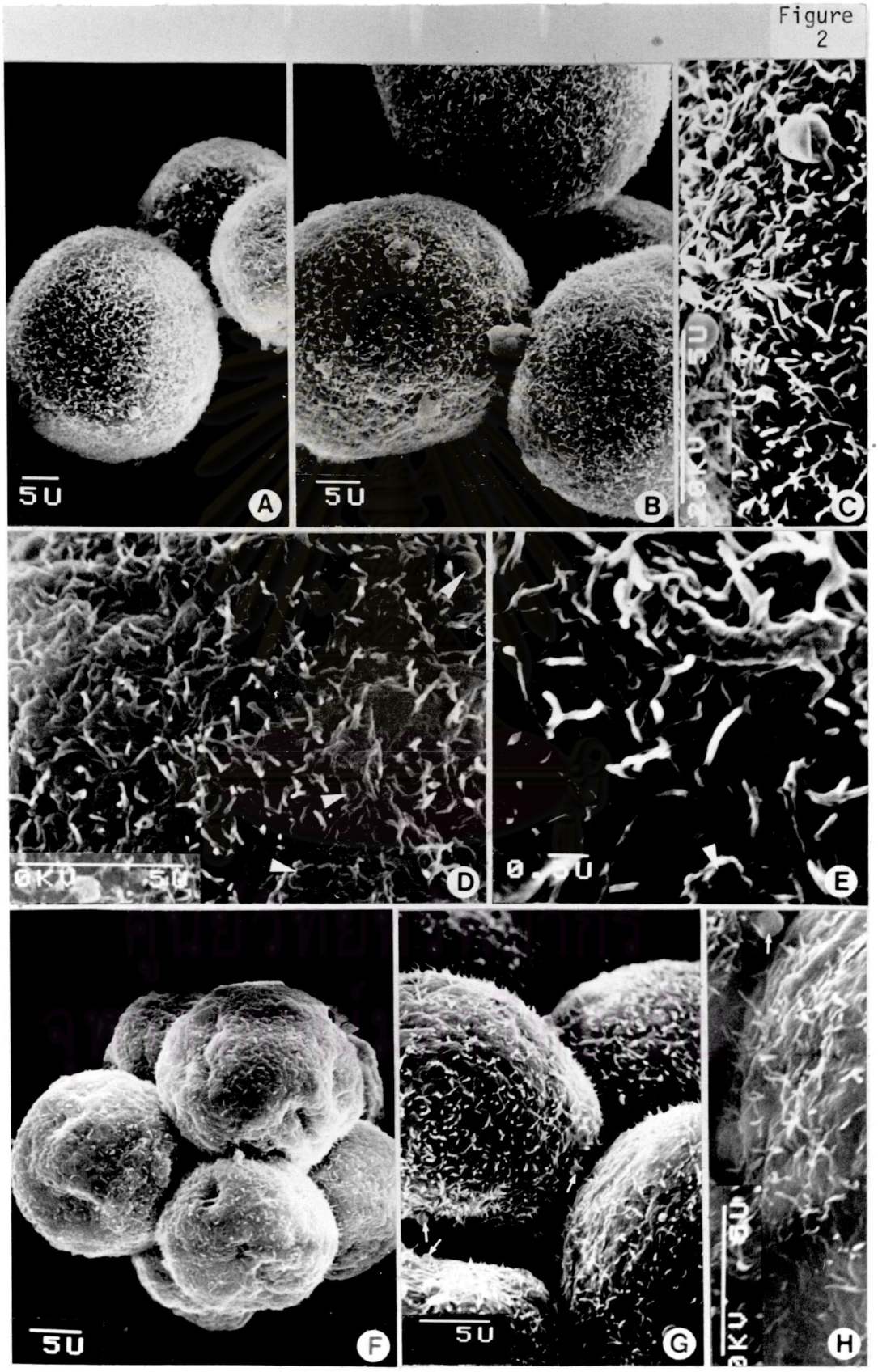

Figure 3 Scanning electron micrograph of morula and early blastocyst

A : Notice the dramatic reduction in length of rod-shaped microvilli on the surface of the morula

B : Intercellular junction (IJ) between blastomeres in morula stage where interdigitation of rod-shaped microvilli was clearly observed

C : Membrane folded on the surface in morula stage (arrow)

D : Early blastocyst stage

E, F, G : High magnification of trophectodermal cell (TC). Notice intercellular junction (arrow heads - E); microfolds (arrow head - F) and interdigitation of microvilli in the intercellular junction (arrow head - G).

Figure 3

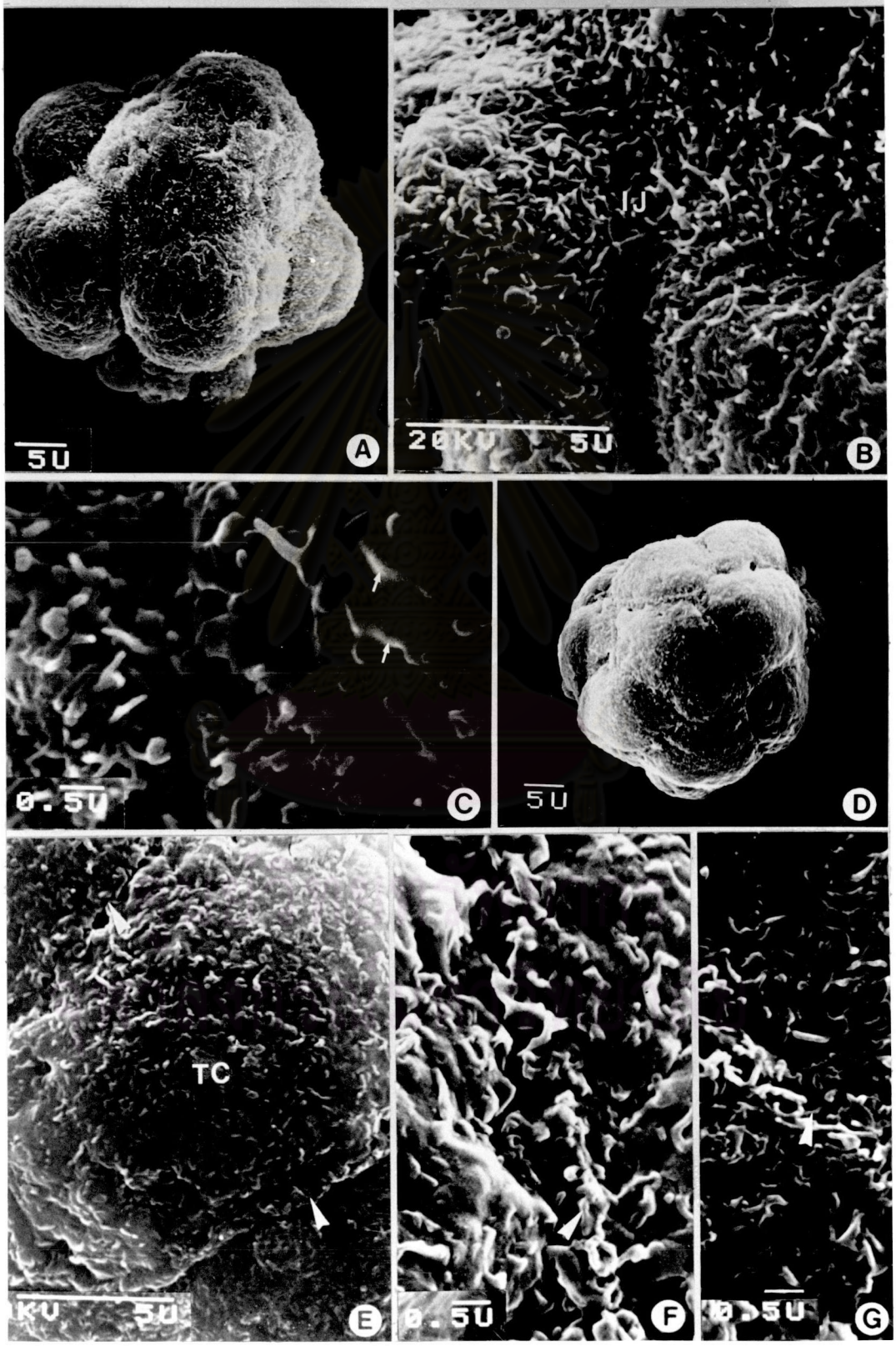

Figure 4 Scanning electron micrograph of a late stage blastocyst

A, D, F : Low magnifications, showing surface structures of three blastocysts. No rod-shaped microvilli was found on the surface of trophectodermal cell (TC)

B, G : High magnifications of the surface of TC , showing uneven contour

C, E, H : High magnifications of intercellular junctions, showing tight interdigitation between microfolds

Figure 4

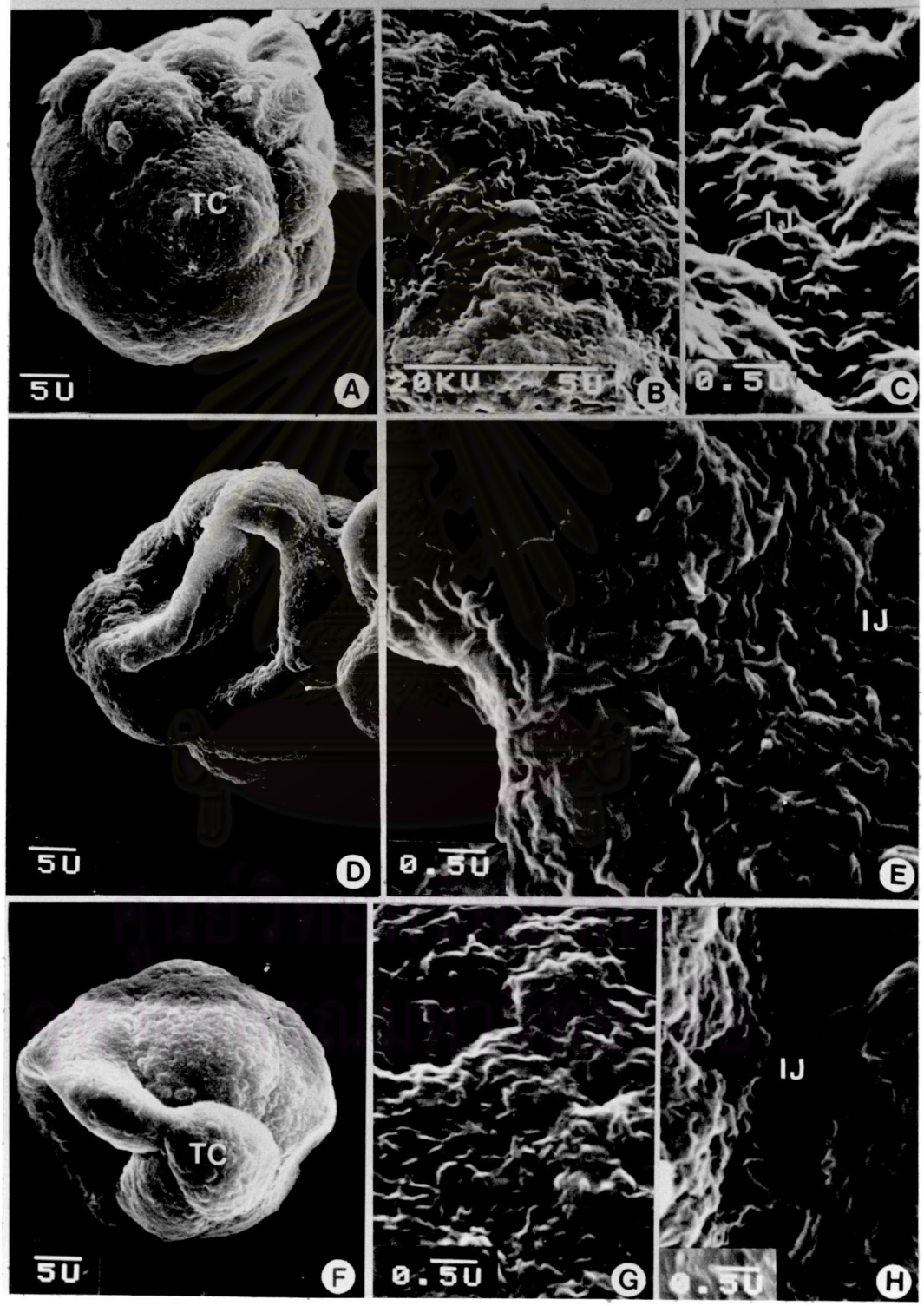

In late stage of blastocyst, trophectoderm became more flattened and no rod-shaped microvilli was found (Figure 4). Nevertheless, the surface appeared undulating and uneven, at high magnification, this was observed to be membrane foldings (Figure 4 : A, B, D, F, G).Intercellular junctions consisted of interdigitation of microridges and a few short microvilli (Figure 4 : C, E, H).

3.2 Ultrastructure of preimplantation embryos as revealed by TEM

All stages of preimplantation embryos were collected and prepared by conventional method for TEM studies.

3.2.1 One-cell embryos

Based on ultrastructural characteristics and the distribution of organelles, the cytoplasm could be divided into three distinctive zones : namely, the cortical zone, the middle zone and the central zone around the nucleus (Figure 5 : A). The cortical zone was a narrow cytoplasmic layer underneath the plasma membrane and microvilli. Prominent cytoplasmic organelles in this zone were numerous cortical vesicles or granules, some mitochondria, multivesicular bodies (MVBs) and a few lamellar structures (LSs). The middle zone contained striking number of parallely-arranged LSs. Various names had been given to these LSs; for examples, cytoplasmic whorls (Hadex, 1966), cytoplasmic lamellae (Weakley, 1967, 1968, 1985), yolk plates (Szollost, 1972) or plaques (Schlafke & Enders, 1968; Tachi et al., 1970). They were designated as LSs in this study because of their bilamellar configuration, each of which exhibited periodicity (Figure 5 : E). In perfect perpendicular sections each lamella appeared as a string of beads; but in grazing section showing an *en face* view, LSs, appeared as sheets with crystal lattice running across their

Figure 5 Electron micrographs of 1-cell embryos prepared by conventional TEM method

A : Low magnification, showing cytoplasm that was divided into 3 distinctive regions. Nu = nucleus X 3,900.

B : Medium magnification of the cortical region (1 from A). Abundant cytoplasmic vesicles (arrow heads) were observed. Some mitochondria (Mi) and multivesicular bodies (MVB) and sperm tail (ST) were also present. X 8,400.

C : Medium magnification of the middle zone (2 from A). Part of the central zone (lower) were also seen. Numerous lamellar structures (BSs) were the prominent organelles of this region. X 12,000.

D,E : High magnification of lamellar structures showing grazing section (D) and perfect cross-section (E). X 36,000, X 36,000.

F : High magnification of inner region, mitochondria (Mi), MVB and vesicles (arrows) were prominent. Golgi complex (Gol) was found in this region. A few Mi with cristae and buddings were clearly seen (upper right insertion X 36,000). X 24,000.

Figure 5

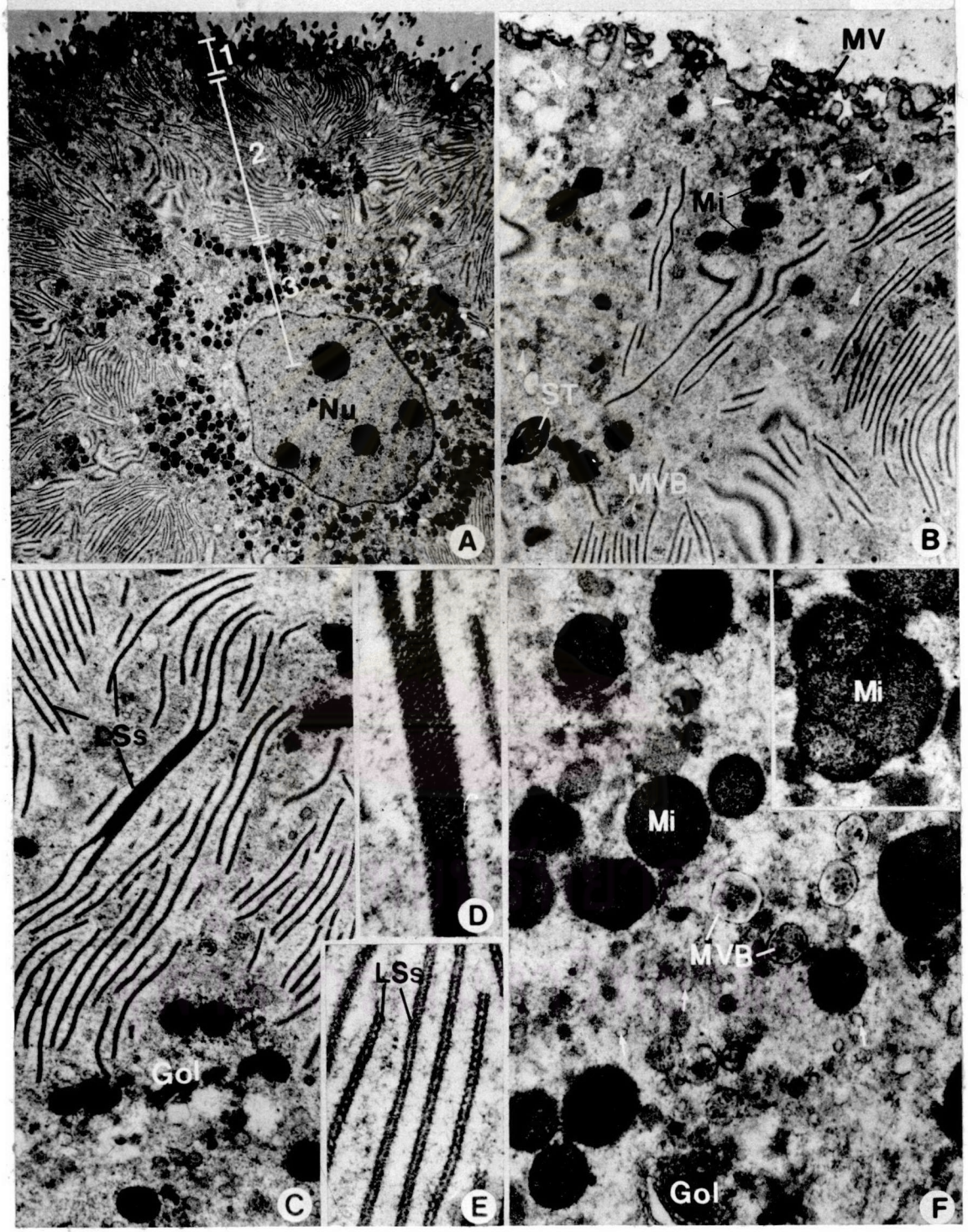

Figure 6 Electron micrographs of 1- and 2-cell embryos prepared by conventional TEM method.

A : High magnification, showing Golgi complex (Gol) found at the periphery of 1-cell embryos. X 24,000.

B,D : High magnification of 1-cell embryos, showing Golgi complex and numerous associated vesicles (arrows) at the perinuclear region. Few multivesicular body (MVB) were also observed in the same area. X 18,000, X 18,000.

C : High magnification of 2-cell embryos, showing Golgi complex and vesicles (arrow heads) at the perinuclear region. Autophagic vacuoles (star) and MVBs (arrows) were noticed. X 24,000.

Figure 6

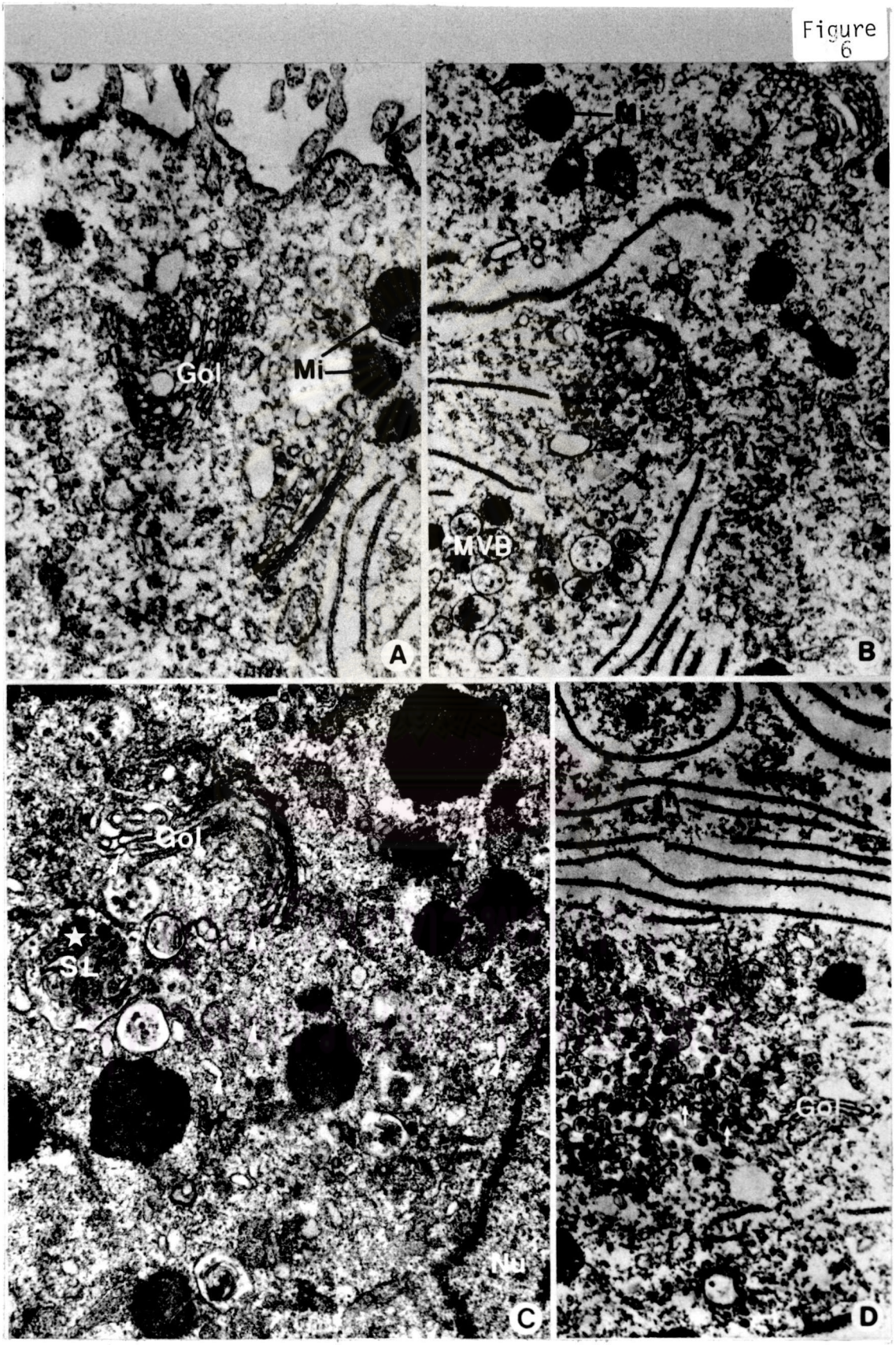

width. Lamellae were the most prominent organelles of the middle zone, and they were usually arranged in stack throughout the cytoplasm. In some regions LSs were composed of many layers of closely-apposed lamellae (Figure 5 : C, D). The central zone prominent organelles consisted of mitochondria and MVBs. Mitochondria were unique in having a round or oval-shaped with few cristae but very dense matrix (Figure 5 : F). Nucleus was surrounded by this zone. Golgi complexes were found in both cortical and central zones but were more numerous in the latter (Figure 5 : C, F; Figure 6 : A, B, D). In the vicinity of Golgi complexes, there were always numerous small vesicles containing electron lucent materials and some MVBs.

3.3.2 Two-cell embryos

The organization of cytoplasm in each blastomere was generally similar to one-cell embryos (Figure 7 : A, C). Two blastomeres were linked by intercellular junctions which appeared similar to desmosomes. Another structure that serve to hold the two blastomeres together was interdigitated microvilli which usually were confined to the region in between two desmosome-like junctions (Figure 7 : B, D).

3.2.3 Four-cell embryos

The organization of cytoplasm of each blastomere was still similar to one-cell embryos with the general decrease in the number of all types of organelle (Figure 8 : A). However, the most numerous organelles found in the cortical zone, which was highly noticable, were secondary lysosomes (SLs) which assumed two types of morphologies; namely, MVB, and autophagic vacuole (AV) (Figure 8 : B, C, E). High degree of interdigitation between microvilli of apposing surfaces of blastomeres was still observed. Another type of

Figure 7 Electron micrographs of 2-cell embryos performed by conventional TEM method

A : Low magnification showing general characteristics of the cytoplasm in two blastomeres. Intercellular junctions (Small rectangle) were observed. High magnification of small rectangle (lower right insertion, X 36,000) indicated that it is desmosome (D). ZP = zona pellucida. X 1,200.

B : Low magnification, showing another type of intercellular junction (arrow) between two blastomeres. X 1,600.

C : Medium magnification, numerous vescles (arrow heads) and some mitochondria (Mi) were observed in the cortical region (1) whereas the lamellar structures (LSs) were prominent in the middle region (2). X 12,000

D : Medium magnification, showing interdigitation of microvilli (arrow) between two blastomeres. X 12,000.

Figure 7

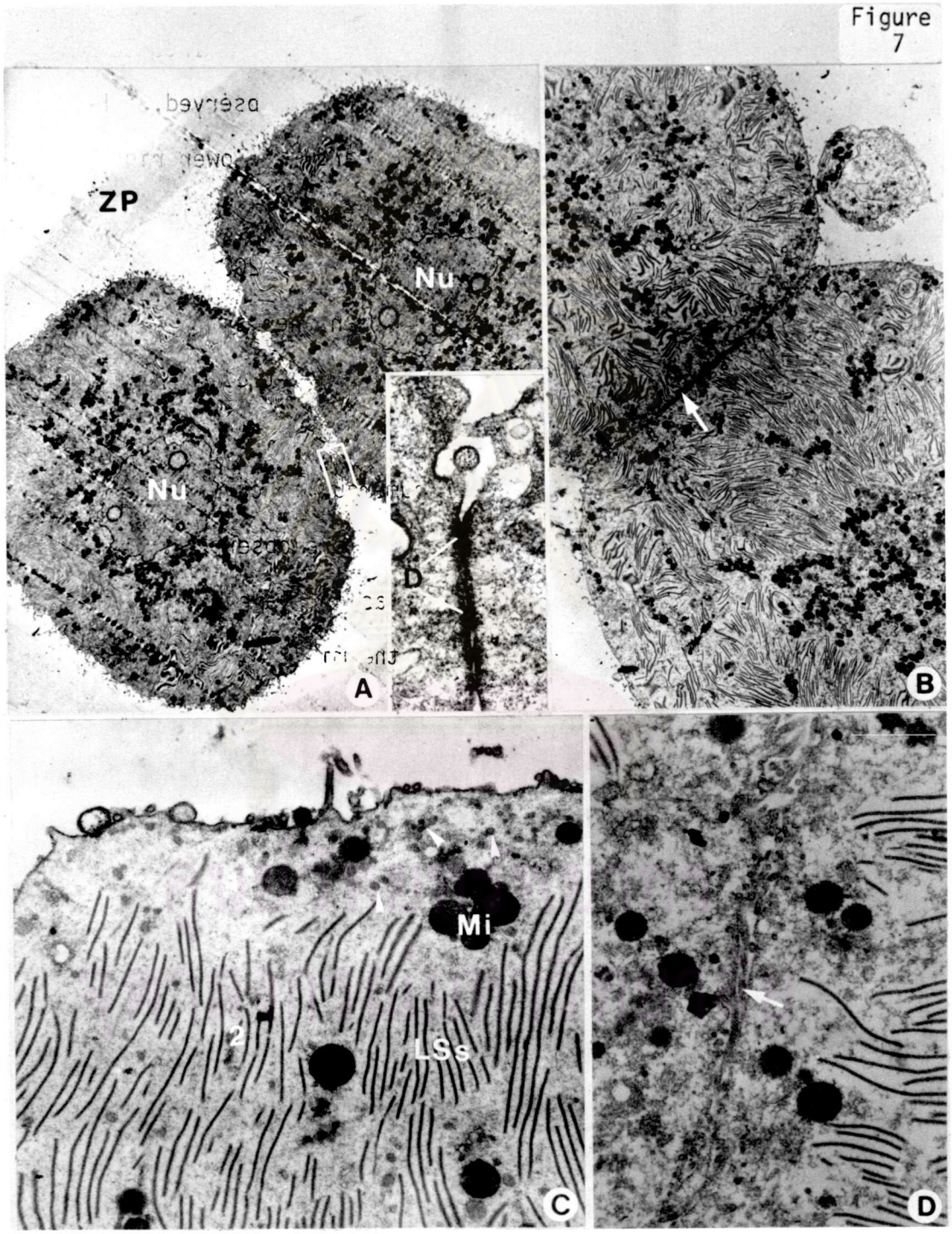

intercellular junction between blastomeres, the gap junction, was first found in this stage (Figure 8 : G, F).

3.2.4 Eight-cell embryos

At this stage the organization of cytoplasm in each blastomere was different from that of one-cell embryo and earlier stages. The polarity of blastomere was first noticed (Figure 9 : A, B). Most cytoplasmic organelles congregated to one side of each blastomere. Numerous vesicles were located in cortical region near the Golgi complexes (Figure 9 : C, D, F). Autophagic vacuoles of different sizes were also observed (Figure 9 : D, E). In some blastomeres, large Golgi complexes with numerous vesicles were observed at the periphery (Figure 10 : A) whereas other Golgi complexes were found close to nucleus (Figure 10 : D). Numerous endocytic vesicles were found beneath the plasma membrane (Figure 10 : B, C) and some of them were confluent with autophagic vacuoles.

3.2.5 Early morulae

This stage of preimplantation embryo consisted composed of two distinctive cell types in different regions. The outer cells were generally flattened, whereas the inner cells tended to be round (Figure 11 : A, C). No distinctive zoning was observed in the cytoplasm of each blastomere as previously described (Figure 11 : B). The junctional complexes between surfaces of the two cell types were more frequently observed, while the interdigitation of microvilli was noticed among cells of the inner region (Figure 11 : D, E). Increasing number of gap junctions was also observed (Figure 11 : F), and numerous vesicles were seen in the cortical region (Figure 11 : D, E).

3.2.6 Morulae

The outer flattened cells were trophectoderm and the

Figure 8 Electron micrographs of 4-cell embryos prepared by conventional TEM method.

A : Low magnification of a blastomere showing the general characteristics of the cytoplasm. X 3,600.

B : Medium magnification from cortical region taken from "A". Mitochondria (Mi), MVB and vesicles (arrow heads) were aggregated to one pole of the blastomere, L = lipid droplet. X 12,000.

C : Medium magnification, showing highly complex plasma membrane (PM) that formed microvilli and cone appeared to be sloughed off. A bundle of microtubules (MTs) was present in the surface protrusions, and MVBs were observed. X 12,000.

D : High magnification of a bundle of microtubules in the surface protrusions. X 18,000.

E : Medium magnification of intercellular junction (IJ) between blastomeres. Interdigitations of microvilli were found and MVB were observed near to this junction. X 12,000.

F : High magnification showing gap junction was also found in some areas of this IJ. X 24,000.

G : High magnification showing GJ. X 36,000.

Figure 8

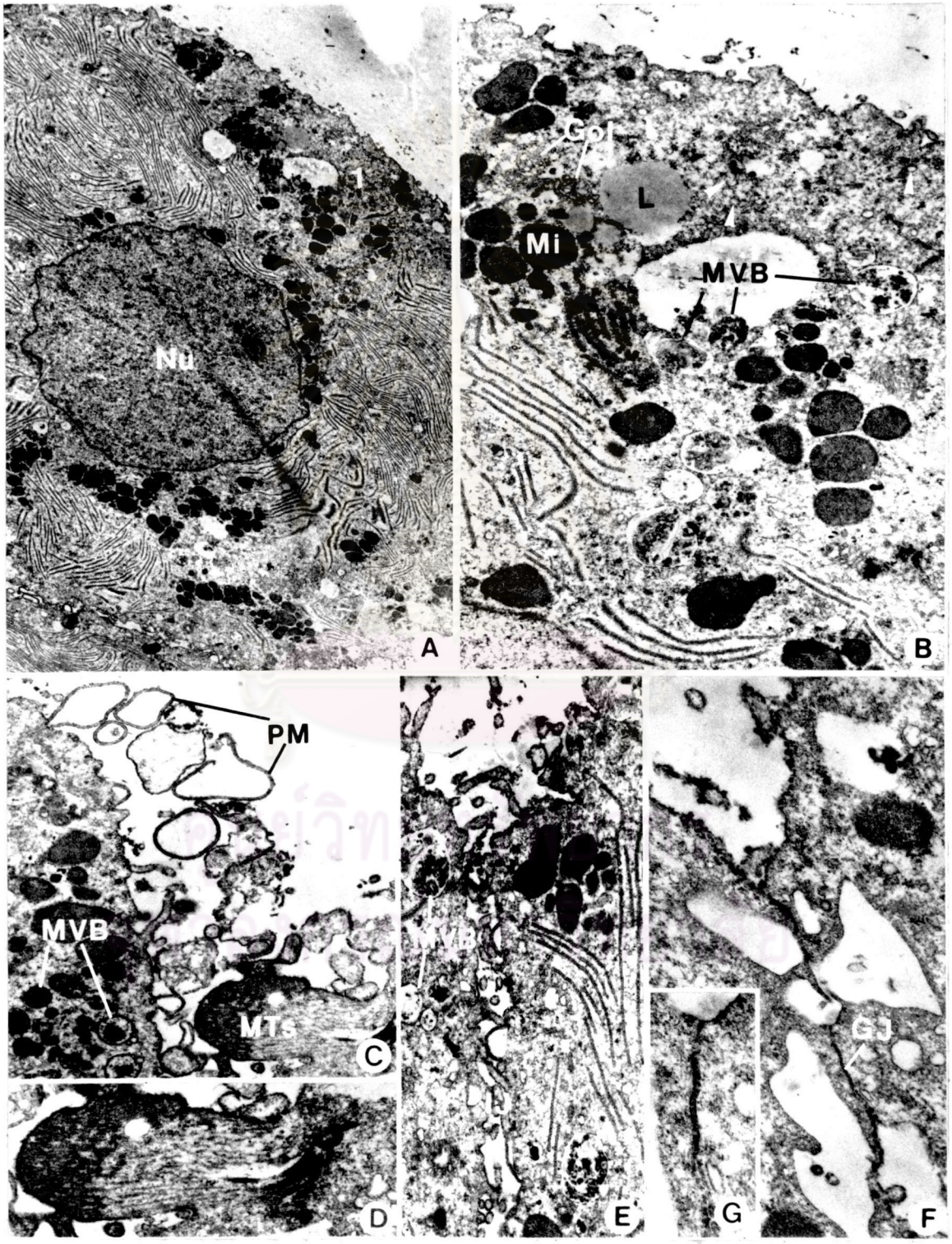

Figure 9 Electron micrographs of 8-cell embryos prepared by conventional TEM method.

A,B : Low magnification, showing the general characteristics of the cytoplasm of each blastomere. The polarity of blastomeric cytoplasm began to be observed. Nu = nucleus. X 2,400, X 4,800.

C,D : High magnification of cortical region showing lipid droplets (L), mitochondria (Mi), autophagic vacuoles (AV), Golgi complex (Gol) and numerous vesicles (V). X 18,000, X 24,000.

E : Medium magnification of inner region, numerous vesicles, mitochondria and autophagic vacuoles (AV) were observed. X 12,000.

F : In apposing area with microvillus interdigitation numerous vesicles (arrow heads) were observed. X 24,000.

Figure 9

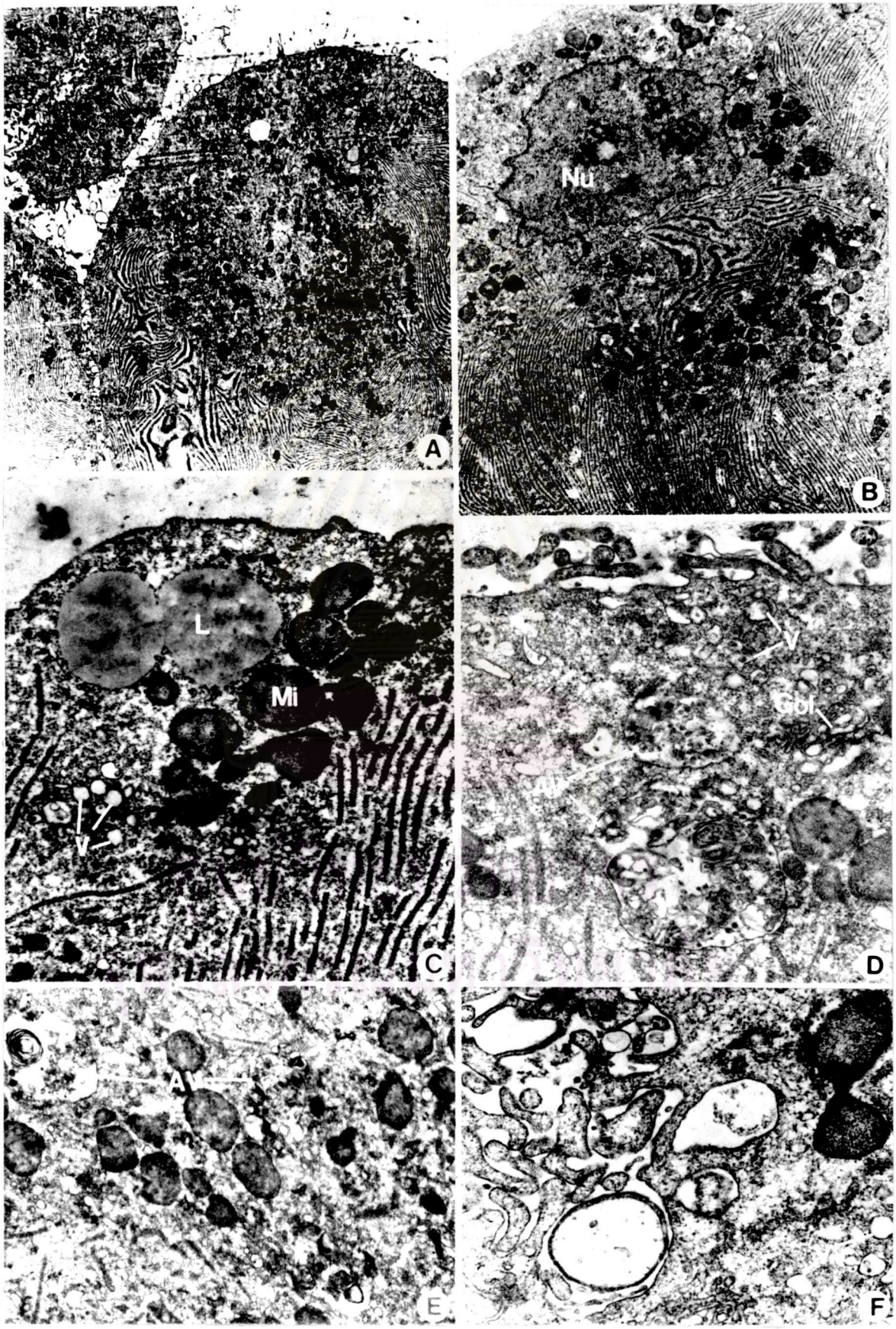

Figure 10 Electron micrographs of 8-cell embryos prepared by conventional TEM method.

A : High magnification of the blastomere, showing the presence of Golgi complexes (Gol), vesicles (V) in the cortical region. X 24,000.

B : High magnification of cortical region, showing large vesicles (arrows) underneath the plasma membrane. X 36,000.

C : High magnification of the blastomere, showing the presence of Gol, AV and numerous vesicles (V) in the cortical region. X 18,000.

D : High magnification of the blastomere, showing the presence of Gol, V and AV in the perinuclear region. X 18,000.

Figure 10

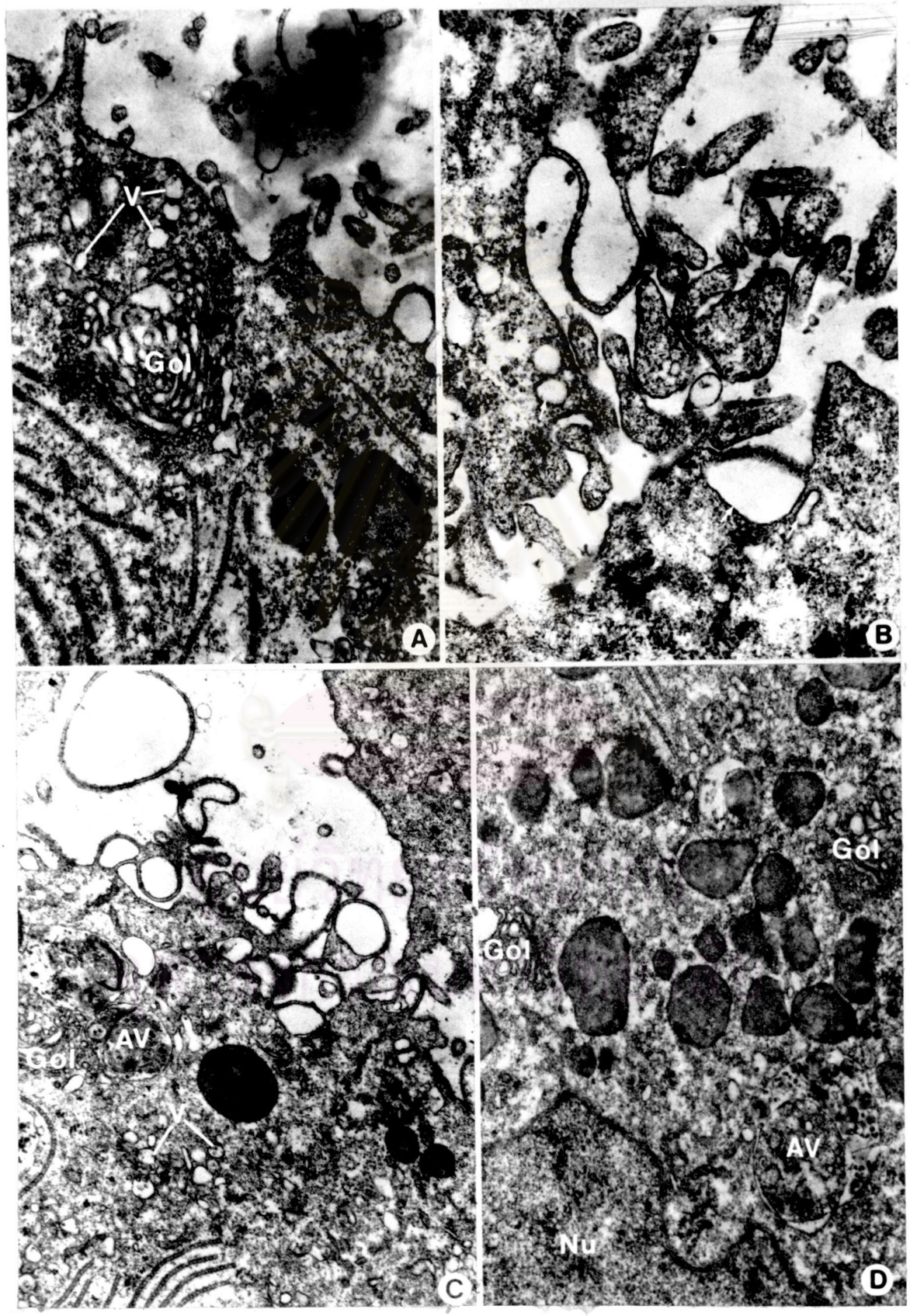

Figure 11 Electron micrographs of early morulae prepared by conventional TEM method.

A : Very low magnification, showing the general ultrastructure of blastomeres. Trophectoderm (Tr) was found (arrow head) at the periphery. X 1,200.

B : Low magnification of a blastomere, showing the distribution of cytoplasmic organelles. X 6,000.

C : Medium magnification from the arrow head region in A, showing intercellular junctions (arrows) L = lipid droplet. X 12,000.

D, E : Medium and high magnification, showing junctional complex (arrow head) between trophectoderm. Interdigitation of microvilli was also observed within the inner part (arrows in D). V = vesicles, MTs = microtubules. X 8,400, X 24,000.

F : High magnification showing the gap junction (GJ), (lower left insertion X 84,000). X 36,000.

Figure 11

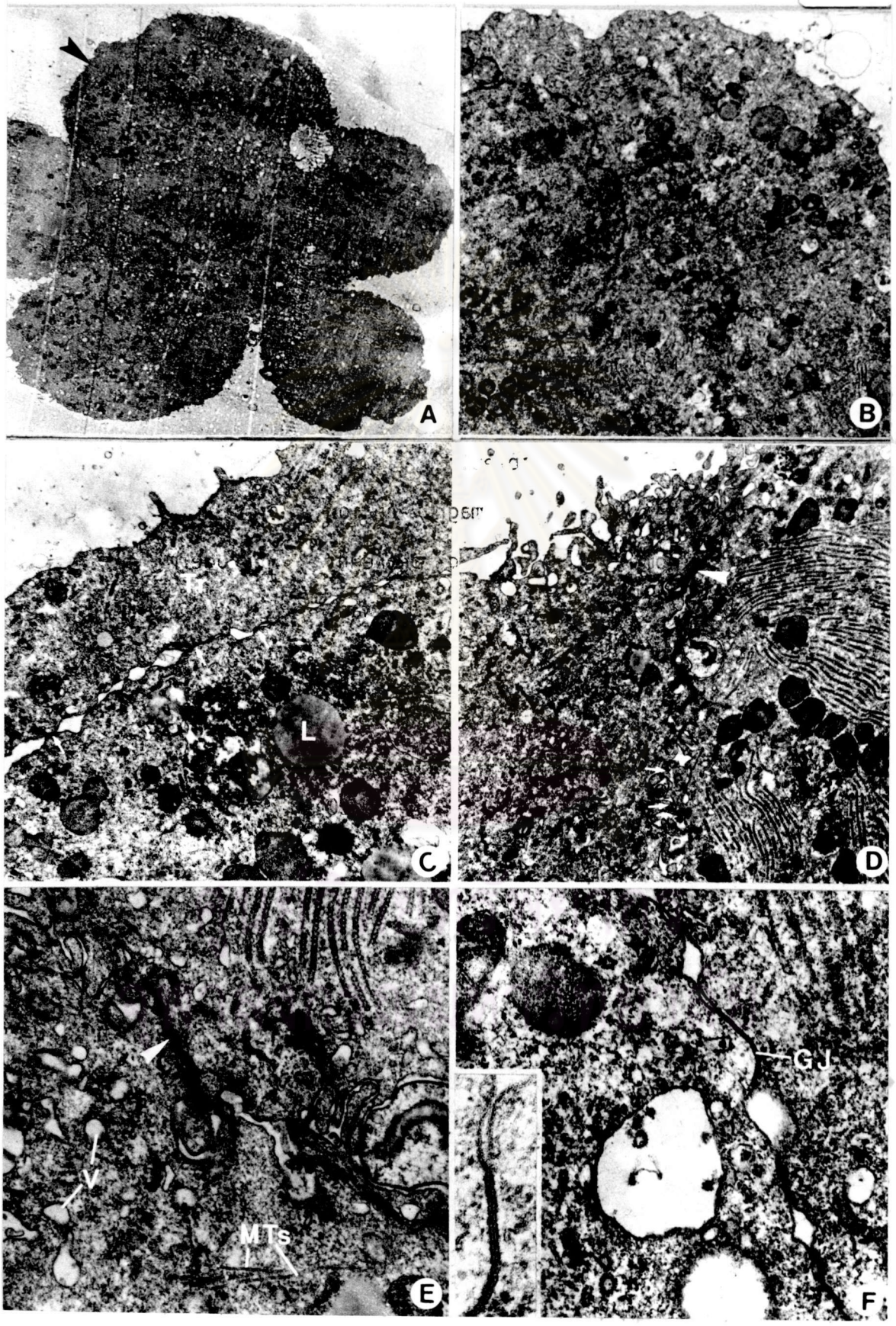

inner round cells were inner cell mass (ICM) (Figure 12 : A). The ultrastructural characteristics of the cytoplasm of trophectoderm resembled the cytoplasm of the cortical region in one-cell embryos. However, there are numerous autophagic vacuoles and various vesicles (Figure 12 : C, D). The cytoplasm of ICM was characterized by the abundance of LSs similar to the middle zone of one-cell embryos. Most of intercellular junctions among ICM resembled desmosomes (Figure 12 : B).

3.2.7 Blastocysts

The blastocysts were composed of two types of cells: trophectoderm and ICM. The trophectoderms that covered ICM were called polar trophectoderm while the opposite side were called mural trophectoderm (Figure 13 : A). The presence of numerous dense bodies in the cytoplasm characterized both polar and mural trophectoderm. In contrast, only a few of these inclusions were observed in ICM(Figure 13 : A, C).

Cells of inner cell mass, which differentiated to become the embryo proper, were loosely apposed to one another and the surrounding trophoblasts, leaving numerous intercellular spaces. At intervals, short regions of cytoplasmic bridges occurred between trophoblasts and other cells of the ICM. Binding these bridges together were various intercellular junctions : gap junctions, interdigitations of microvilli and desmosomes (Figure 13 : B). Ultrastructurally, the contents of ICM were similar to those described previously, except that LSs appeared more abundant than in the trophectoderm.

Microvilli on the surface of the trophectoderm were short and sparse when compared to previous stage. Morphological changes continued to occur in mitochondria within both trophectoderm and ICM.

Figure 12 Electron micrographs of morulae prepared by conventional TEM method.

A : Low magnification, showing the distribution of outer flatten, and inner round cells. Tr = trophectoderm. X 1,200.

B : Low magnification, showing intercellular junctions (IJ) among inner cells. A few autophagic vacuoles (AV) were observed. X 8,400.

C,D . High magnification, showing the cortical cytoplasm of outer cells. Numerous vesicles (V) and autophagic vacuoles (AV) were observed. Golgi complex (Gol) was also found in this region. X 24,000, 24,000.

Figure 12

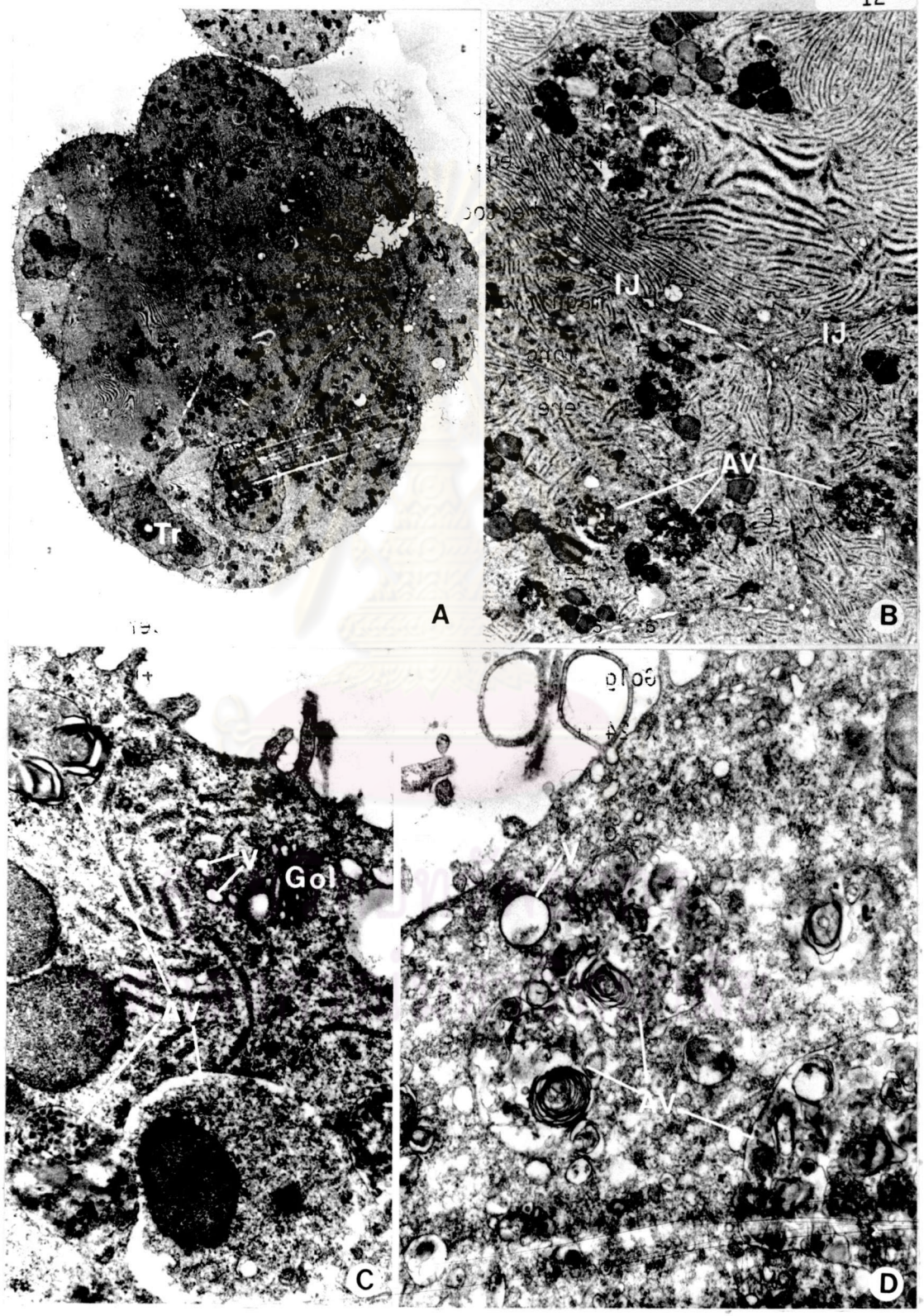

Figure 13 Electron micrographs of blastocyst prepared by conventional TEM method.

A : Very low magnification, showing general morphology of blastocyst. Interval of intercellular spaces (arrow heads) between polar trophectoderm (pTr) and ICM were observed. mTr = mural trophectoderm, Bl = blastocoel. X 1,200.

B : Medium magnification, showing numerous various size of dense bodies (DB) in trophectoderm. X 8,400.

C : Medium magnification of ICM, showing numerous LSs. Interdigitation of microvilli (arrow) between ICM and pTr was observed. X 18,000.

D : Low magnification, showing general characteristic of ICM. A few DB were observed. X 4,800.

E : Medium magnification, showing intercellular junctions between polar trophectoderm (pTr) and ICM; gap junction (GJ), interdigitation of microvilli (arrow) and desmosome (D). Cylindrical-shaped mitochondria (mi) were observed in both trophectoderm and ICM. IS = intercellular space. X 12,000.

Figure 13

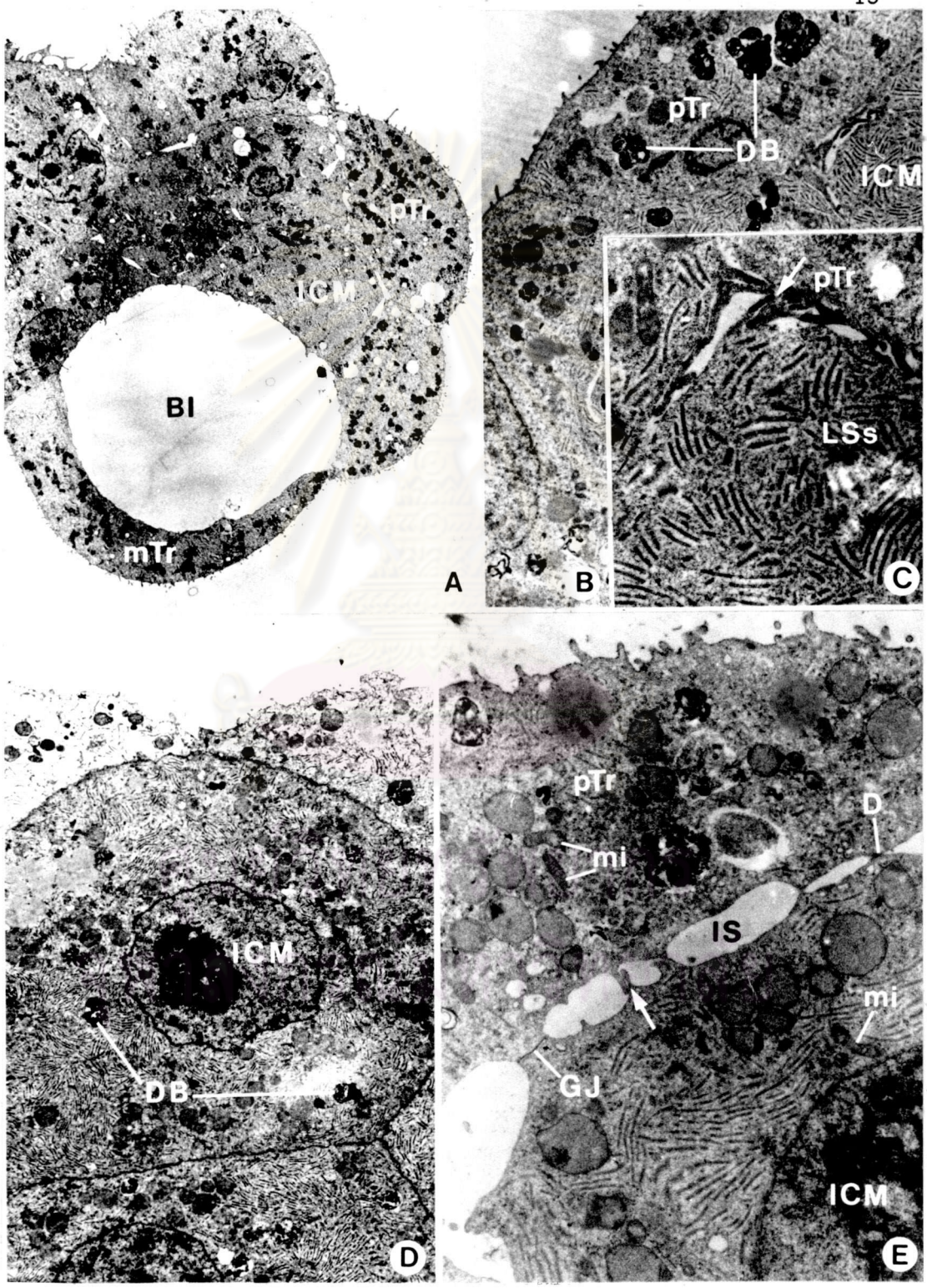
pTr
ICM
Bl
mTr
A
pTr
DB
ICM
B
pTr
LSs
C
ICM
DB
D
pTr
mi
D
IS
mi
GJ
ICM
E

These organelles became more cylindrical with an increased number of cristae (Figure 13 : B).

In this study, normal rough endoplasmic reticulum (RER) and smooth endoplasmic reticulum (SER) as observed in most somatic cells was not present. However, it is possible that the LSs may actually be another form of RER with embedded ribosomes (Bachvarova et al., 1981).

3.3 The organization of cytoskeletons in preimplantation embryos

The organization of cytoskeleton in zona-free preimplantation embryos treated with Triton X-100 for 1 hr was studied by TEM. There appeared to be four types of cytoskeletal elements; namely, the thin straight microfilament, microtubule, bundle of intermediate filaments and microtrabecular lattice (Table 3.1).

3.3.1 The organization of microfilaments

By varying the time of Triton X-100 extraction, it was found that the most suitable time for extraction with Triton X-100 was 1 hr , in which most of the soluble materials in the cytoplasm of preimplantation embryos were dissolved out, as well as the plasma membranes. Some cytoskeletons were presumably lost but the majority probably remained intact. The most peripheral elements appeared as the network of long straight filaments, each of which was about 53 Å in diameter, and these were designated as microfilaments (MFs) (Figure 14).

In one-cell embryos, it was clearly shown that MFs were localized preferentially in the cores of microvilli and in the narrow area immediately underneath the plasma membrane (Figure 15 : B, C). Most peripherally-disposed MFs were arranged either longitudinally along with long axes of microvilli or parallel to the plasma membrane. They also appeared as closely-packed fibers whose individual elements

may be cross-linked. These microfilaments were designated as cortical MF. Within the inner part of cytoplasm, designated as cytoplasmic MF, were the organization of loose networks whose fibrous components were much less prominent and less-tightly packed than those in the cortical area (Figures 15: E; 16 : D).

In two-cell embryos to blastocysts, cortical MFs were clearly seen (Figures 17-22) while the cytoplasmic MFs were less prominent except those in the trophectoderms (Figure 21 : D).

3.3.2 The organization of microtubules (Figures 15-22)

Microtubules (MTs) in the cytoplasm of preimplantation embryos were about 230 Å in diameter. They were distributed in all directions and were clearly observed in both longitudinal and cross sections underneath the plasma membrane and inside the cell (Figure 18 : C, D, E; 21 : B-F), and also between lamellar structures (Figure 17 : D, E, F; 19 : C, E). Furthermore, MTs were abundant in the area where the polar body was being extruded (Figure 16 : A, B, C), and in the regions where the peripheral cytoplasm protruded. In four-cell embryos (Figure 7 : C, D) and early blastocysts, (Figure 20 : C) MTs were longitudinally arranged along the extended region. MTs were also localized close to the intercellular junction between the trophectoderm (Figure 20 : D, E), inner cell mass (ICM) and ICM (Figure 22 : A, B, C).

3.3.3 The organization of intermediate filaments

In the cytoplasm of developing embryos, there was also another type of cytoskeletal element. They were designated as intermediate filaments (IFs) as called in most other cells, each with 80-100 Å in diameter. In this study, IFs were clearly observed in one- and two-cell embryos. In one-cell embryo, they were organized as both tightly-packed and loose bundles (Figure 23 : B-E) while in

Table 3.1 Size and distribution of cytoskeletal elements in preimplantation embryos

Types	Diameters (Å)	Stage of embryos found	Organization & Distribution
MFs	53	all	in the cores of microvilli and underneath the plasma membrane
MTs	230	all	disposed in all directions in cytoplasm and became peripherally disposed in trophectoderm of blastocyst
IFs	80-100	1-and 2-cell	cortical cytoplasm
MNs	165 (beads) 92 (strings)	all	interconnecting other cytoskeletal elements and among all the cytoplasmic organelles

two-cell embryos, IFs were observed only as closely-packed bundles of different sizes (Figure 24). In addition, another type of IFs which were arranged in smaller bundles was also found (Figure 25). All types of IFs were found in the cortical region, and these IF bundles were not often seen in other regions.

3.3.4 The organization of microtrabecular network

Even after the extraction by Triton X-100 for 2 hrs, this network of highly cross-linking fibers still remained in the cytoplasm (Figure 14 : A, B, C), they were, therefore, designated as microtrabecular network (MN) in this study. MN was the major component of cytoskeleton which was distributed evenly all over the cytoplasm of preimplantation embryos, except in the regions between lamellar structure where they appeared loosely-arranged. They were present among microtubules (Figure 16 : C) and LSs (Figures 14 B; 18 : C, D). MNs were also observed to link with IFs (Figure 23, 24, 25) and MFs (Figure 21 : D). Most microtrabeculae appeared as zig-zag fibers which resemble beads on-a-string with consecutive diameters of 165 and 92 Å, respectively. They not only were cross-linked among themselves but also served to interconnect other cytoskeletal elements and cytoplasmic organelles.

3.4 Binding of lectins to embryos (Table 3.2)

3.4.1 Binding of Con A

Embryos were fixed with glutaraldehyde and subsequently labelled with Con A, HRP and DAB + H_2O_2. Reaction products were found on the surface plasma membrane and microvilli of 1-, 2-, 4-cell embryos and blastocysts (Figures 26, 27, 28, 29). The distribution and intensity of Con A bindings shown by this technique were uniform throughout the entire surface of embryos. The staining intensity

Figure 14 Electron micrographs of preimplantation embryos extracted with Triton X-100 for 2 hrs.

A,B : Medium and high magnifications of 1-cell embryos, showing microtrabecular lattices (arrow heads) among lamellar structures and mitochondria (Mi). X 12,000, 32,000.

C,D,E: High magnification of 8-cell embryos in which most of soluble materials in the cytoplasm were extracted. Microfilaments (MFs) were apparently seen as long fibers. Microtrabecular network (arrow heads), microtubules (arrow) and microvilli (MV) were also observed. X 36,000, X 48,000, X 36,000.

F,G : High magnification of trophectodermal cells showing that plasma membrane which were partially destroyed by longer extraction (asterisks). MFs and numerous microtubules (arrows) were clearly seen in the zone underneath the plasma membrane. X 36,000, X 36,000.

Figure 14

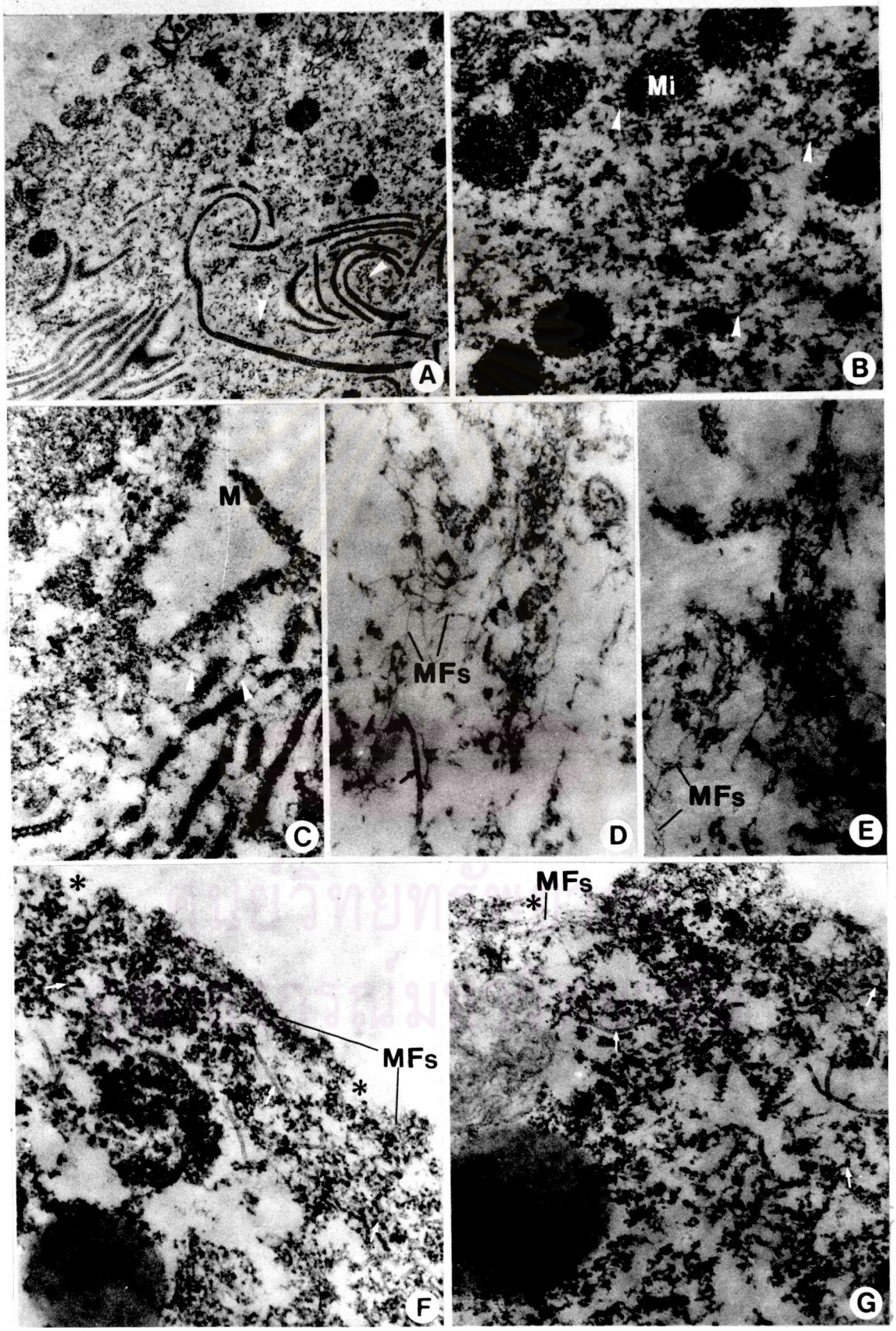

Figure 15 Electron micrographs of 1-cell embryos extracted with Triton X-100 for 1 hr.

A : Low magnification of 1-cell embryo showing the organization of cytoplasmic organelles. X 2,400.

B,C : High magnification of microvilli (MV) and plasma membranes, showing the organization of cortical MFs. X 48,000, X 36,000.

D : Sperm's tail (ST) which remained in the cytoplasm. Microtubule (arrow) and microtrabeculae lattices (arrow heads) were observed. X 36,000.

E : High magnification, showing microtubules (arrows), microtrabecular network (arrow heads) and cytoplasmic MFs. X 48,000.

Figure 15

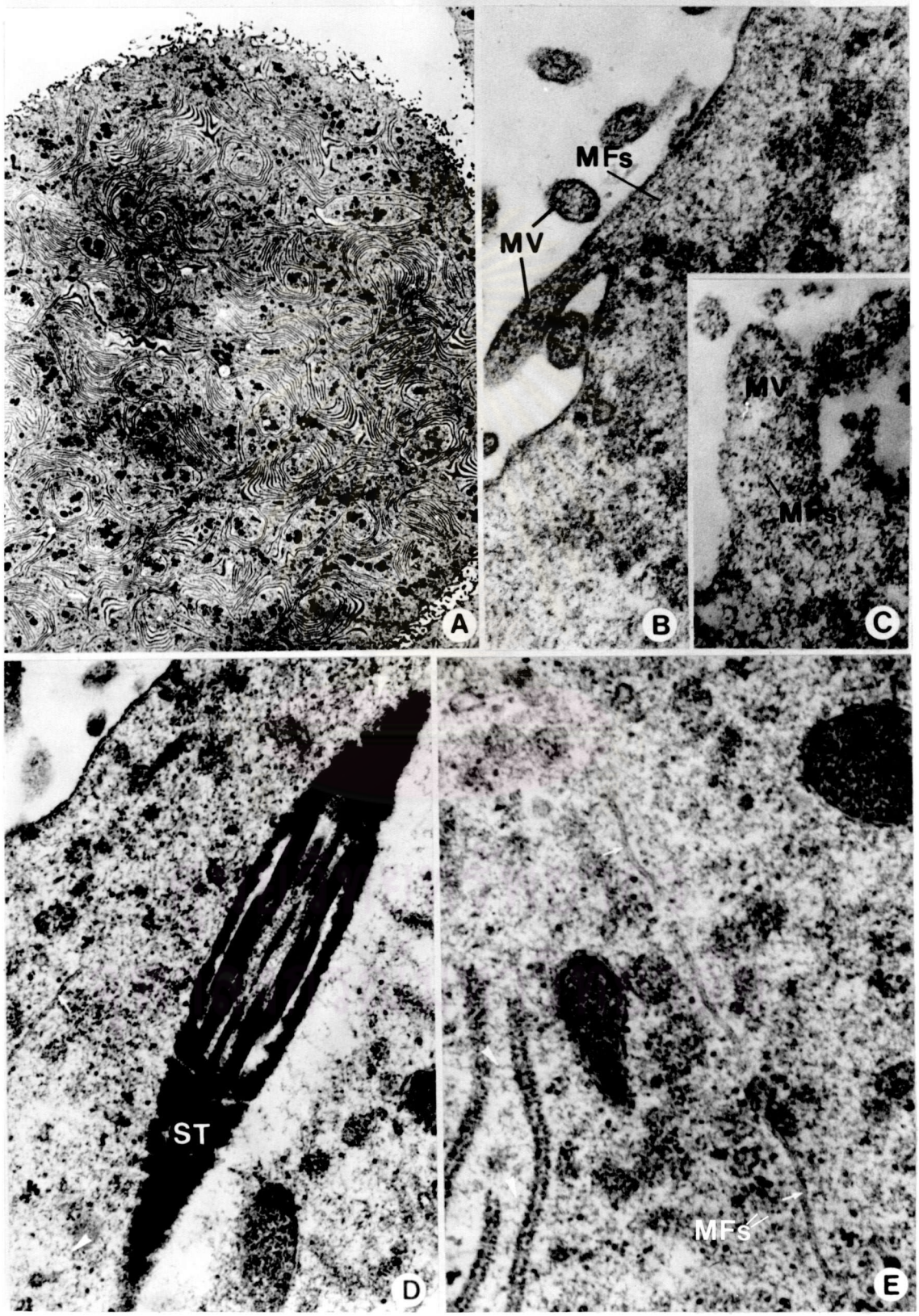

Figure 16 Electron micrographs of 1-cell embryos extracted with Triton X-100 for 1 hr.

A : Low magnification of 1-cell embryo in the region of polar body (PB) formation. X 2,400.

B,C : Medium and high magnification of an area in A which contain microtubule (MTs) : both longitudinal and transverse sections of MTs were observed. Microtrabecular lattices (arrows) filled up the space. X 8,400, X 64,000.

D : Cross-section of sperm's tail (ST) was still found in 1-cell embryo. Cytoplasmic microfilaments (arrow heads) were also observed. X 48,000.

Figure 16

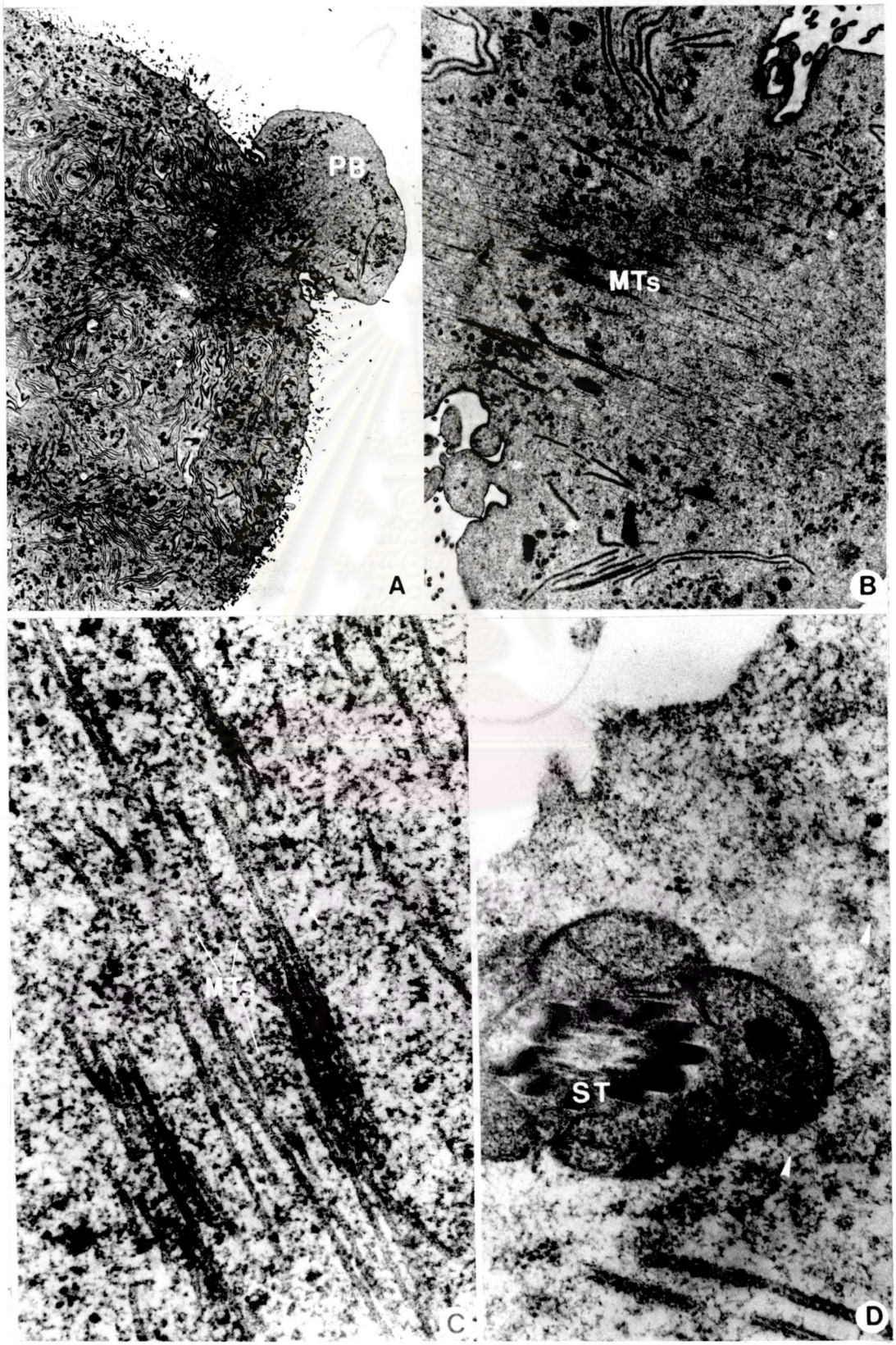

Figure 17 Electron micrographs of 2-cell embryos extracted with Triton X-100 for 1 hr.

A : Low magnification, shown the organization of cytoplasmic organelles in the place close to the nucleus. X 2,400.

B,C : High magnification, showing the presence of cortical microfilaments (MFs), microtubules (arrow head) and intermediate filaments (IFs). X 36,000, X 48,000.

D,E,F: Both cross and longitudinal sections of microtubules (arrow heads) were found between lamellar structures. X 36,000, X 36,000, X 36,000.

Figure 17

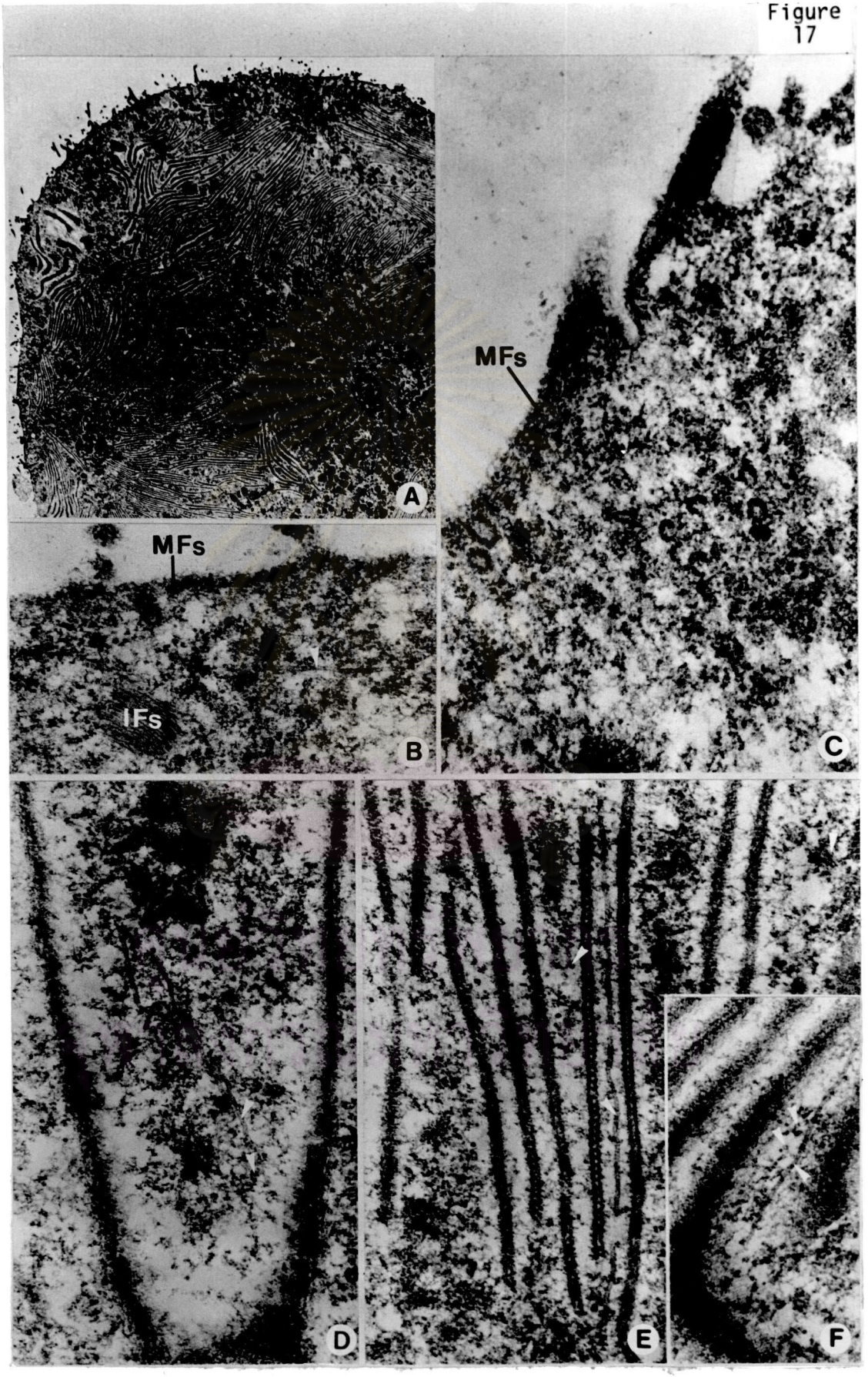

Figure 18 Electron micrographs of 4-cell embryos extracted with Triton X-100 for 1 hr.

A : Low magnification of two blastomeres, showing the general organization of cytoplasm and the nucleus (Nu). X 12,000.

B : High magnification of a blastomere showing cortical microfilaments (MFs) in microvilli and underneath the plasma membrane and micro-trabecular network (arrows) linked between lamella structures. X 36,000.

C,D,E: High magnification showing the organization of microtubules in both longitudinal and cross sections (arrow heads), and microtrabecular network (arrows) that link between lamellar structures and MTs. X 36,000, X 36,000, X 48,000.

Figure 18

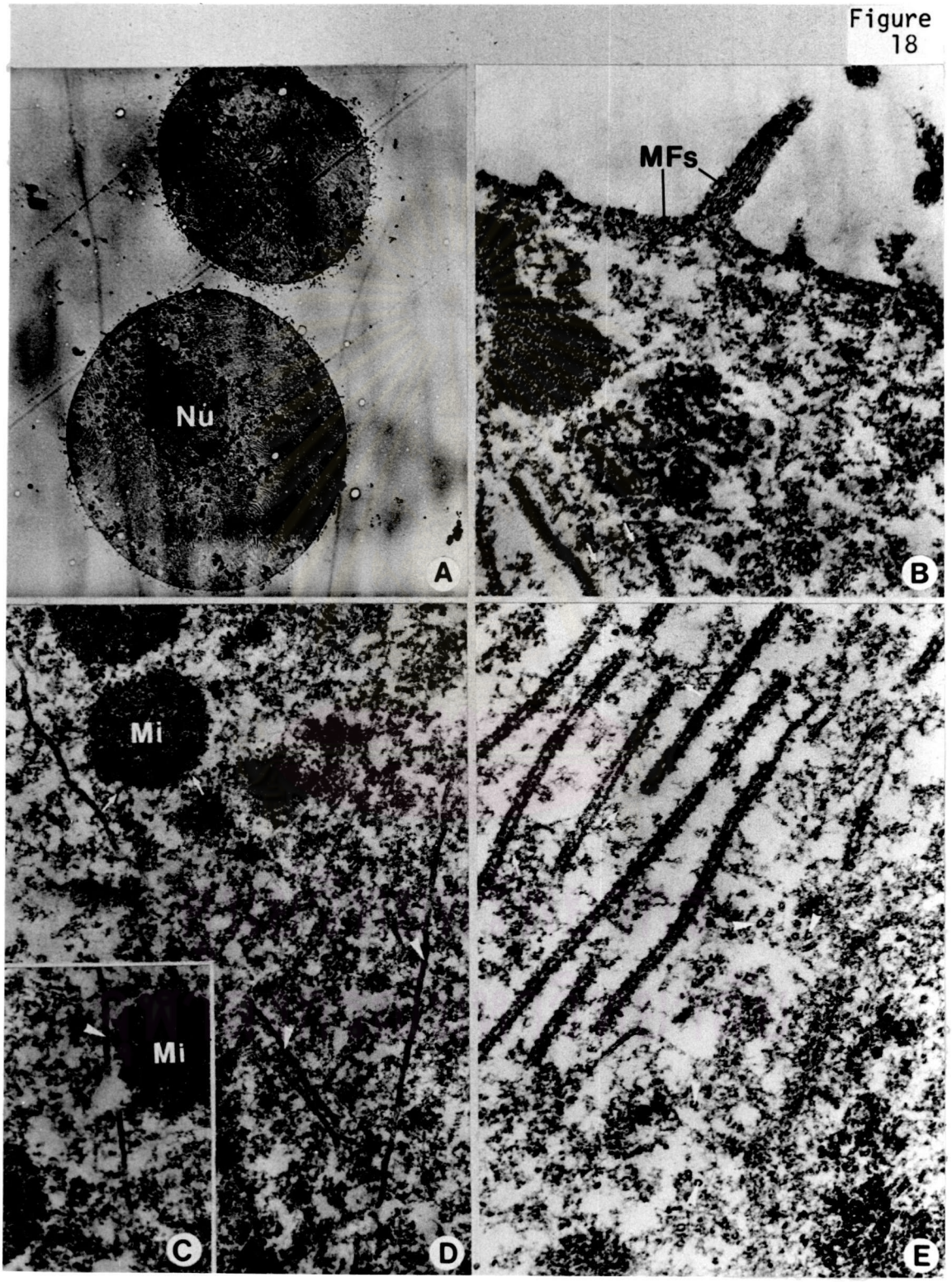

Figure 19 Electron micrographs of 8-cell embryos extracted with Triton X-100 for 1 hr.

A : Low magnification of five blastomeres, showing general distribution of cytoplasmic organelles. X 1,200.

B : High magnification showing straight cortical microfilaments (MFs) and cross sections of microtubules (arrow). X 36,000.

C,D,E,F : The distribution of microtubules (arrows) were observed in many directions. Microtrabecular network (arrow heads) filled up most of the cytoplasmic space. X 36,000, X 36,000, X 36,000.

Figure 19

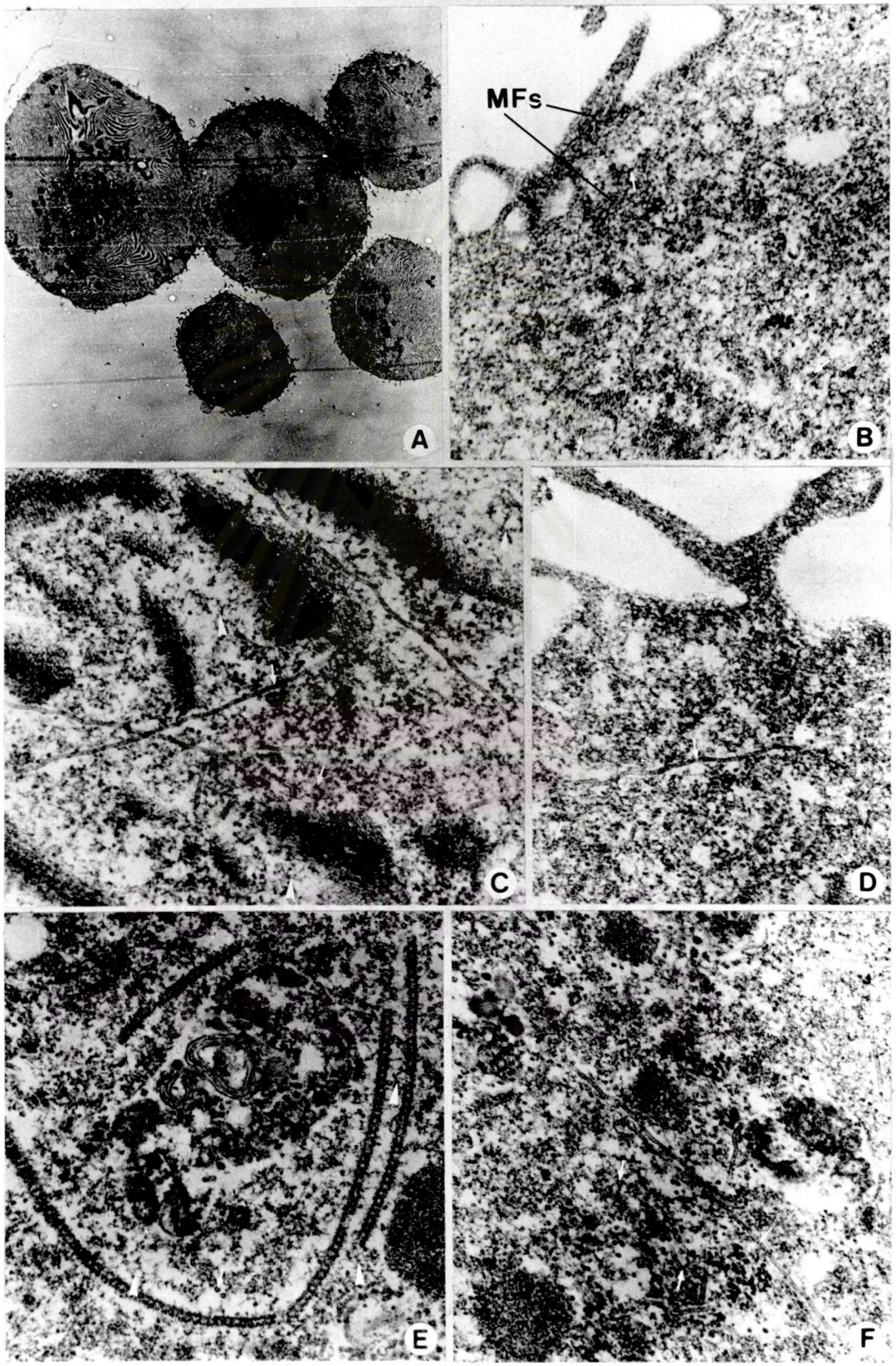

Figure 20 Electron micrographs of early blastocysts extracted with Triton X-100 for 1 hr.

A : Low magnification of early blastocyst, showing early blastocoel (Bl), trophectoderms (Tr) and inner cell mass (ICM). X 2,400.

B : Microtubules (arrow heads) were arranged in many directions close to plasma membrane of trophectoderm. X 3,600.

C : High magnification from small rectangle in A. A large bundle of closely-packed microtubules (MTs) were observed. X 24,000.

D,E : The distribution of microtubules (arrow heads) in the junctional region between adjacent trophectoderm (Tr). IS = intercellular space. X 36,000, X 36,000.

Figure 20

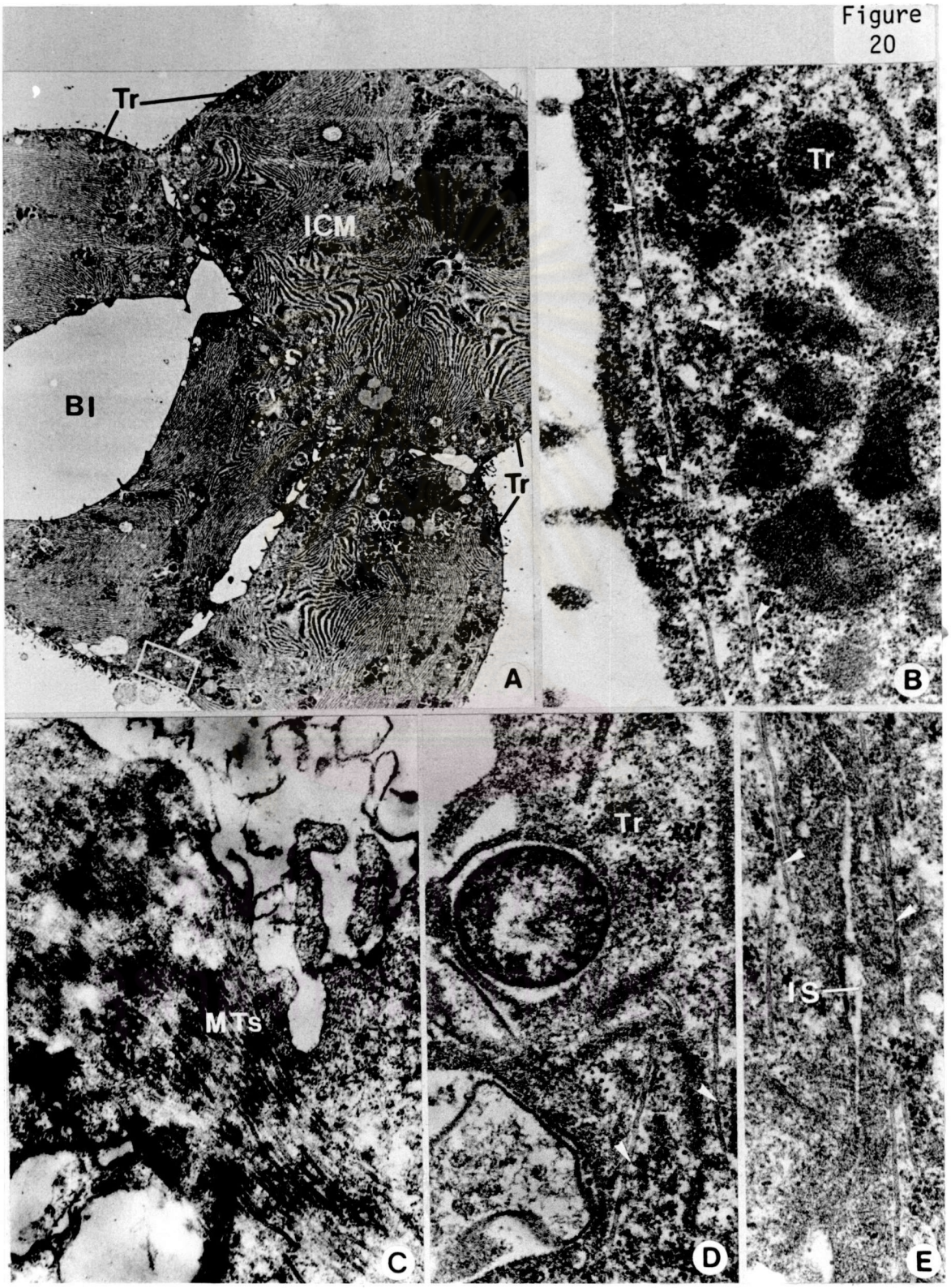

Figure 21 Electron micrographs of blastocysts extracted with Triton X-100 for 1 hr.

A : Low magnification of blastocyst showing only mural trophectoderms and large blastocoel. OM = outer membrane; IM = inner membrane; Bl = blastocoel. X 1.200.

B : Medium magnification of trophectoderm showing the distribution of microtubules (arrows). X 12,000.

C,E,F : High magnification of trophectoderms showing inner membrane (IM) regions. The distribution of microtubules (arrows) and microfilaments (MFs) were observed. X 36,000, X 36,000, X 36,000.

D : High magnification of trophectoderm showing the distribution of microtubules (arrows) and microfilament (MFs) in outer membrane (OM) region. X 36,000.

Figure 21

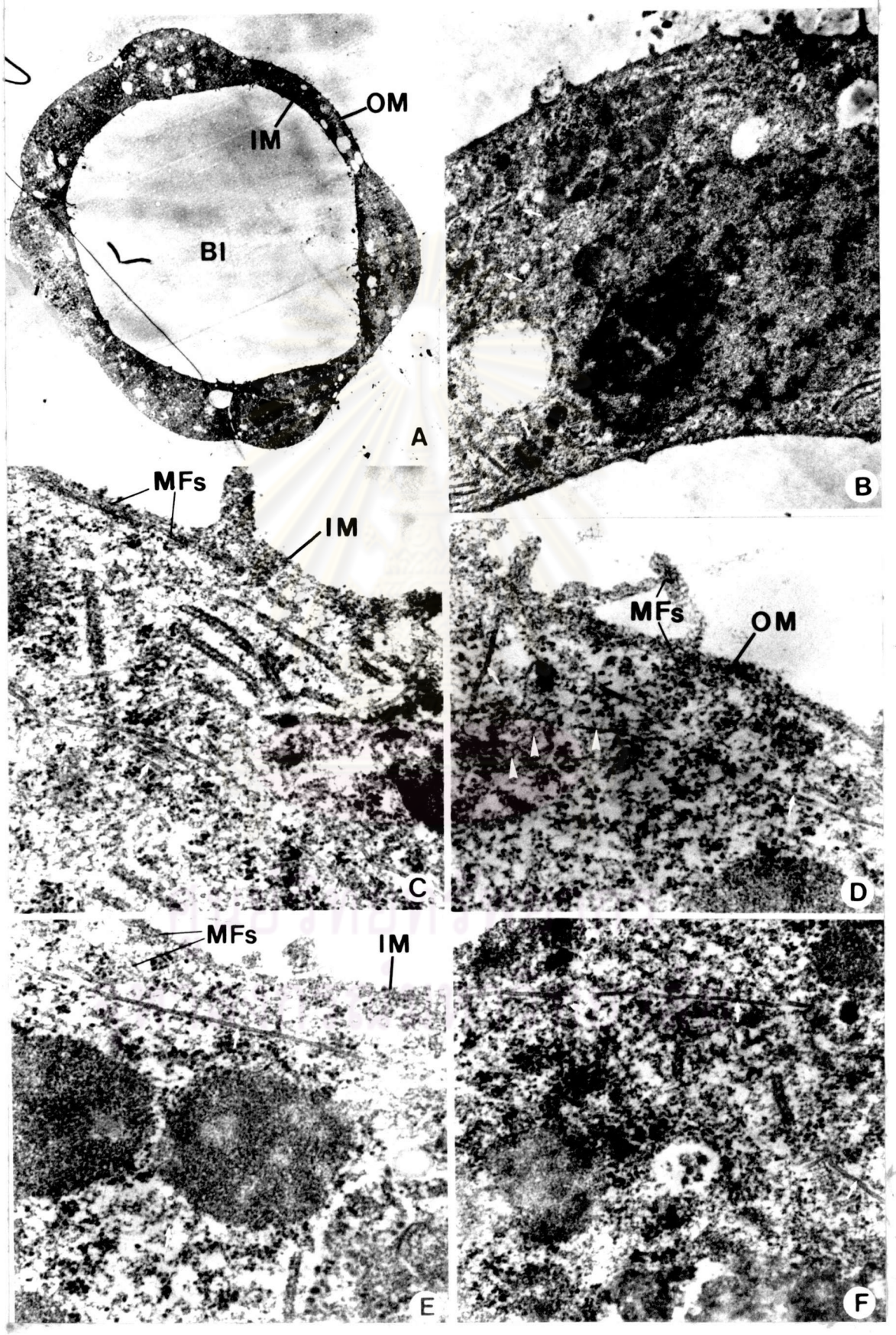

Figure 22 Electron micrograph of blastocysts extracted with Triton X-100 for 1 hr.

A,B,C: High magnification of intercellular junction (IJ) between two inner cell masses (ICM). Microtubules (arrows) were often arranged paralelly to the IJ and tangential arrangement (arrows) was also observed. X 36,000, X 36,000. X 36,000.

D : Microtubules (arrows) were found near gap junction (GJ). X 36,000.

E : Numerous microtubules were observed in the cytoplasm of ICM. X 36,000.

Figure 22

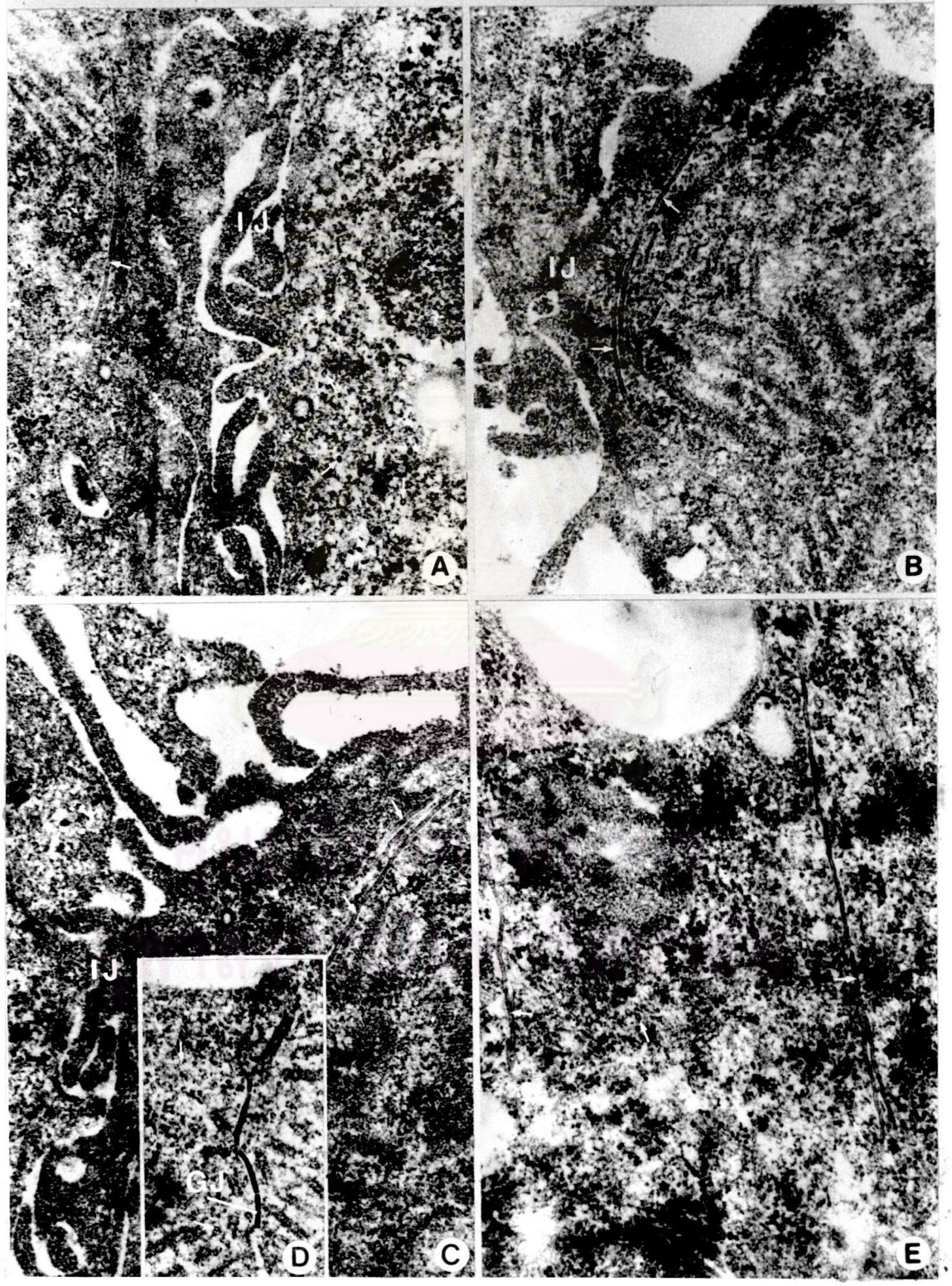

Figure 23 Electron micrographs of 1-cell embryos extracted with Triton X-100 for 1 hr.

A : High magnification showing microtrabecular network (arrows) linking between adjacent mitochondria (Mi) and lamellar structures. X 48,000.

B,C,D,E : The different organization of intermediate filaments (IFs) were observed. Microtrabecular network (arrows) were also linked to IFs (in D, E). X 36,000, X 48,000, X 82,500, X 82,500.

Figure 23

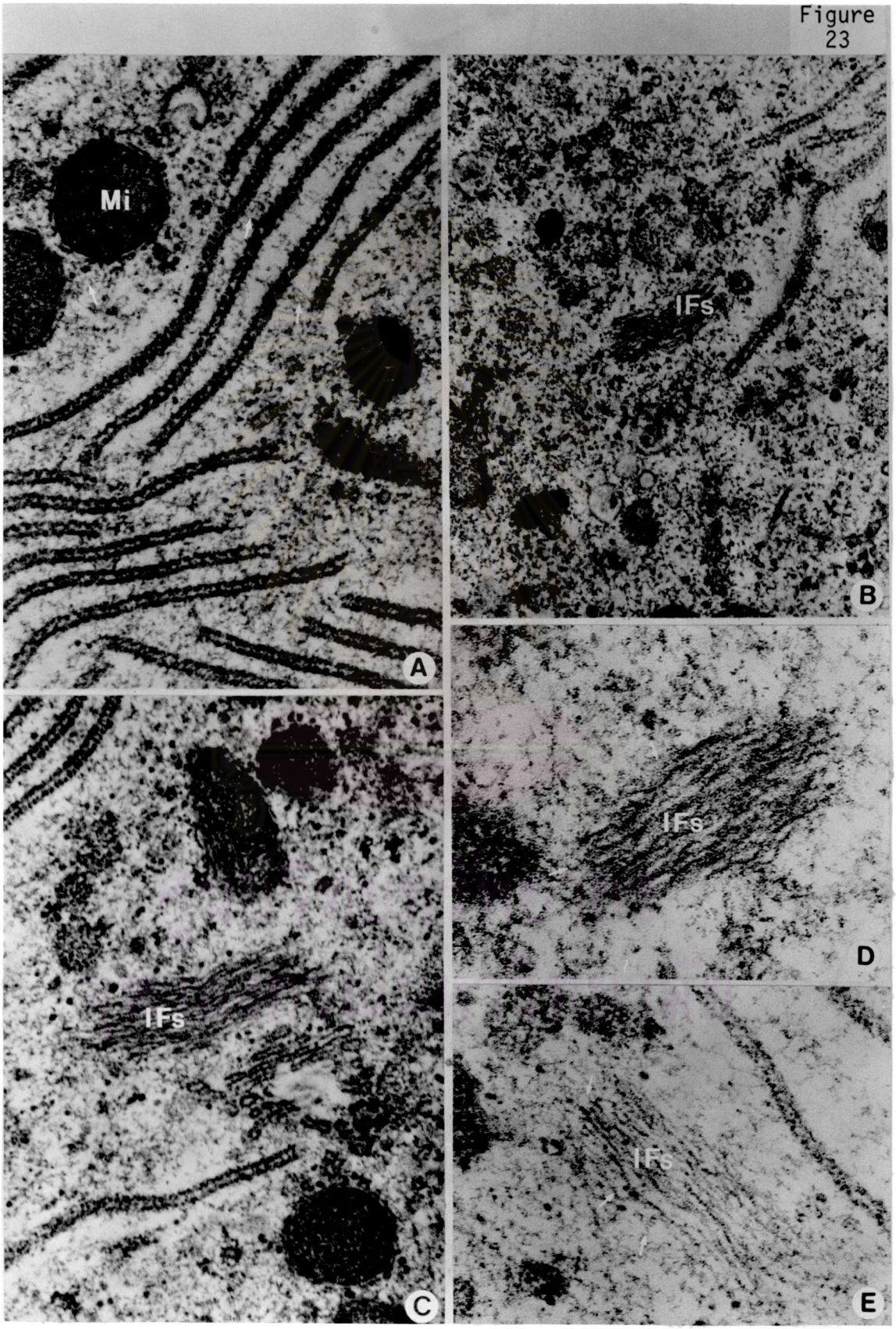

Figure 24 Electron micrographs of 2-cell embryos extracted with Triton X-100 for 1 hr.

A. : Cross section of intermediate filaments (IFs) were clearly seen. At high magnification (left insertion) it appears as mesh work. X 49,500, X 36,000.

B,C,D,E,F, : The bundles of IFs were found along the cell periphery. X 36,000, X 36,000, X 36,000, X 36,000, X 36,000.

Figure 24

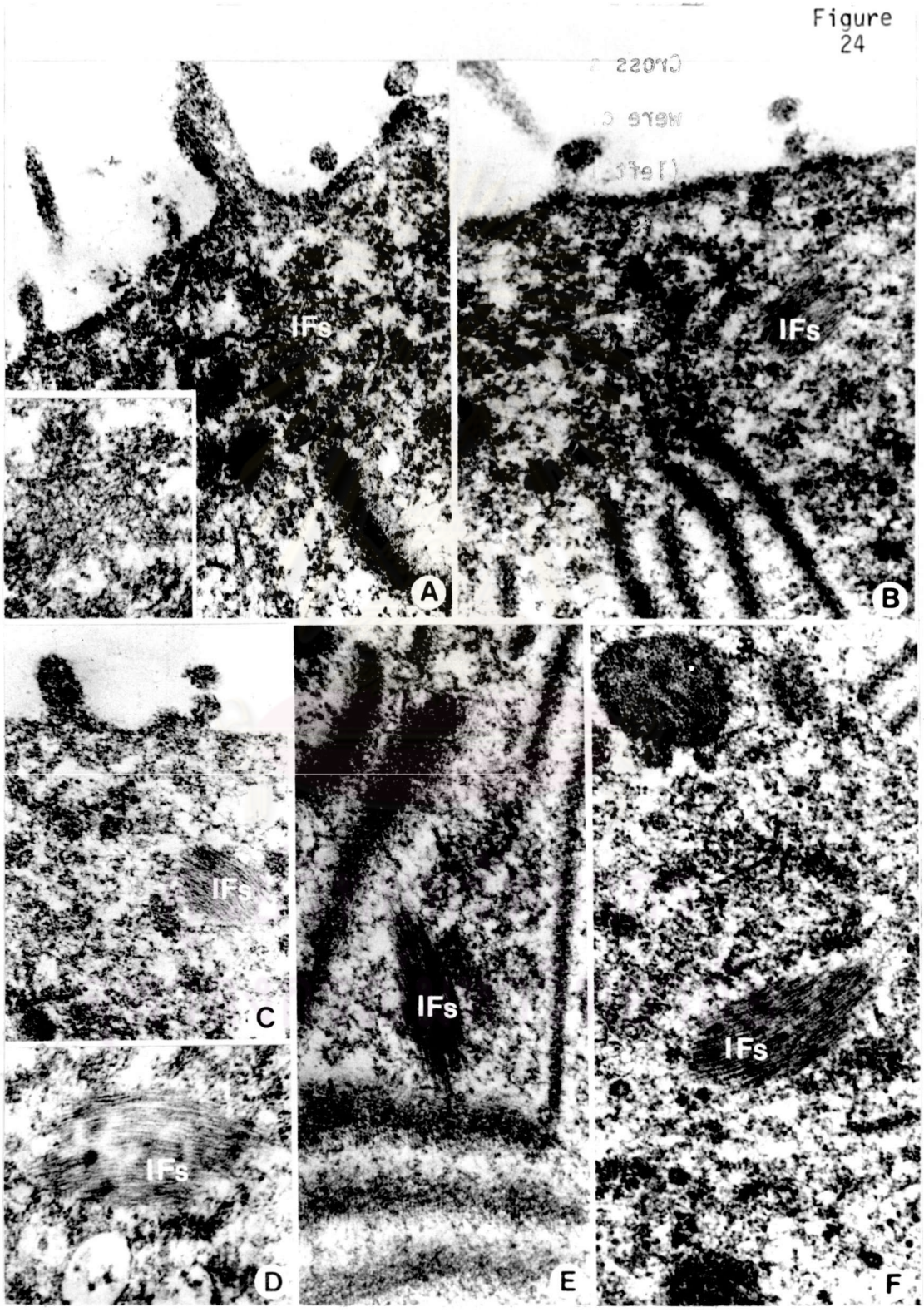

Figure 25 Electron micrographs of 2-cell embryos extracted with Triton X-100 for 1 hr.

A,B,D : The distribution of intermediate filaments (IFs) (arrow heads) were observed throughout the cell periphery. This type of IF bundle was smaller than the previous type (Figure 24). X 36,000, X 36,000, X 48,000.

C,E : High magnification showing small bundles of IFs. X 64,000, X 64,000.

Figure 25

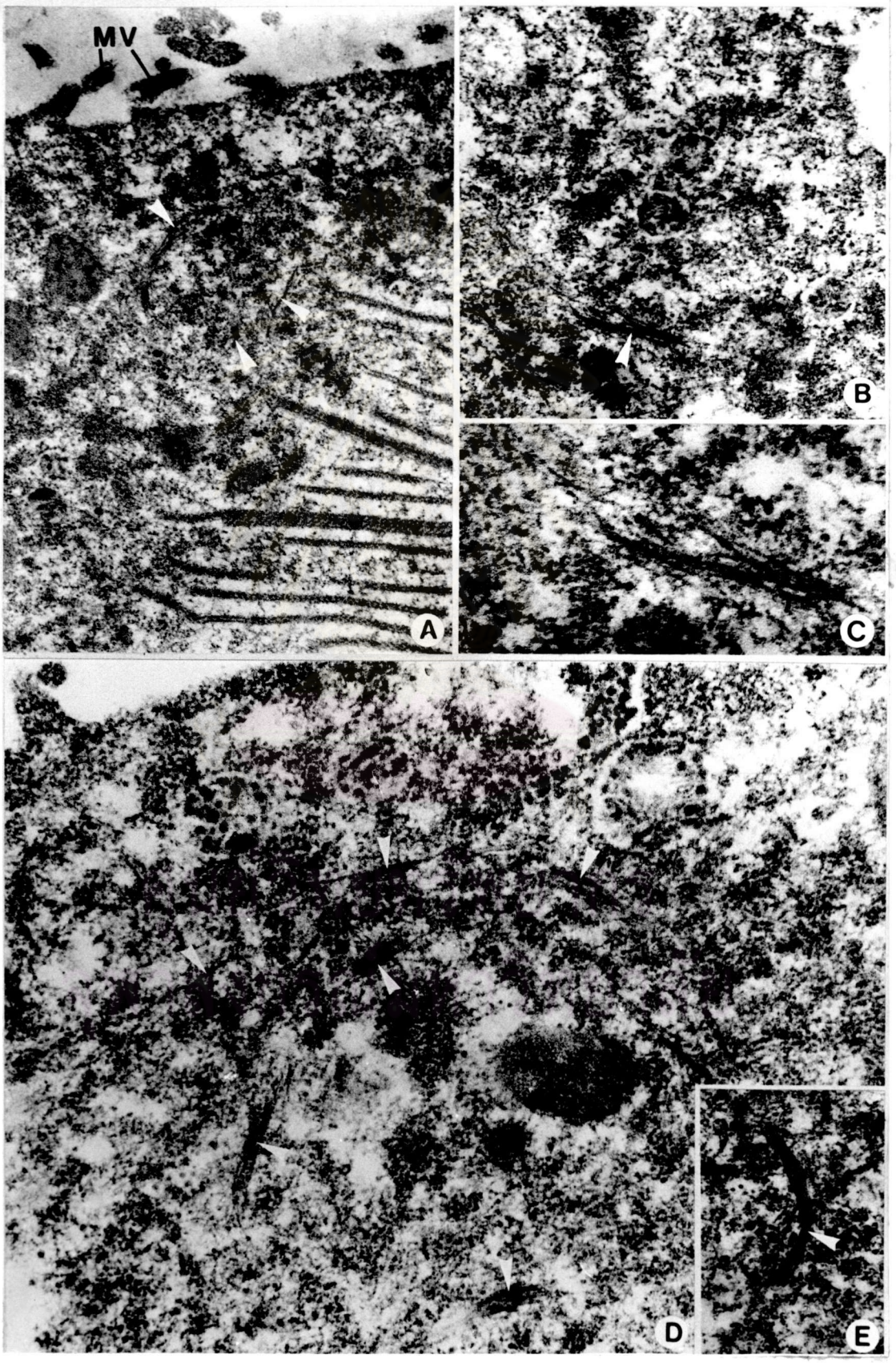

was strong in 1-cell embryo, especially in the areas where cortical granules released its content. This might be because of the abundance of glycoproteins released. The intensity of reaction products was gradually decreased in 2-cell embryos and was only sparingly observed in 4-cell embryos and blastocysts (summarized in Table 3.2).

3.4.2 Binding of WGA

Embryos were fixed with glutaraldehyde and subsequently labelled with WGA-HRP and DAB + H_2O_2. Reaction product were observed on both plasma membrane and microvilli of 1-, 2-, 4-cell embryos and blastocysts (Figures 30, 31, 32, 33). These reaction products appeared as small dense particles on embryonic membrane and also on the membrane of the polar body (Figure 30 : F). WGA binding was uniformly distributed throughout the entire surface of all stages of embryo. The intensity of reaction product was already strong in 1-cell embryo. However, the stronger intensity was observed in the 2-, 4-cell embryos and blastocysts. In addition, the cell coat was rather thick in these stages.

3.4.3 Binding of RCA_1

Embryos were fixed with glutaraldehyde and subsequently labelled with RCA_1-HRP and DAB + H_2O_2. Reaction products were observed on both plasma membrane and microvilli of 1-, 2-, 4-cell embryos and blastocyst (Figures 34, 35, 36, 37). The reaction products were uniformly distributed throughout the entire surface and the intensity of the stain was very strong on the surface of all stages of embryos. In some regions, the reaction product was also found in the most peripheral part of embryonic cytoplasm (Figure 34 : A, B), which on high magnification was due to invagination of the surface membrane. The cell coat was also thick in these embryos.

Table 3.2 Lectins binding to hamster embryos and uterine epithelia during preimplantation stage

Stages	Controls	Lectin Stained*		
		Con A	WGA	RCA_1
Embryos				
1-cell (D_1)	-	+++	+++	++++
2-cell (D_2)	-	++	++++	++++
4-cell (D_3)	-	+	++++	++++
blastocyst (D_4)	-	+	++++	++++
Uterine epithelia				
D_1	-	+	++++	++++
D_2	-	++	++++	+++
D_3	-	++	++++	+++
D_4	-	++	+++	+

* The intensity of lectin stained was designated as : + for light staining; ++ for medium staining; +++ for strong staining, ++++ for very strong staining.

\- No reaction product

Notice that small dots found around the surfaces of embryos in figures 30-37 might be the reaction products from remaining ZP.

Figure 26-29 TEM micrographs of the surface of preimplantation embryos exposed to Con A + HRP + DAB + H_2O_2

Figure 26 (A-E) One-cell embryos, showing the uniform distribution of reaction products on microvilli (Mv) and plasma membrane. The staining intensity was very strong in cortical granules (CG).
A, X 12;000, B, X 2;400, C, X 24,000; D, X 24,000; E, X 24,000.

Figure 26

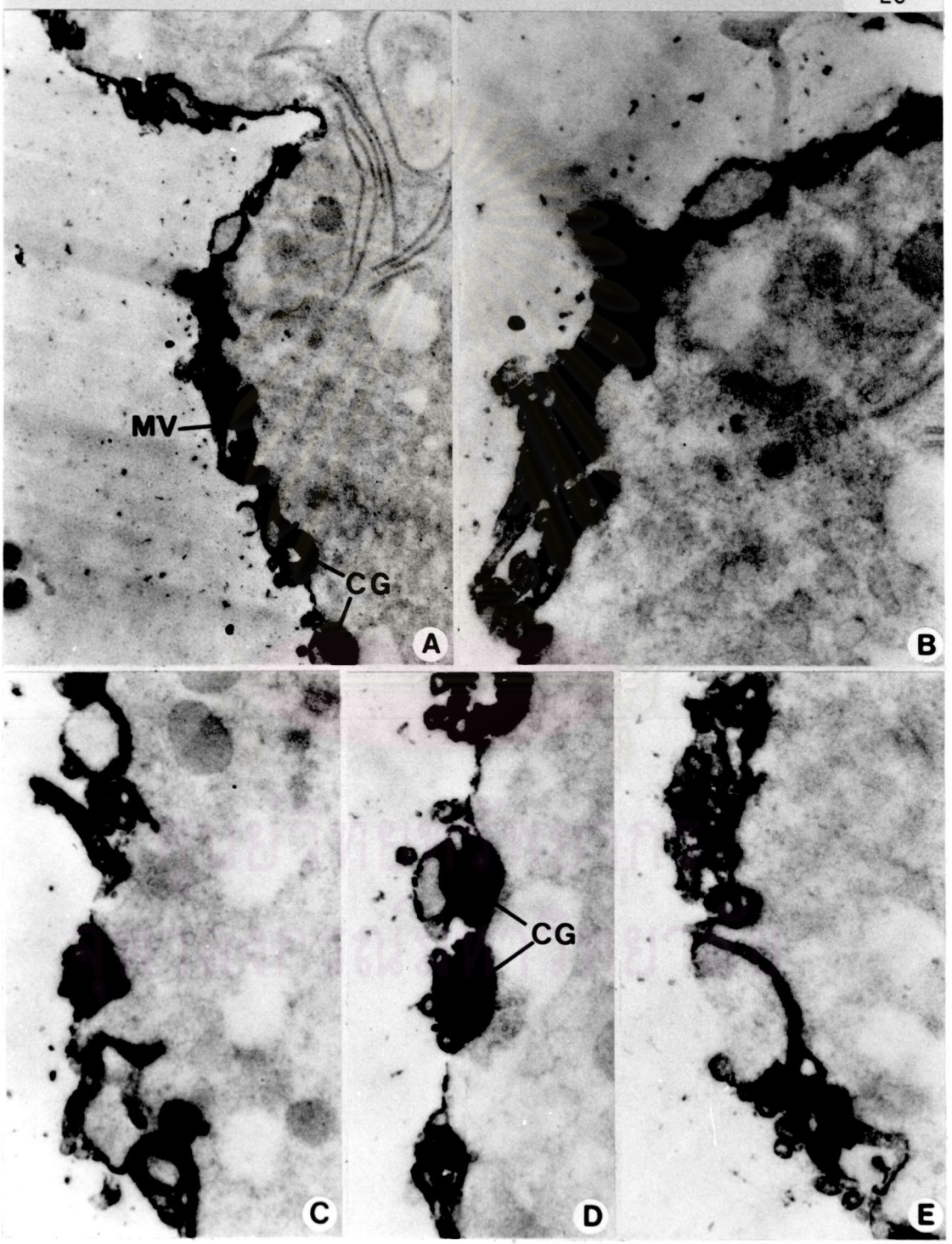

Figure 27 (A-E) Two-cell embryo, showing the uniform distribution of reaction products on both microvilli and plasma membrane. The intensity of staining was decreased when compared to one-cell embryos.
A, X 12,000; B, X 18,000; C, X 18,000; D, X 18,000; E, X 24,000.

Figure 27

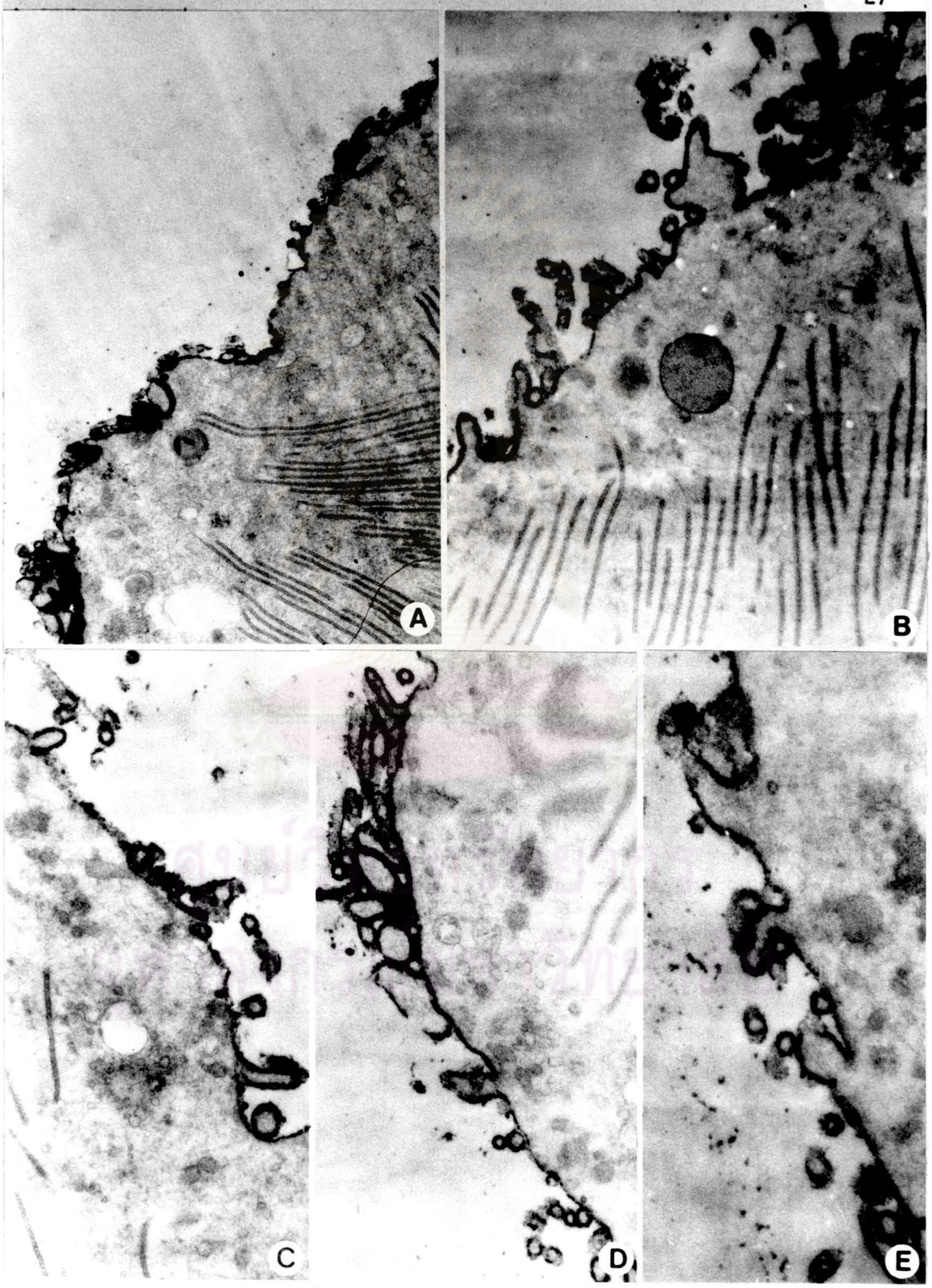

Figure 28 (A-D) Four-cell embryos, showing the uniform distribution of reaction products or both microvilli and plasma membrane. A, X 24,000; B, X 24,000; C, X 24,000; D, X 24,000.

Figure 28

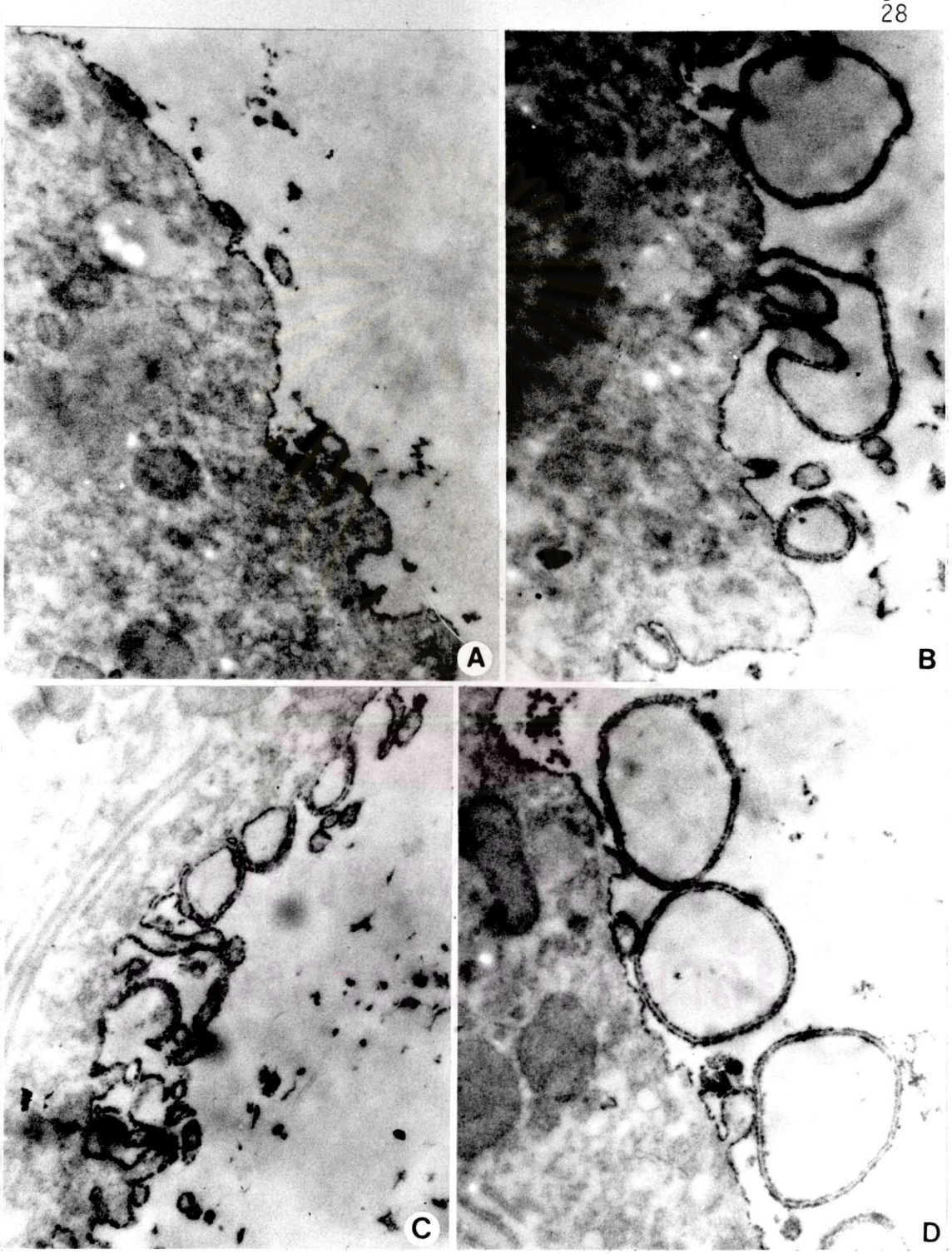

Figure 29 (A-E) Blastocysts, showing the uniform distribution of reaction products on both microvilli and plasma membrane.
A, X 12,000; B, X 24,000; C, X 24,000; D, X 24,000;
E, X 24,000.

Figure 29

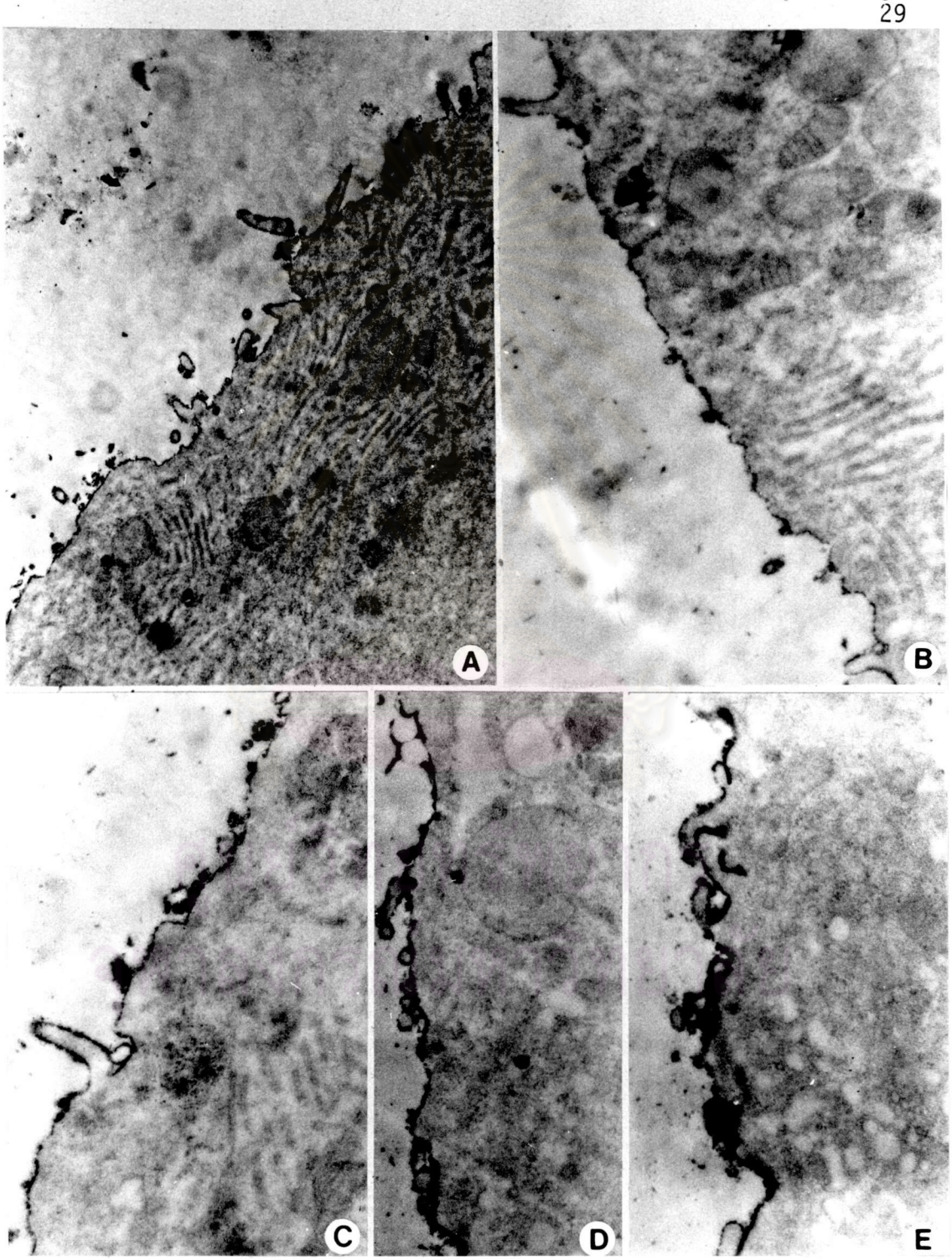

Figure 30-33 TEM micrographs of the surface of preimplantation embryos exposed to WGA-HRP+DAB+H_2O_2.

Figure 30 One-cell embryos, showing the reaction products were uniformly distributed on both microvilli and plasma membrane (A-E). The reaction product was also found on polar body (F). A, X 12,000; B, X 18,000; C, X 18,000; D, X 24,000; E, X 24,000; F, X 24,000.

Figure 30

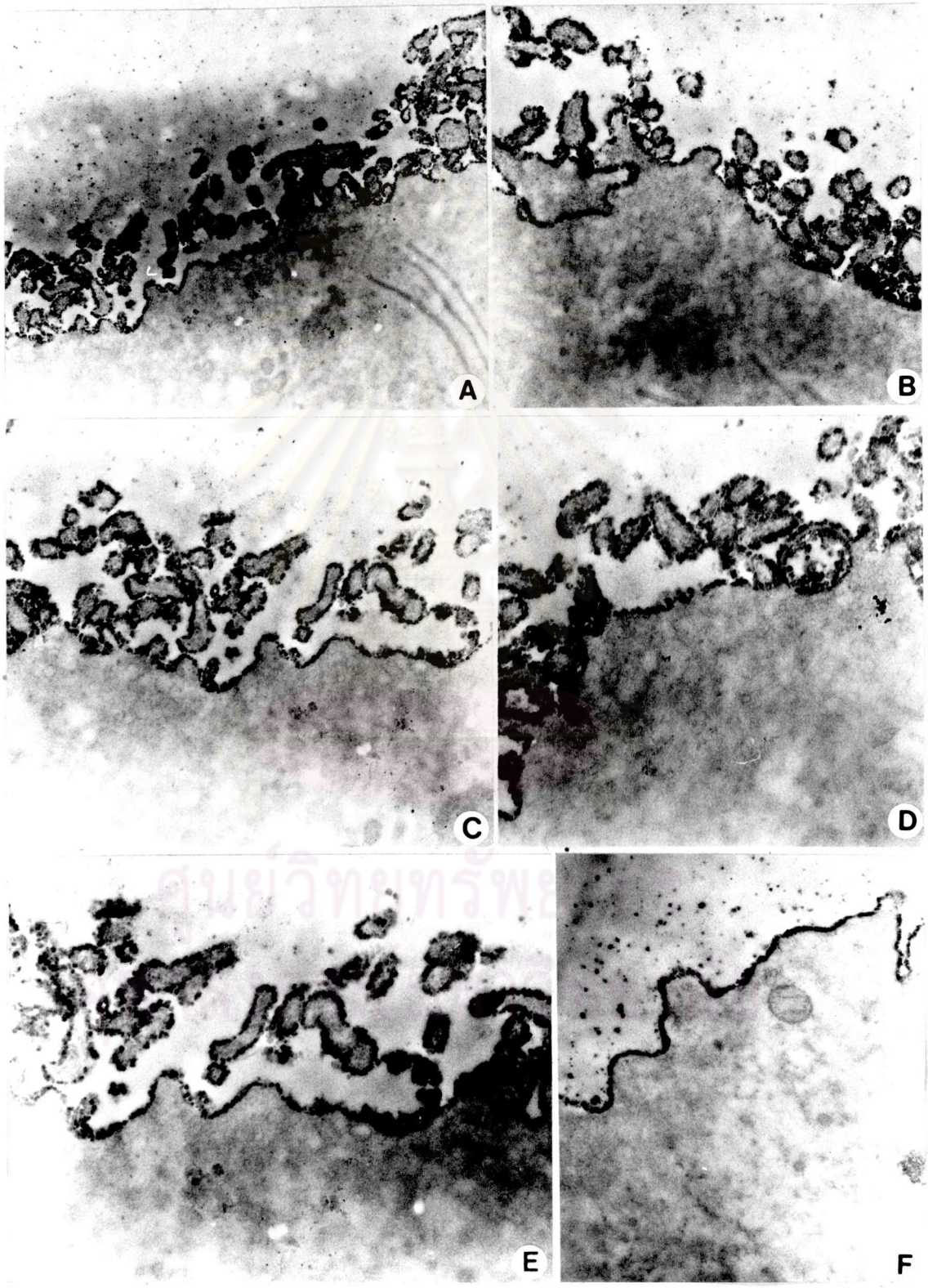

Figure 31 (A-E) Two-cell embryos, showing the high intensity of reaction products. They were uniformly distributed on both microvilli and plasma membrane. A, X 18,000; B, X 18,000; C, X 24,000; D, X 18,000; E, X 18,000.

Figure 31

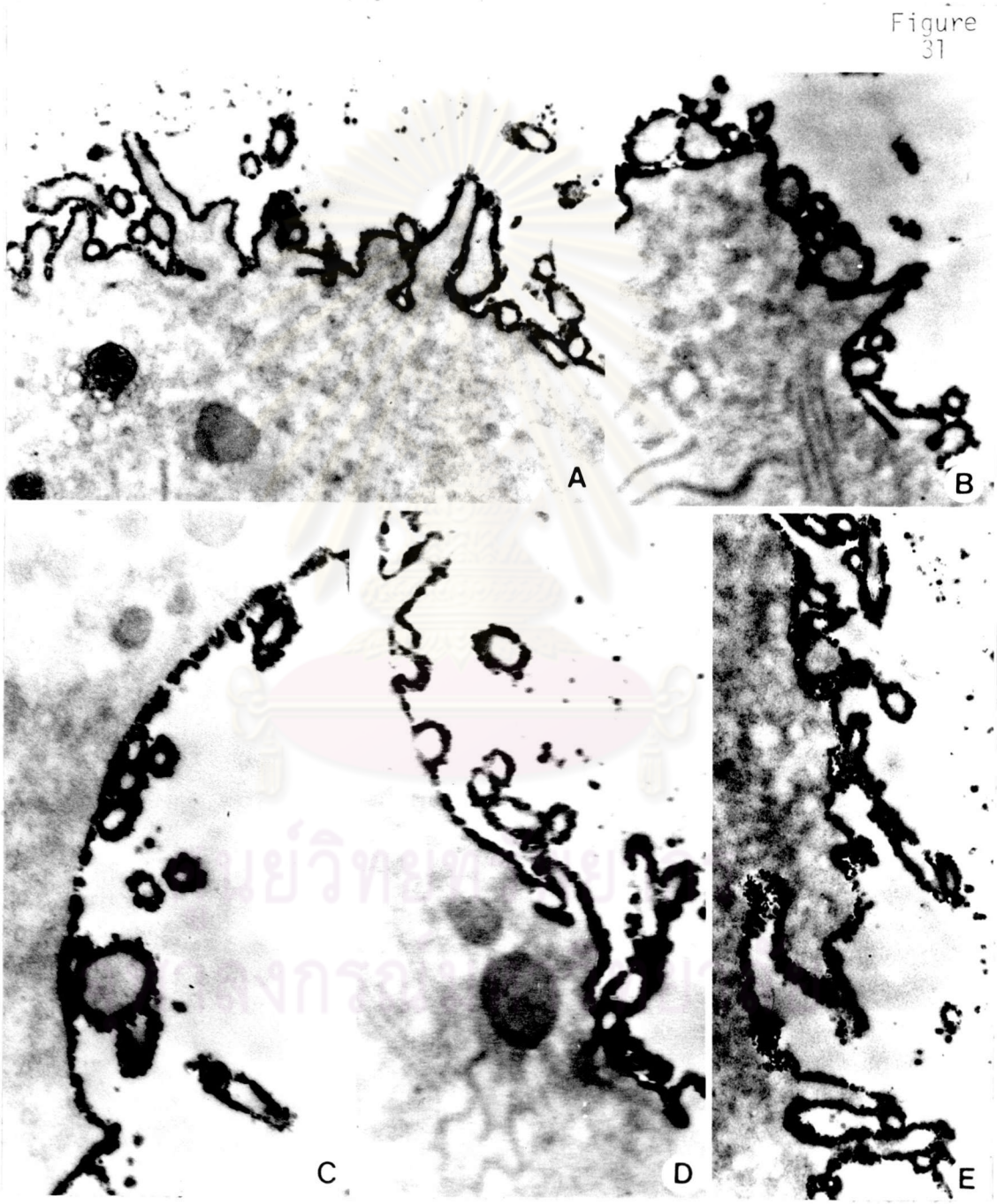

Figure 32 (A-D) Four-cell embryos, showing the uniform distribution of reaction products on both microvilli and plasma membrane. A, X 18,000; B, X 18,000; C, X 24,000; D, X 24,000.

Figure 32

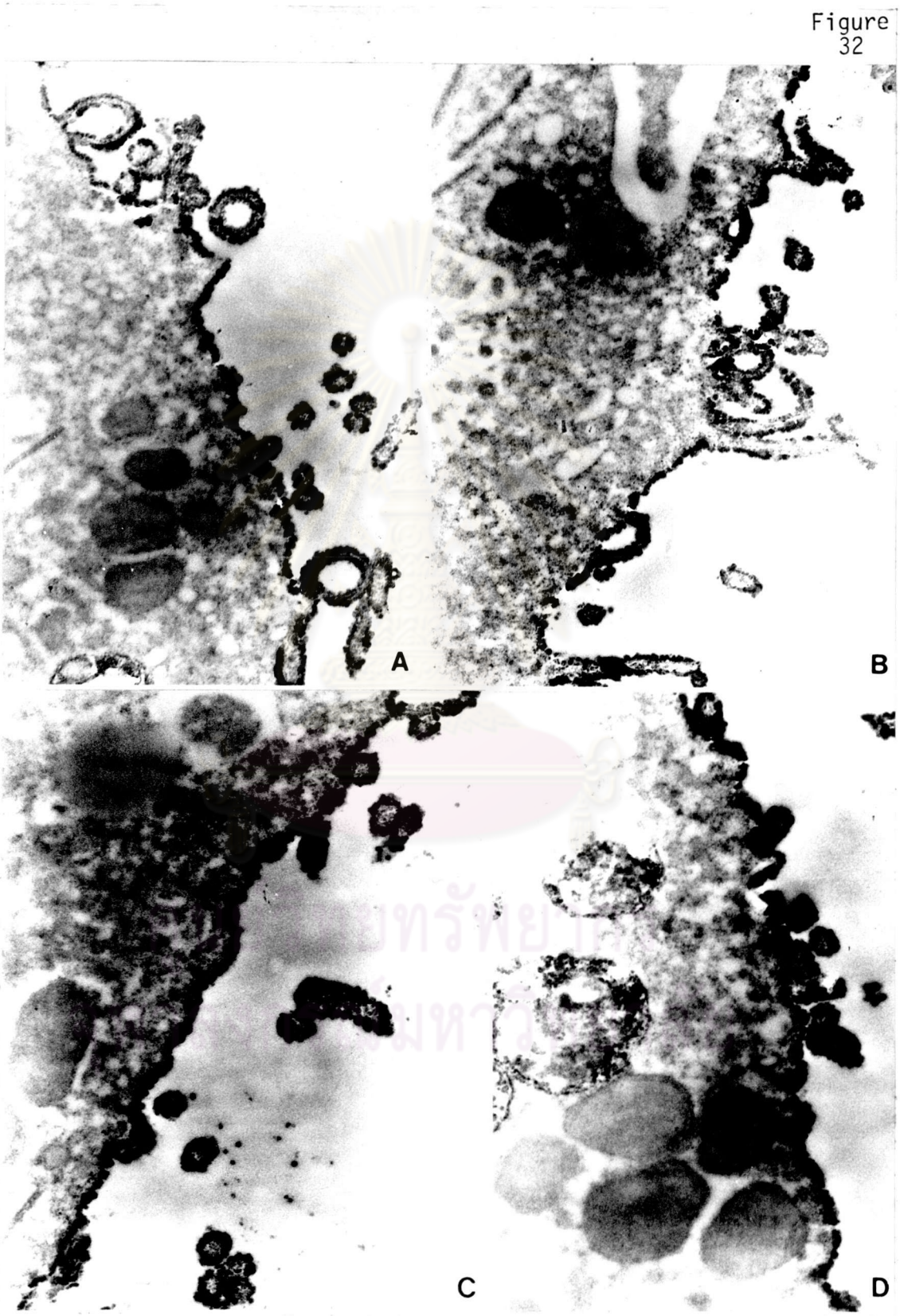

Figure 33 (A-D) Blastocyst, showing the uniform distribution of reaction products on both microvilli and plasma membrane. The intensity of staining was very intense when compared to the previous stage. E = embryo. A, X 18,000; B, X 18,000; C, X 24,000; D, X 24,000.

Figure 33

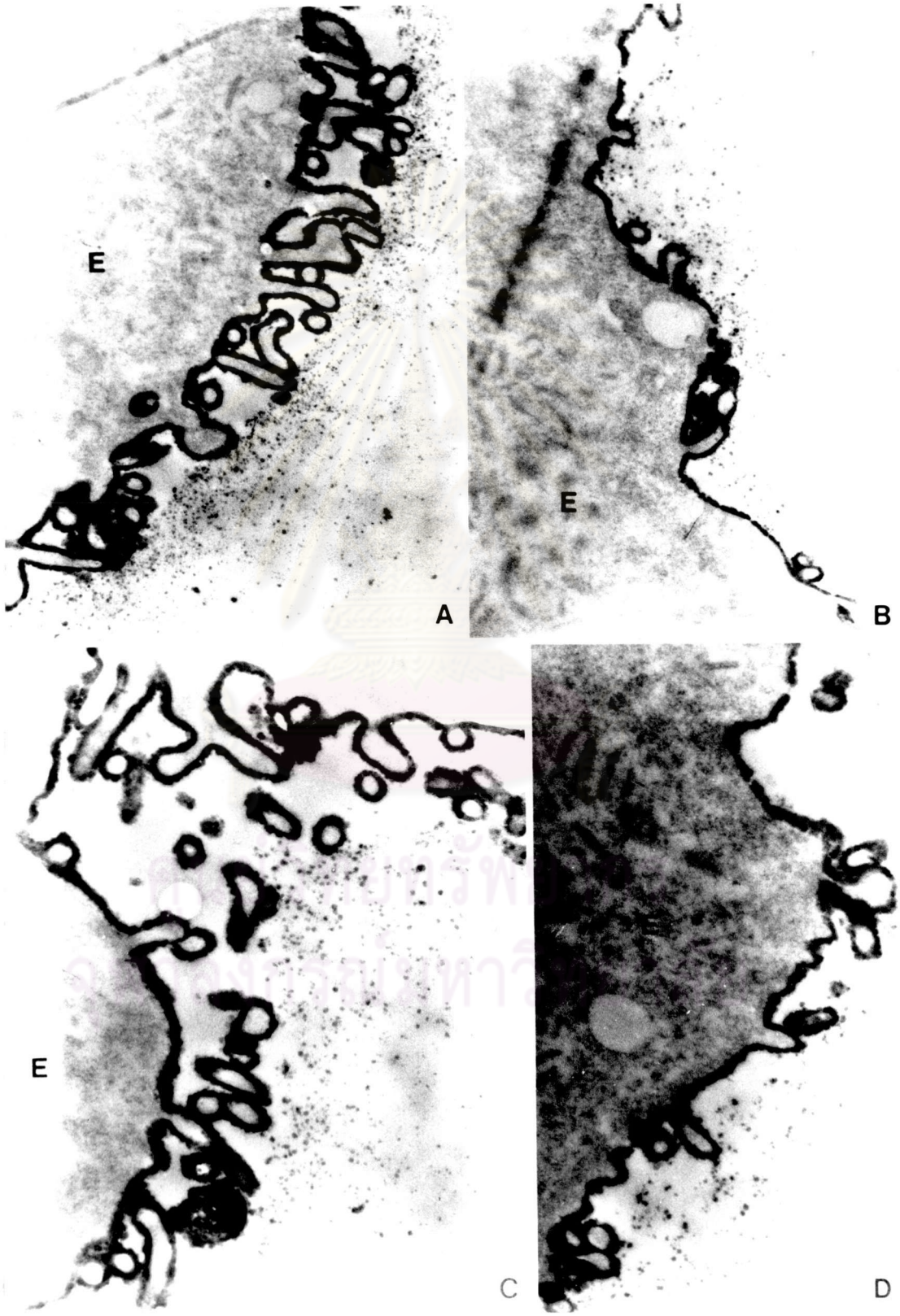

Figure 35 (A-D) Two-cell embryos, showing the uniform distribution of intense reaction products on both microvilli and plasma membrane. A, X 24,000; B, X 24,000; C, X 24,000; D, X 24,000.

Figure 35

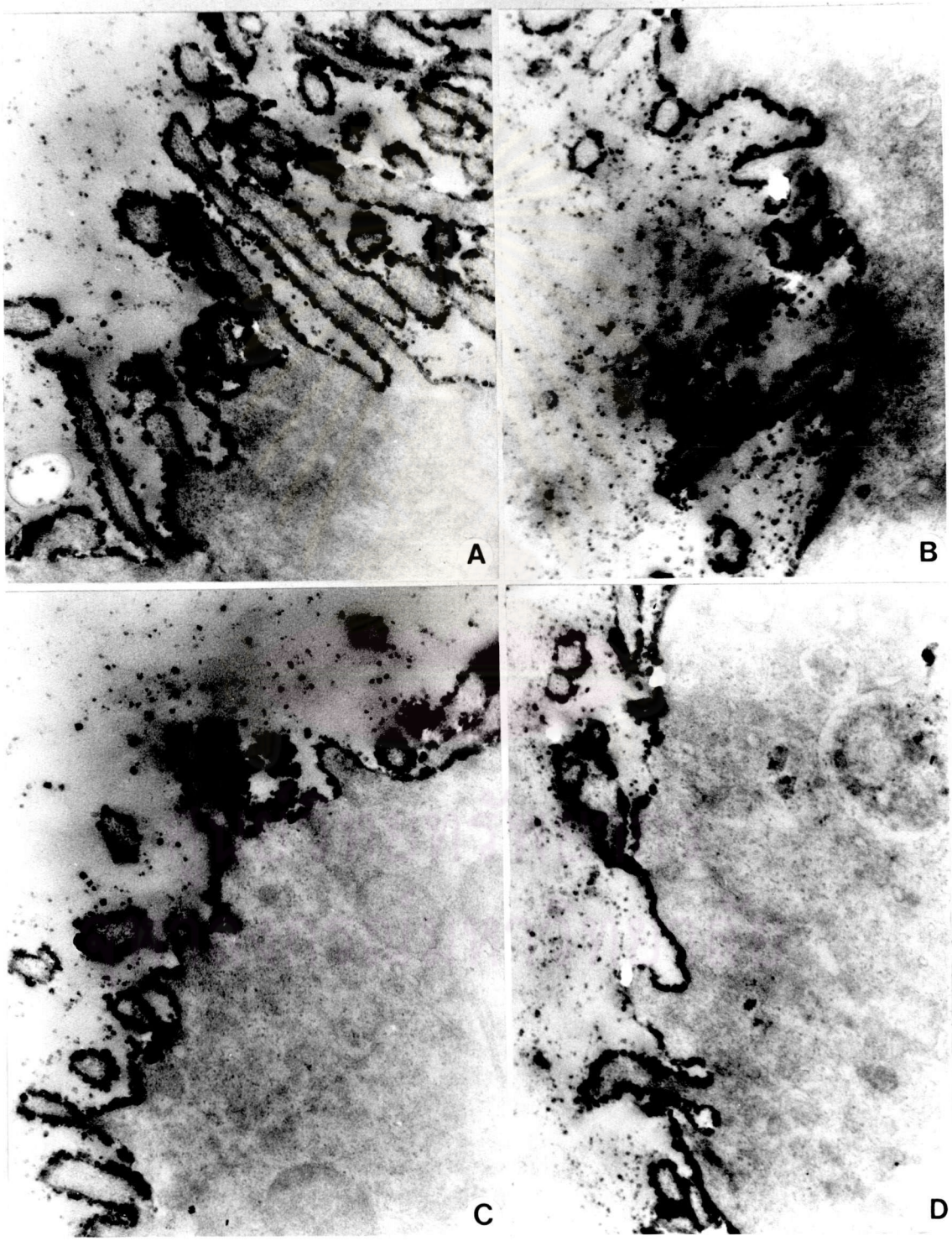

Figure 36 (A-F) Four-cell embryos, showing the uniform distribution and intense reaction products on both microvilli and plasma membrane. A, X 18,000; B, X 18,000; C, X 24,000; D, X 24,000; E, X 36,000; F, X 36,000.

Figure 36

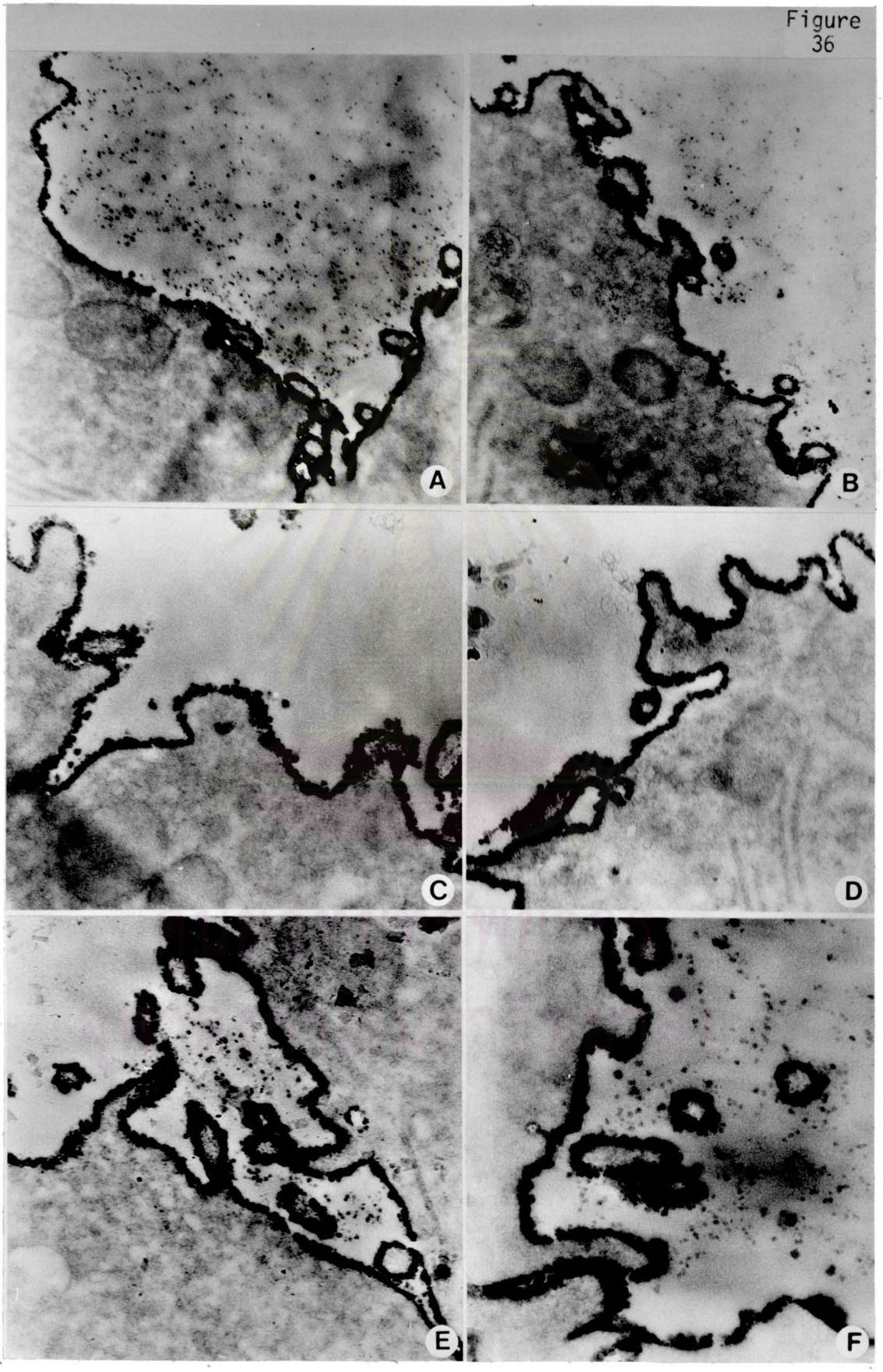

Figure 37 (A-E) Blastocyst, showing the uniform distribution of intense reaction products on both microvilli and plasma membrane. A, X 18,000; B, X 18,000; C, X 24,000; D, X 24,000; E, X 24,000.

Figure 37

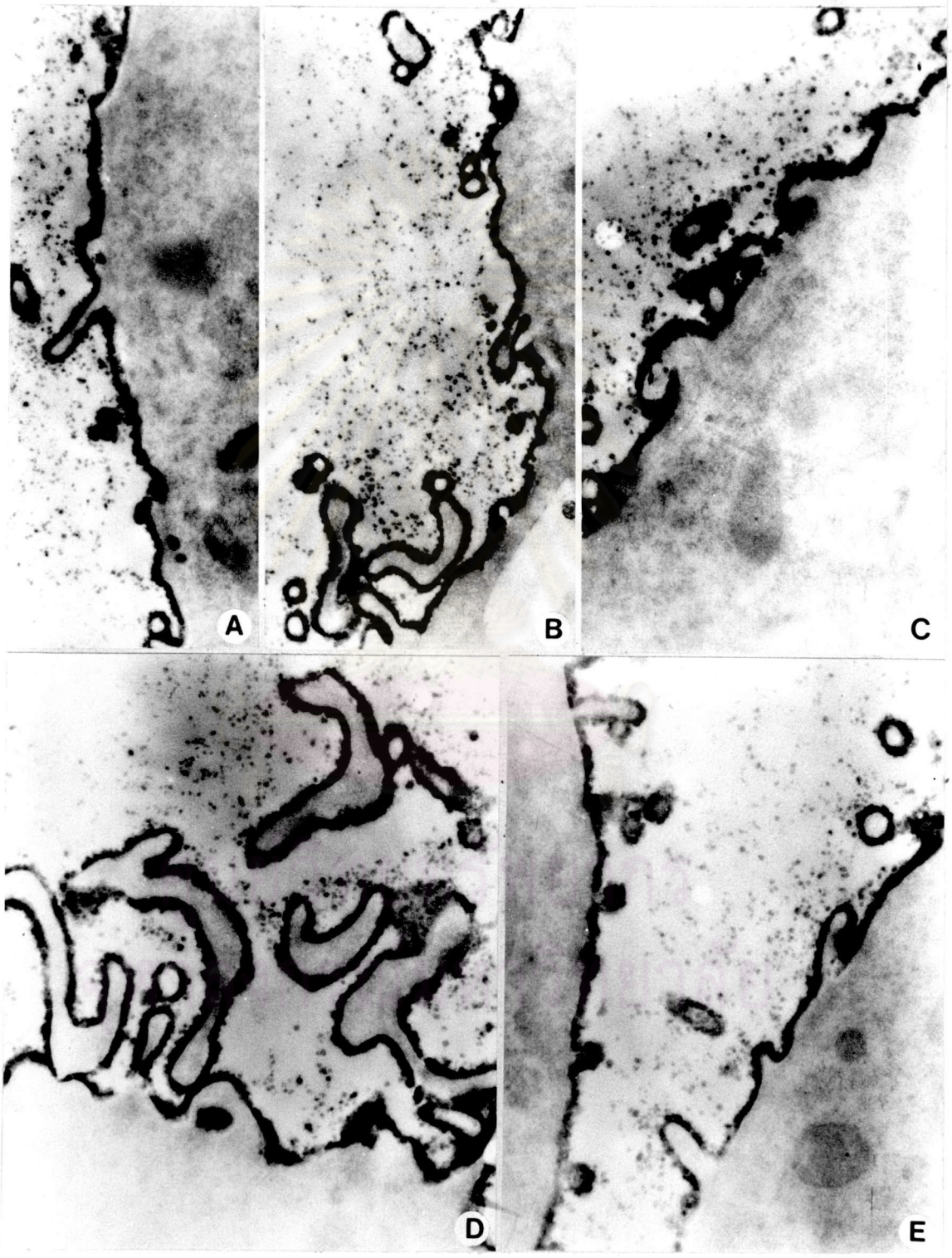

Figure 38 TEM micrographs of control groups of preimplantation embryos that were exposed to HRP + DAB + H_2O_2. No reaction product was observed on both microvilli and plasma membrane of 1-cell (A), 2-cell (B), 4-cell (C) embryos and blastocyst (D). A, X 18,000; B, 18,000; C, X 18,000; D, X 18,000.

Figure 38

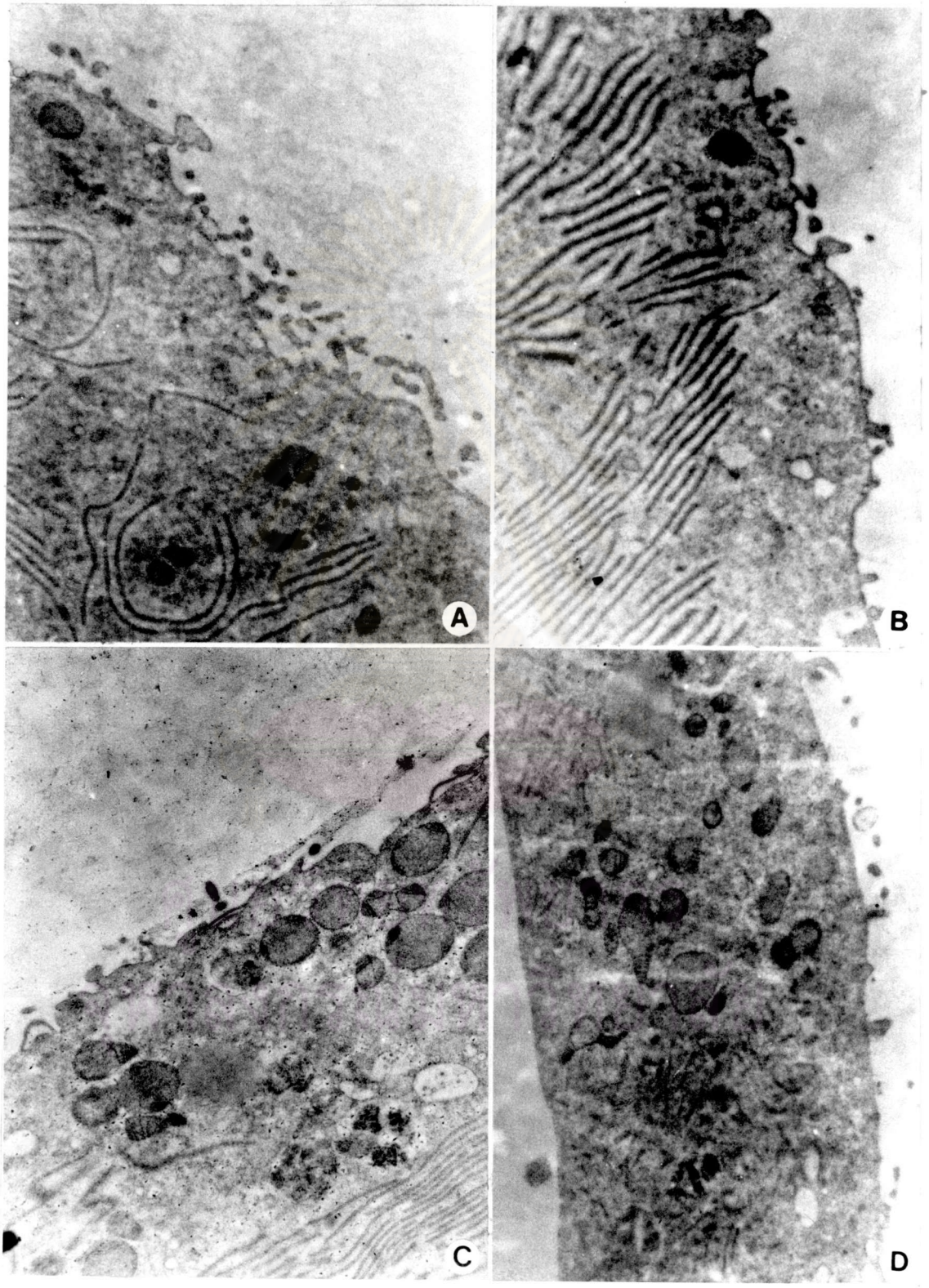

3.4.4 Control groups

Embryos were fixed in glutaraldehyde and subsequently incubated with HRP and DAB + H_2O without prior incubation with lectins. No reaction product was found on both the embryonic microvilli and plasma membrane of 1-, 2- and 4-cell embryos and blastocysts (Figure 38 : A, B, C, D).

3.5 Binding of lectins to uterine epithelium

3.5.1 Binding of Con A

D_1- to D_4- uteri were fixed with glutaraldehyde and sequentially labelled with Con A, HRP and DAB + H_2O_2. Reaction products found in D_1- and D_3-uteri were uniformly distributed on both microvilli and plasma membrane of the lining epithelial cells (Figures 39; 40). The staining intensity on D_1-uterus was not strong compared with that of D_2-,D_3- and D_4-uteri. The distribution of reaction product in D_2-uterus was not uniform and the stain appeared as patches on the plasma membrane (Figure 40 : A, B, D). Likewise, the uterine epithelium of D_4-uterus showed similar pattern of patchy stain (Figure 42 : D, F, G). The staining intensity of Con A in D_2-, D_3- and D_4-uteri was fairly strong and showed similar pattern. (Figures 40, 41, 42).

3.5.2 Binding of WGA

D_1- to D_4-uteri were fixed with glutaraldehyde and sequentially labelled with WGA-HRP and DAB + H_2O_2. Reaction products were found on the entire surface of both plasma membrane and microvilli of D_1- to D_4-uterine epithelia (Figures 43, 44, 45, 46). The distribution of reaction products was uniform on the plasma membrane of uterine epithelia. They appeared on the microvillus membrane like what appeared to be the bristles of glycocalyx projecting perpendicularly

out of the membrane (Figure 43 : B, C, D, E; Figure 44 : A, D, E, F; Figure 45 : A, G, H). The latter implies the thickness of glycocalyx containing WGA receptors on the luminal surface membrane as such, the glycocalyx coat of D_1-, D_2- and D_3-uteri appeared rather thick, and the thickness was much lesser reduced in D_4-uterus (Figure 46). The intensity of the stain was very strong in D_1-, D_2- and D_3-uteri and appeared to decrease in D_4-uterus.

3.5.3 Binding of RCA_1

D_1- to D_4-uteri were fixed with glutaraldehyde and sequentially labelled with RCA_1-HRP and DAB + H_2O_2. It was found that the glycocalyx of the membrane on the luminal surface of D_1, D_2 and D_4 uterine epithelia contained abundant of RCA_1 binding sites (Figures 47, 48, 49). The distribution of the reaction product was quite uniform in all stages with little staining on the glycocalyx bristles in comparison to WGA. The product was abundant in uterine epithelium of D_1 and gradually decreased in D_2 and D_3. The dramatic reduction of the product was observed in D_4-uterine epithelium (Figure 50) which appeared to locate close to both the apical plasma membrane and microvilli.

3.5.4 Control groups

D_1- to D_4-uteri were fixed with glutaraldehyde and subsequently incubated in HRP and DAB + H_2O_2 without prior incubation with lectins. No reaction product was found on the apical surface membrane and microvilli of these uteri (Figure 51).

Figure 39-42 TEM micrographs of the surface of uterine epithelium during preimplantation period that was exposed to Con A + HRP + DAB + H_2O_2.

Figure 39 (A-D) D_1-uteri, showing the uniform distribution of small reaction products on both microvilli (MV) and plasma membrane. A, X 12,000; B, X 24,000; C, X 36,000; D, X 36,000.

Figure 39

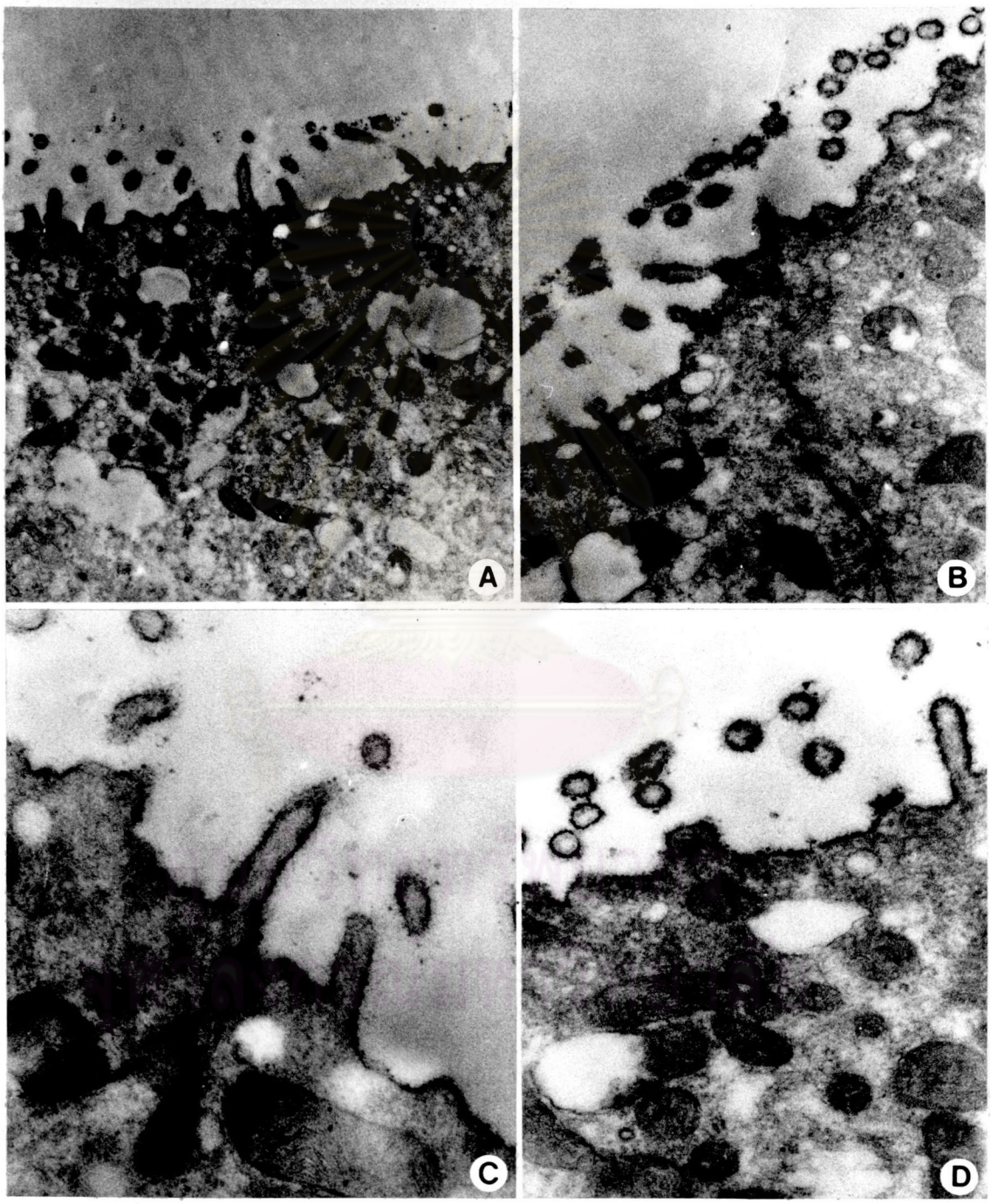

Figure 40 (A-E) D_2-uteri, showing the distribution of reaction products on microvilli and plasma membrane. The clumping of reaction products were observed on plasma membrane (arrow heads). A, X 12,000; B, X 12,000; C, X 24,000, D, X 24,000; E, X 36,000.

Figure 40

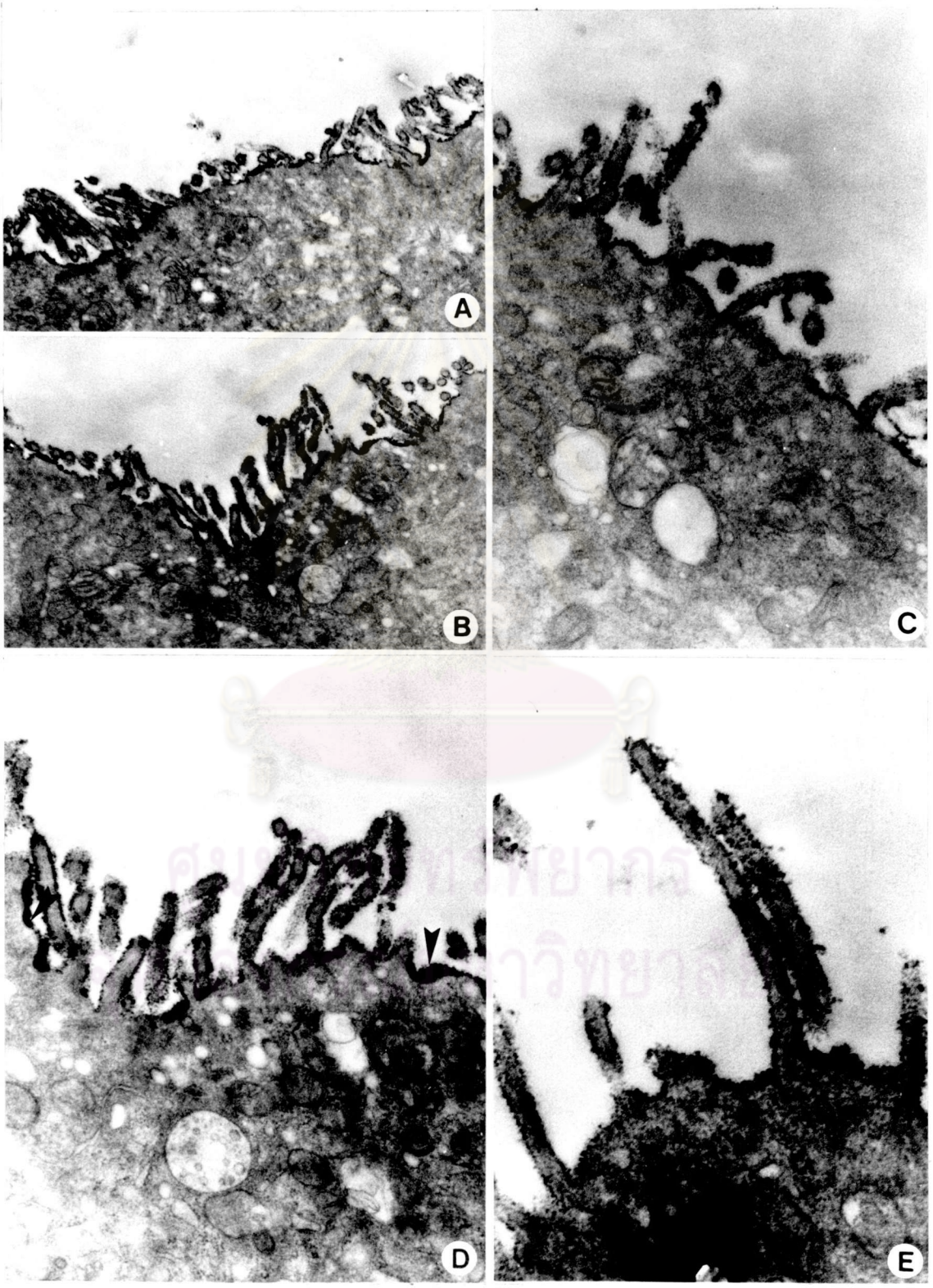

Figure 41 (A-F) D_3-uteri, showing the uniform distribution of reaction products on both microvilli and plasma membrane.

A, X 12,000; B, X 12,000; C, X 24,000; D, X 24,000; E, X 36,000; F, X 36,000.

Figure 41

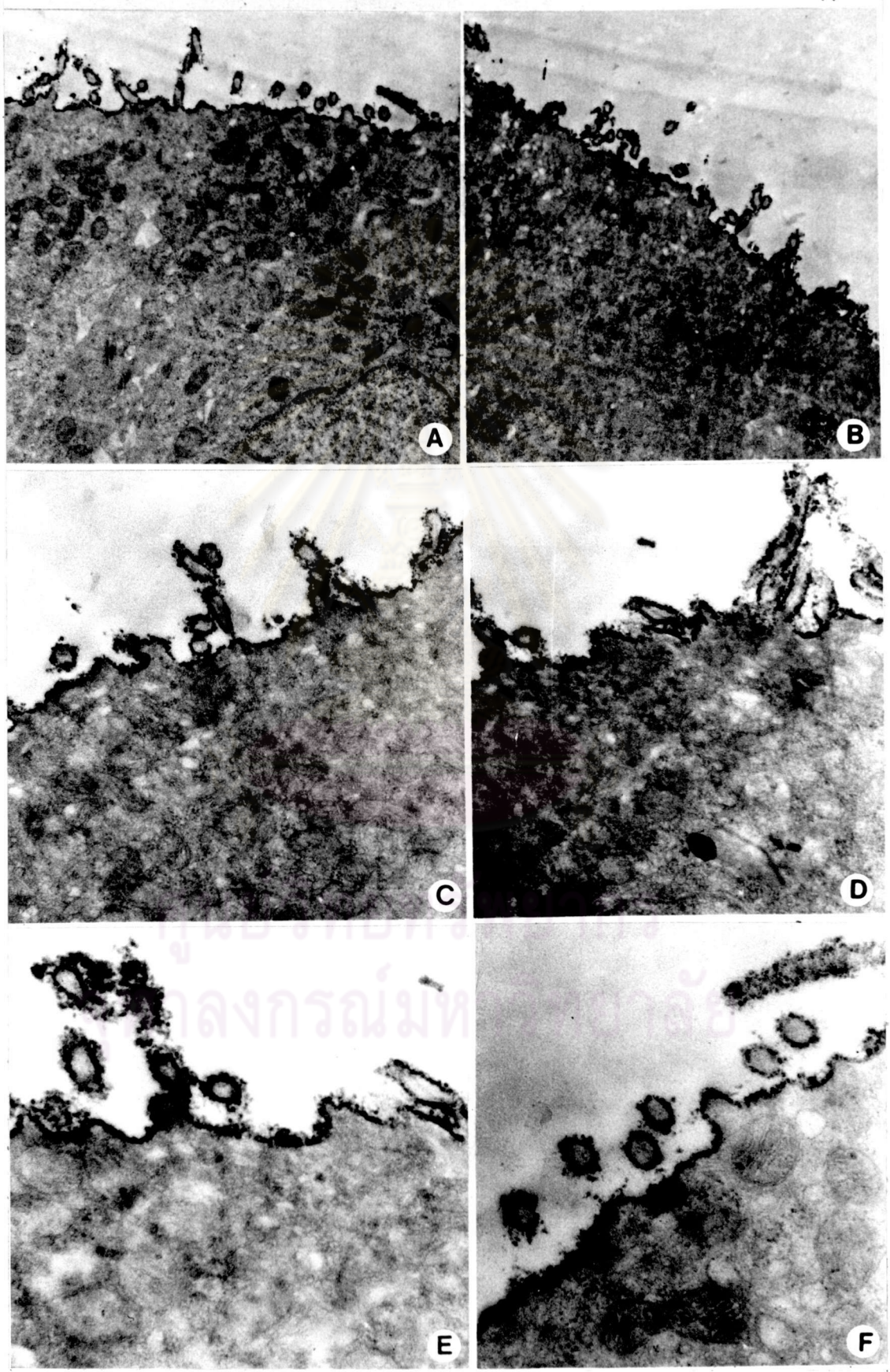

Figure 42 D_4-uteri, showing the distribution of reaction products on microvilli and plasma membrane. The rupture of plasma membrane was observed (arrow head in C) and the clumping of reaction product was also found (arrow head in F). A, X 12,000; B, X 12,000; C, X 24,000; D, X 24,000; E, X 24,000; F, X 24,000; G, X 24,000.

Figure 42

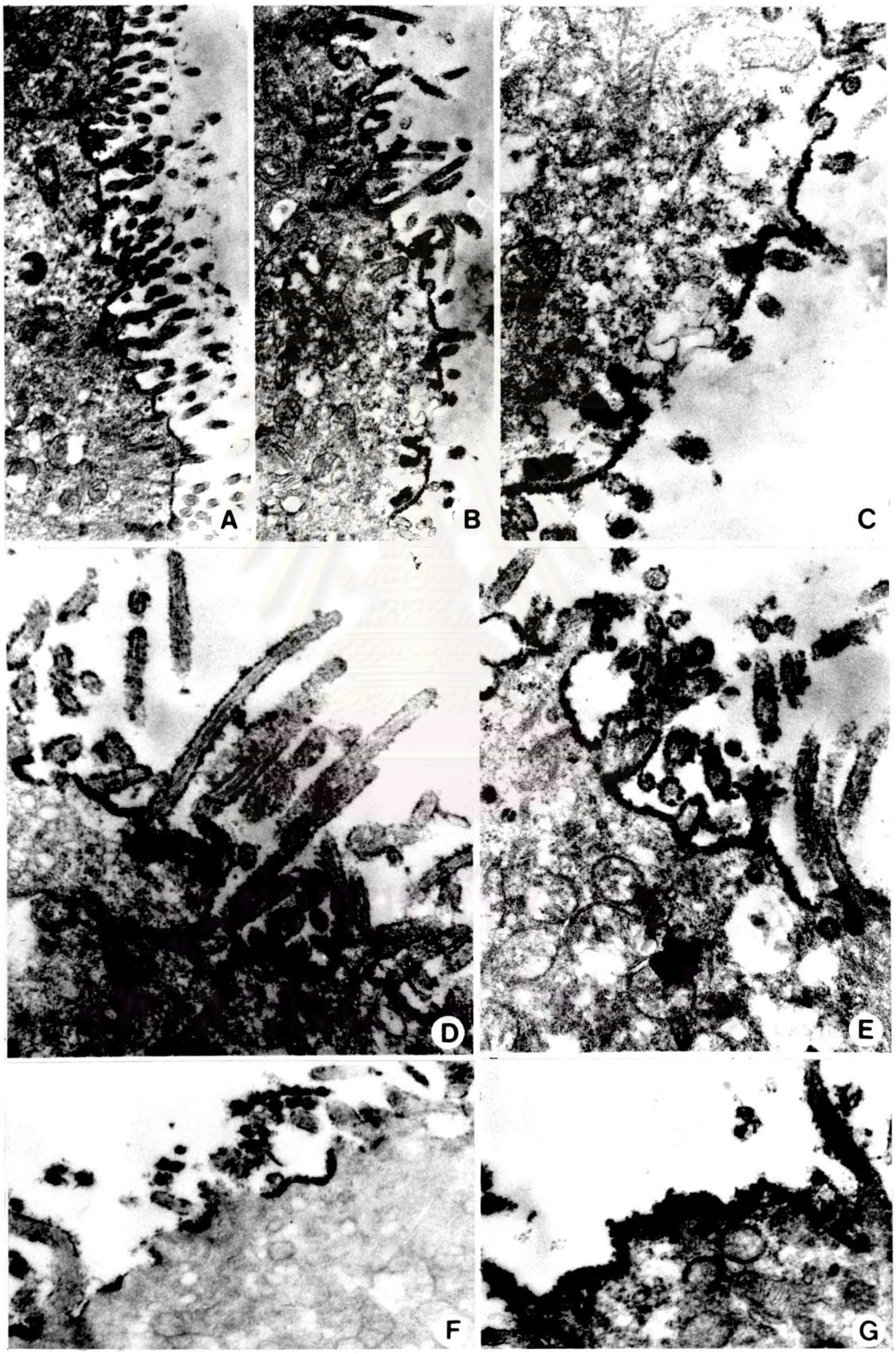

Figure 43-46 TEM micrographs of the surface of uterine epithelium during preimplantation period exposed to WGA - HRP + DAB + H_2O_2 respectively.

Figure 43 D_1-uteri, showing the distribution of reaction products on microvilli and plasma membrane. The reaction products were rather intense (arrow heads) around microvillous area. A, X 12,000; B, X 12,000; C. X 18,000; D, X 24,000; E, X 24,000; F, X 24,000.

Figure
43

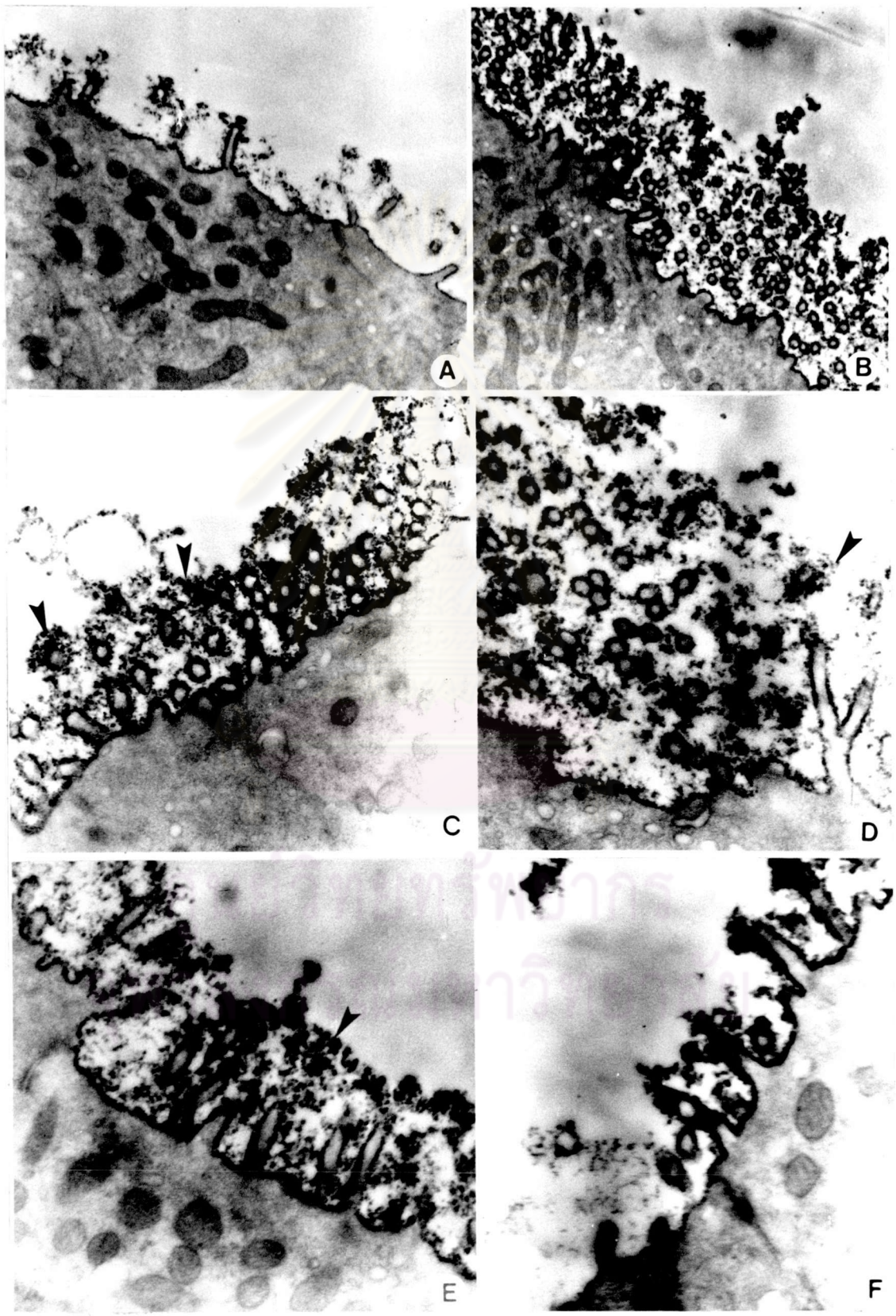

Figure 44 (A-F) D_2-uteri, showing the distribution of reaction products on both microvilli (black arrow heads) and plasma membrane (white arrow heads). The reaction products were very intense around microvillous area. (D, E, F). A, X 12,000; B, X 12,000; C, X 24,000; D, X 24,000; E, X 24,000; F, X 24,000.

Figure
44

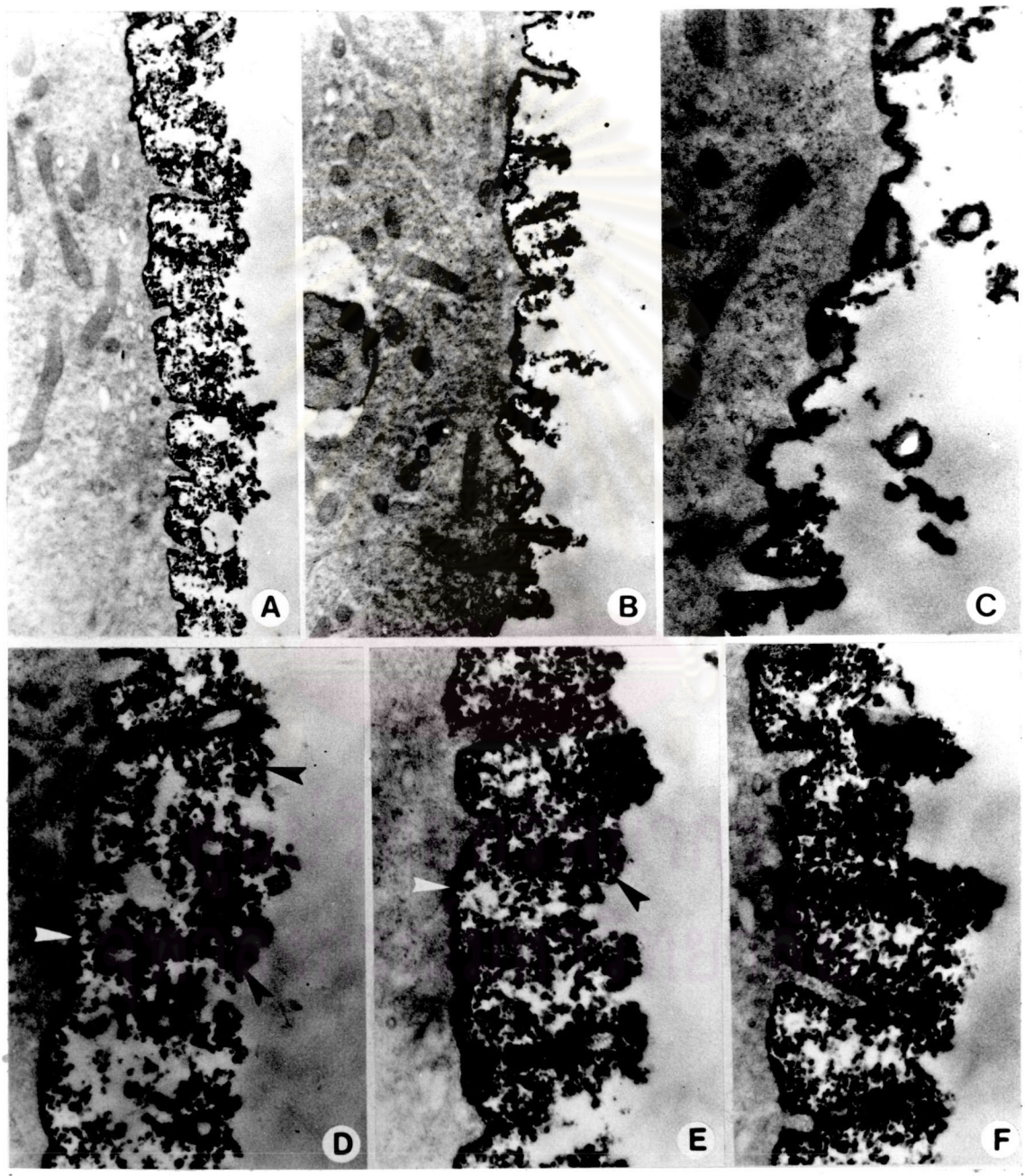

Figure 45 (A-I) D_3-uteri, showing the distribution of intense reaction products on both microvilli and plasma membrane.

A, X 12,000; B, X 18,000; C, X 18,000; D, X 24,000; E, X 24,000; F, X 24,000; G, X 24,000; H, X 24,000; I, X 24,000.

Figure 45

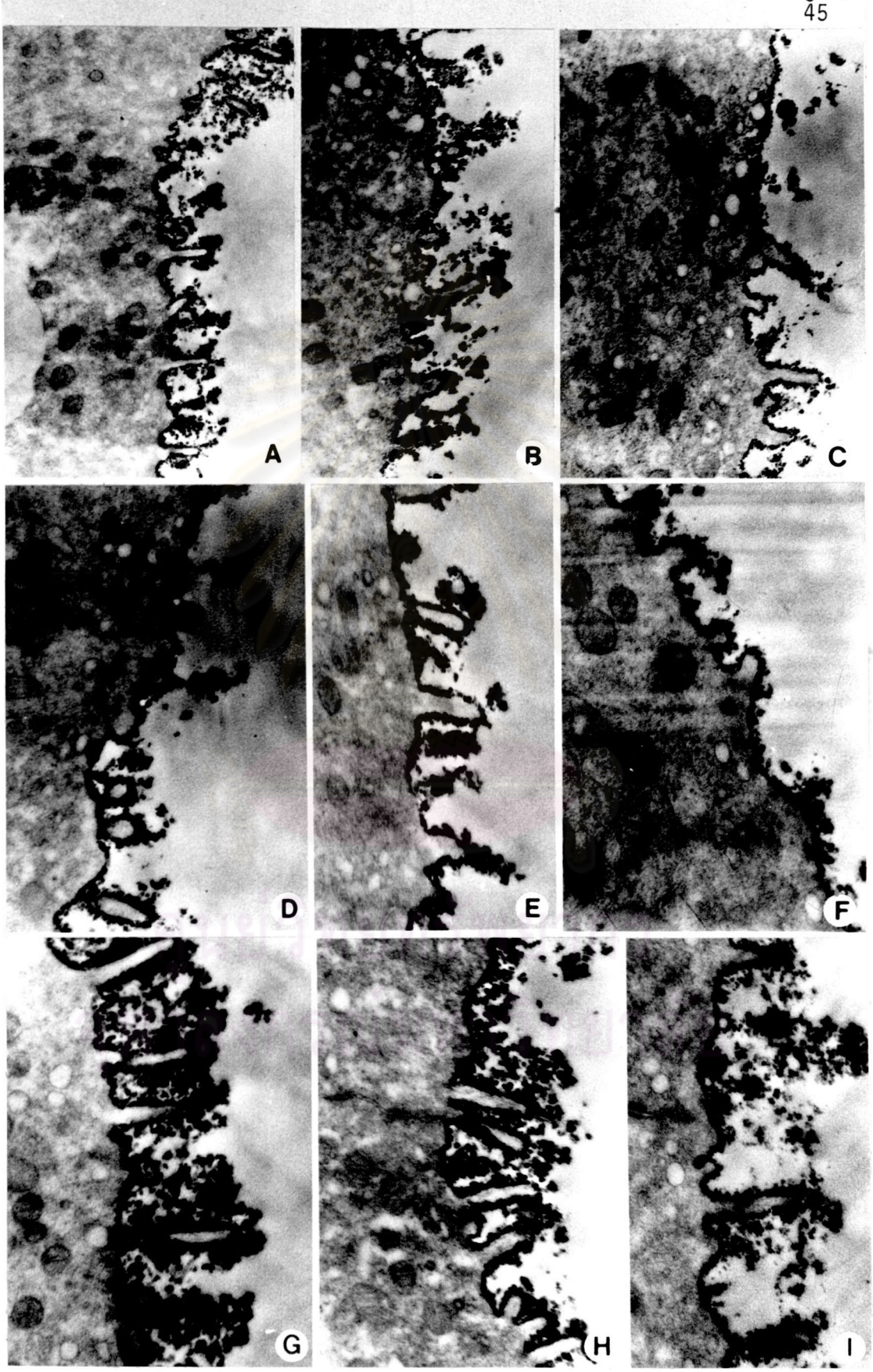

Figure 46 (A-F) D_4-uteri, showing the distribution of reaction products on both microvilli and plasma membrane. The intensity of stainign was less than in previous stage. A, X 12,000; B, X 12,000; C, X 12,000; D, X 24,000; E, X 24,000; F, X 24,000.

Figure 46

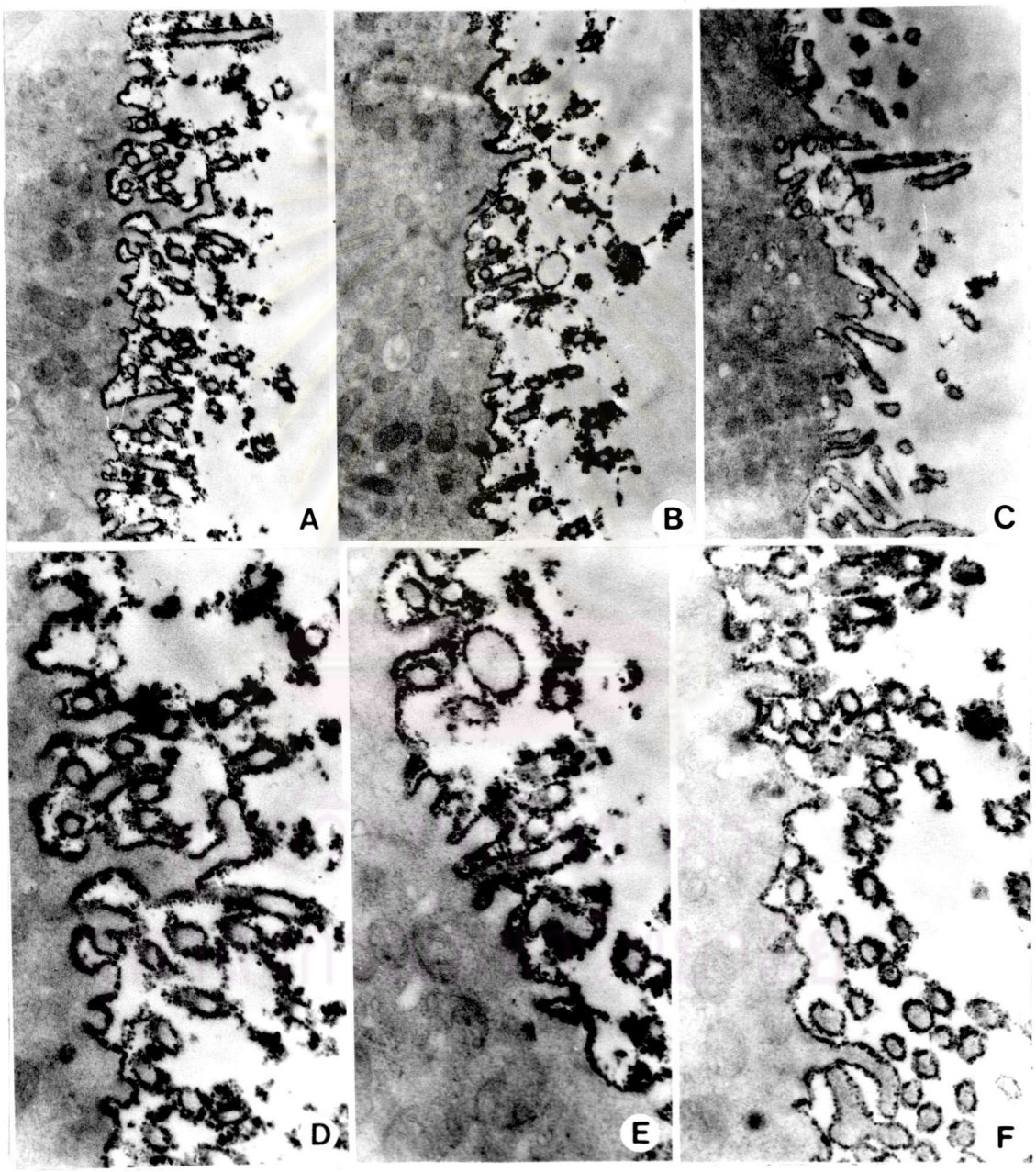

Figure 47-50 TEM micrographs of the surface of uterine epithelium during preimplantation period exposed to RCA - HRP + DAB + H_2O_2.

Figure 47 (A-G) D_1-uteri, showing the distribution of reaction products on both microvilli and plasma membrane. A, X 12,000; B, X 12,000; C, X 12,000; D, X 24,000; E, X 24,000; F, X 24,000; G, X 24,000.

Figure 47

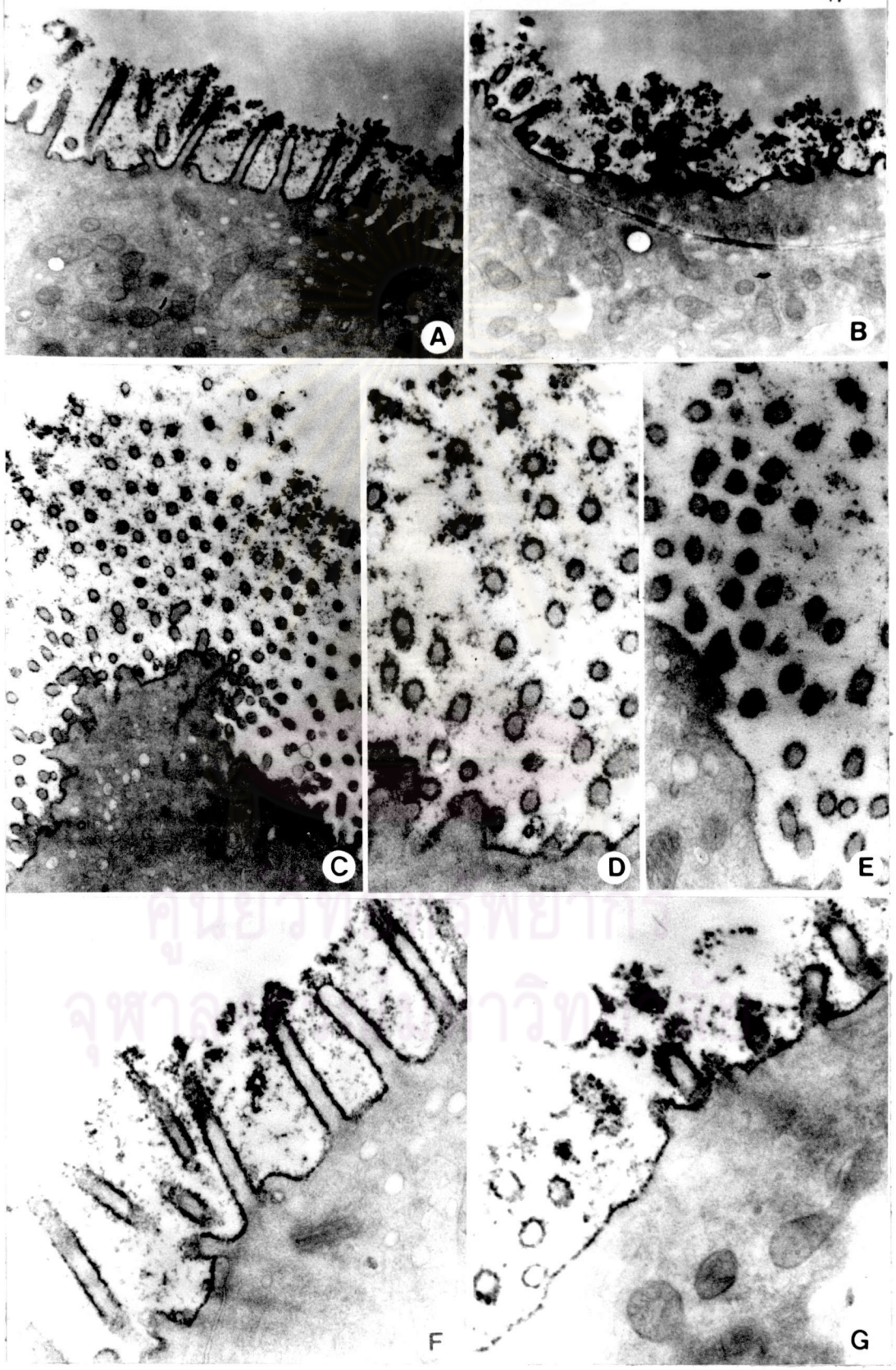

Figure 48 (A-F) D_2-uteri, showing the distribution of reaction products on both microvilli and plasma membrane. A, X 12,000; B, X 12,000; C, X 24,000; D, X 24,000; E, X 24,000; F, X 24,000.

Figure 48

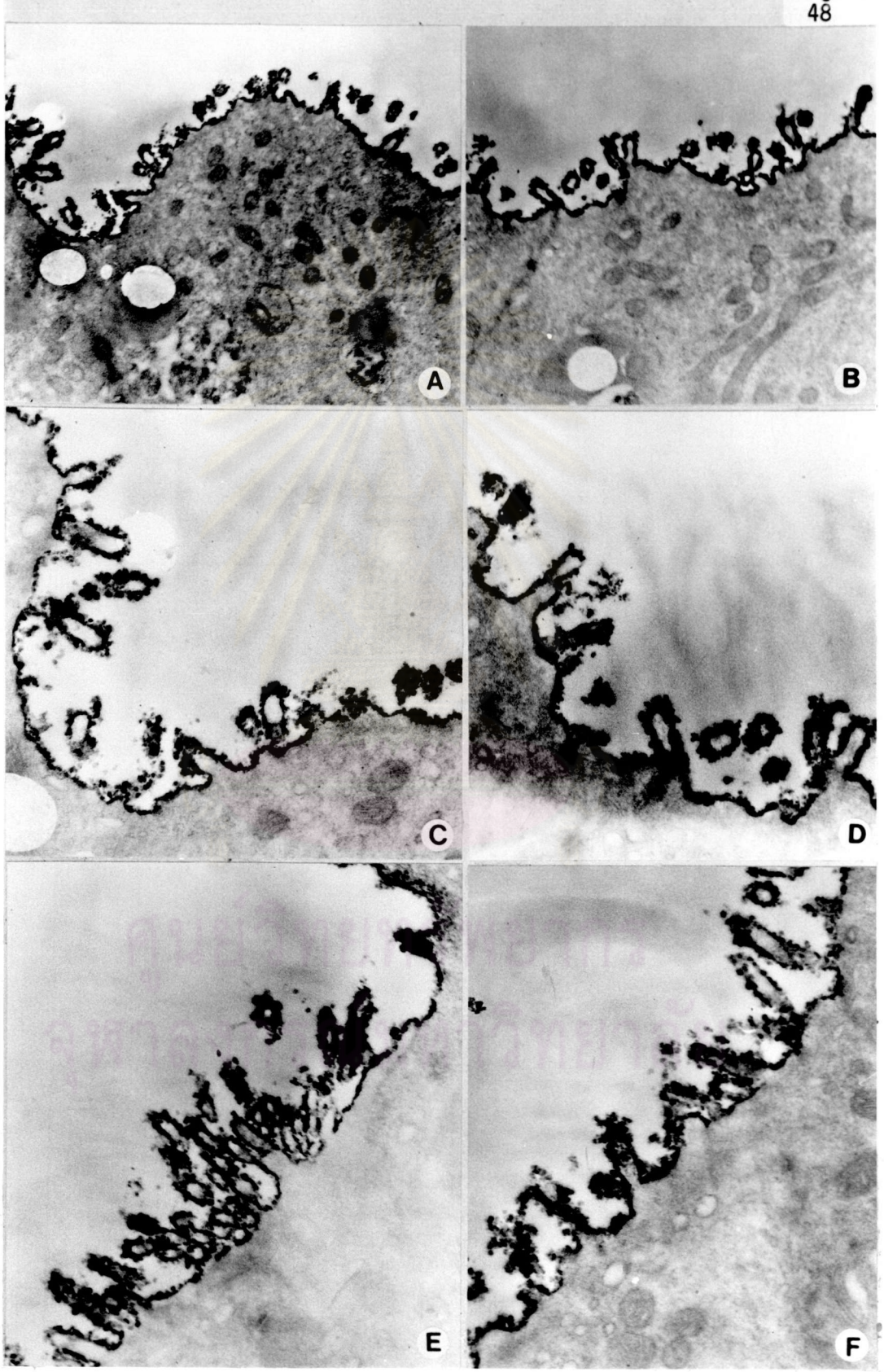

Figure 49 (A-F) D_3-uteri, showing the distribution of reaction products on both microvilli and plasma membrane. A, X 12,000; B, X 12,000; C, X 24,000; D, X 24,000; E, X 24,000; F, X 24,000.

Figure
49

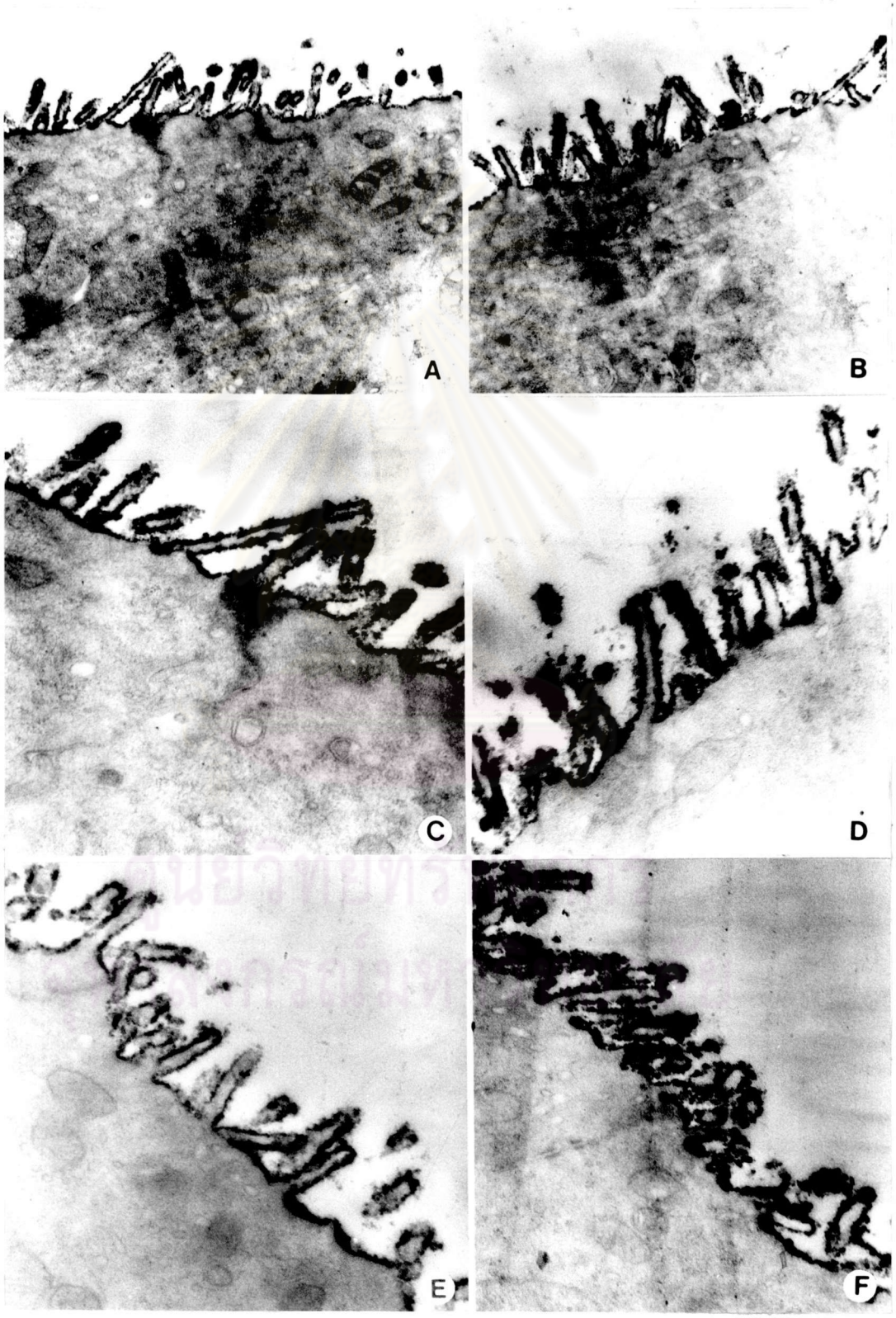

Figure 50 (A-G) D_4-uteri, showing the distribution of reaction product on both microvilli and plasma membrane. The intensity of staining was less than previous stage. A, X 12,000; B, X 12,000; C, X 12,000; D, X 24,000; E, X 24,000; F, X 24,000; G, X 24,000.

Figure 50

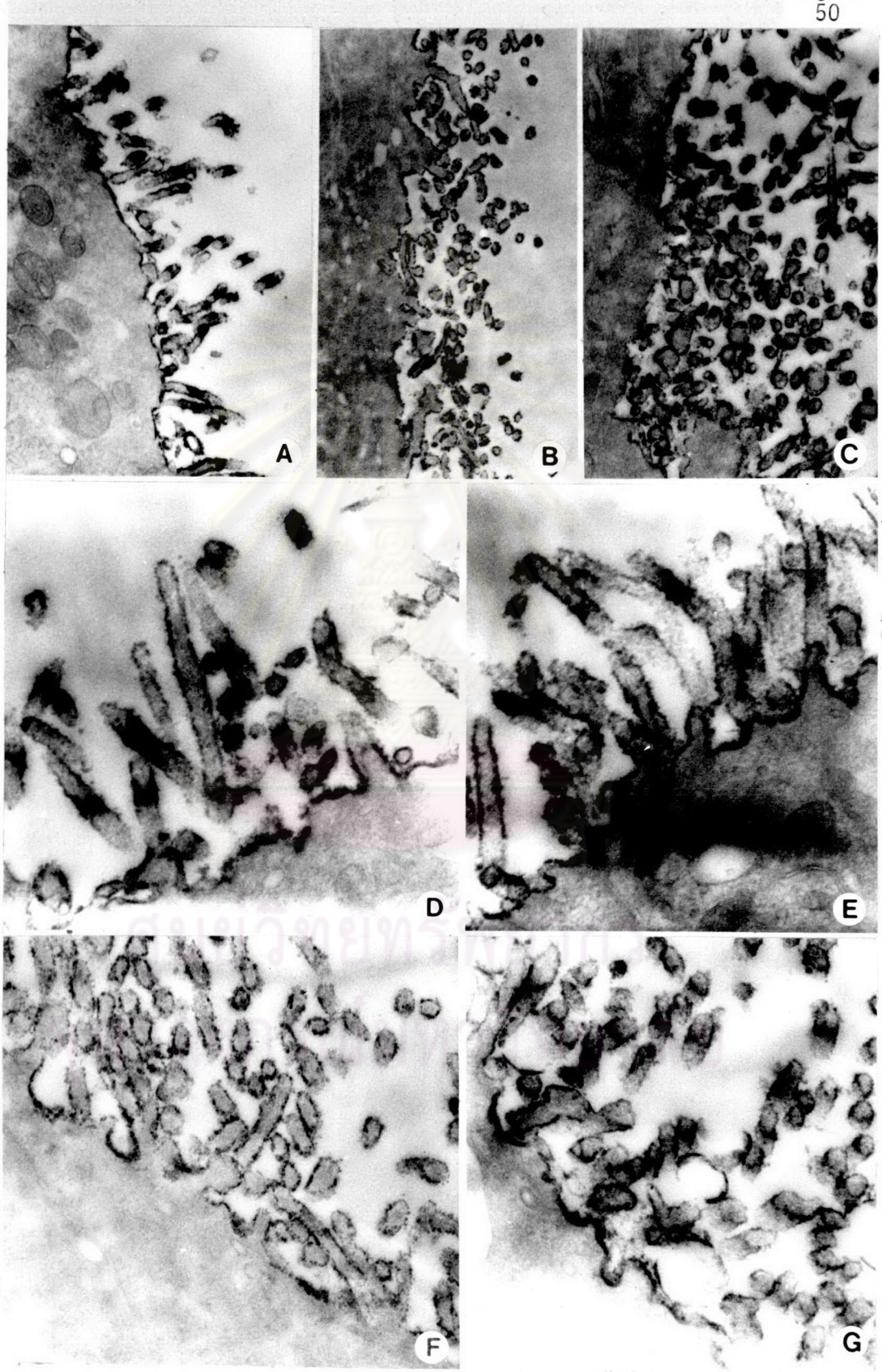

Figure 51 TEM micrographs of control uteri exposed to HRP + DAB + H_2O_2. No reaction product was observed on both microvilli and plasma membrane of D_1 - (A), D_2 - (B), D_3 - (C) and D_4 - uteri (D). A, X 12,000; B, X 12,000; C, X 12,000; D, X 12,000.

Figure 51

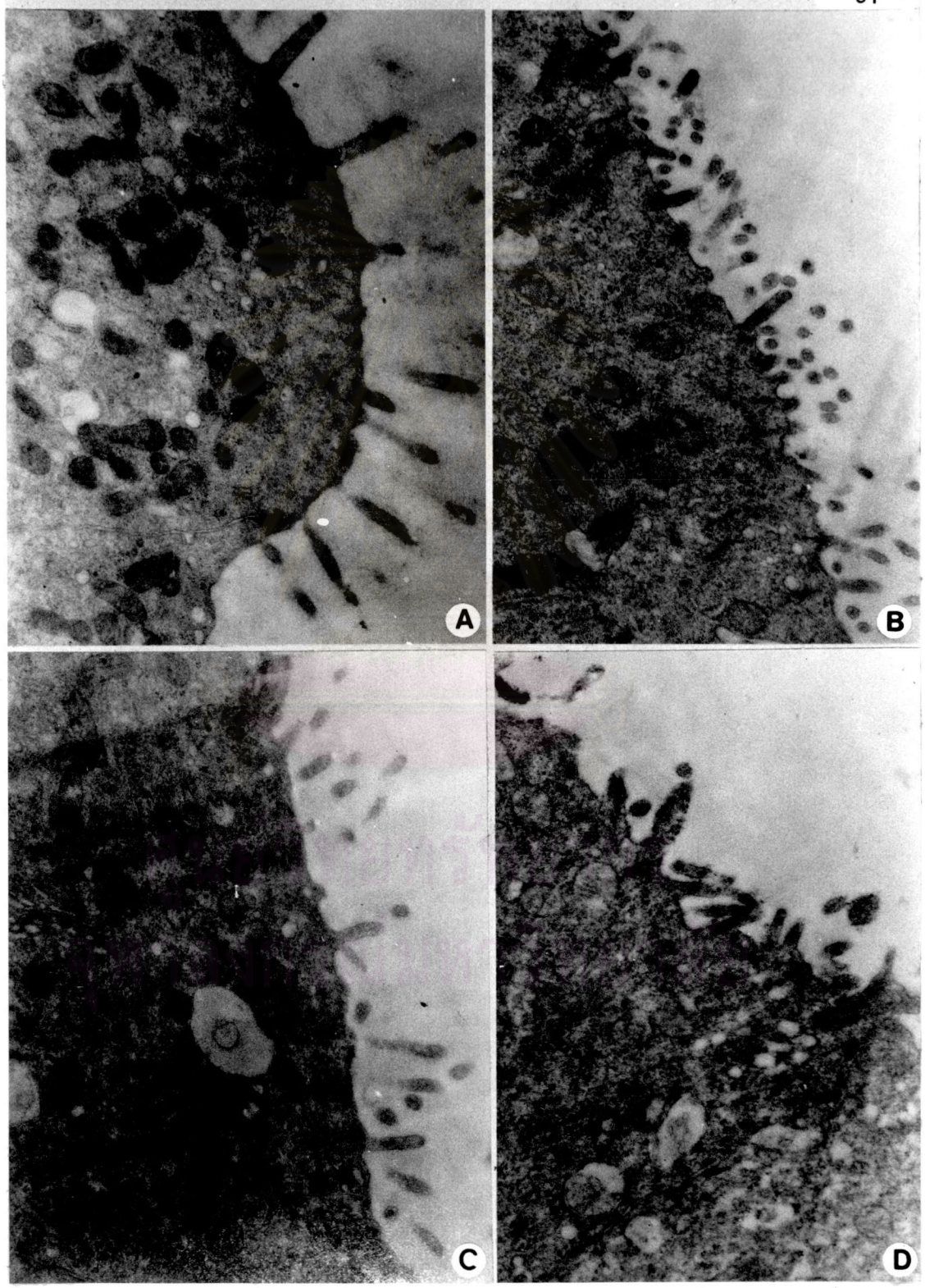

3.6 Implantation after lectins administrations

Implanted embryo develops into fetus and causes swelling of the uterine horn at the site of implantation. In hamster, from D_6 onward, rows of white opaque bodies on both horns (Figure 52:A) indicated growing live fetuses. If development was interrupted and the fetus died, the dead fetus appeared as clumps of blood which can easily be distinquished from the live one (Figure 52 : C).

In the untreated animal,normal pregnancy yielded an average of 14.2 implantations per animal (Figure 52 : A). This was designated as 100% successful implantation (Table 3.5). When 0.1 ml normal saline was given on D_3 (group 2) the average number of implantations was reduced to 11 (77.5%) per animal (Table 3.3), and was significantly different ($P< 0.001$) from the untreated control group. Implantation was decreased but not completely inhibited in Con A-treated animals (Table 3.4). The average number of implantations in groups 3, 4, 5 were 3.6 (25.4%), 3 (21.1%) and 2.9 (20.4%), respectively (Table 3.6). These were significantly different ($P < 0.001$) from that observed in normal-saline treated animals. However, there was no significant difference in the number of implantations among grcups of animals treated with various dosages of Con A. In WGA-treated groups (6, 7, 8, 9), implantation was completely inhibited (Table 3.5). All results were summarized in Table 3.6 and Figure 53.

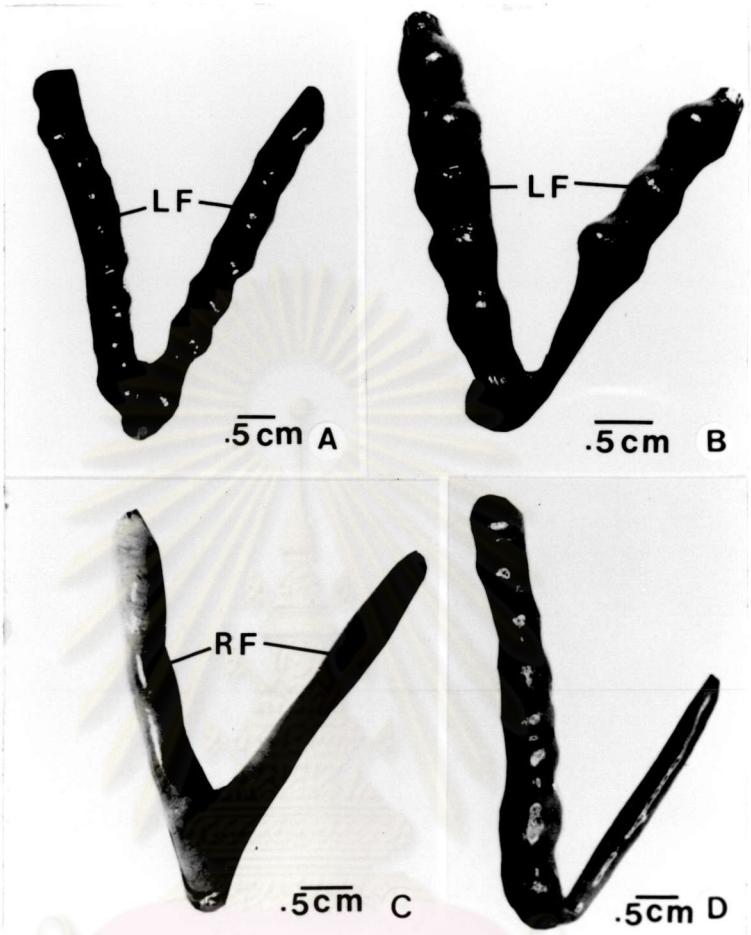

Figure 52 Gross structure of uterine horns with implanted fetuses

A : Both untreated uterine horns with normal pregnancy. Noticed beads of alive fetus (LF).

B : Implantations of fetuses were decreased in uterus treated with 0.1 ml normal saline (left horn), and 200 - 400 µg Con A (right horn)

C : Both uterine horns were treated with 800 µg Con A, all fetuses were resorbed (RF = resorbed fetus)

D : Untreated uterine horn with normal number of alive fetuses (left horn) as compared to WGA-treated horns (right horn). No implanted fetus was found.

Table 3.3 The effect of administration of 0.1 ml normal saline (NS) intraluminally on implantation

Female No.	No. of Implantations	
	Intact	NS
1	14	11
2	16	13
3	16	10
4	15	11
5	10	10
6	15	11
7	14	12
8	14	11
9	14	11
10	16	10
Mean	14.2	11

Table 3.4 The effect of Con A administered intraluminally on implantation

Female No.	No. of Implantations		
	200 µg/ 0.1 ml NS	400 µg/ 0.1 ml NS	800 µg/ 0.1 ml NS
1	0 + $7R^X$	0 + $4R^X$	0 + $2R^X$
2	0 + $6R^X$	1	0 + $4R^X$
3	3	3	0 + $2R^X$
4	0	0 + $3R^X$	0 + $2R^X$
5	6	3	0 + $7R^X$
6	0	0 + $6R^X$	0 + $2R^X$
7	6	0 + $3R^X$	0 + $1R^X$
8	1	1	0 + $3R^X$
9	2 + $1R^X$	0 + $4R^X$	0 + $1R^X$
10	3 + $1R^X$	0 + $2R^X$	0 + $5R^X$
Mean	2.1 + 1.5R	0.8 + $2.2R^X$	0 + $2.9R^X$

R^X = Resorbed fetuses

Table 3.5 The effect of WGA administered intraluminally on implantation

Female No.	No. of Implantations			
	50 µg/ 0.1 ml NS	100 µg/ 0.1 ml NS	200 µg/ 0.1 ml NS	400 µg/ 0.1 ml NS
1	0	0	0	0
2	0	0	0	0
3	0	0	0	0
4	0	0	0	0
5	0	0	0	0
6	0	0	0	0
7	0	0	0	0
8	0	0	0	0
9	0	0	0	0
10	0	0	0	0

Table 3.6 The effects of lectins administered intraluminally on implantation (summarizes of tables 3.3 - 3.5)

Group	Treatments	No. of fetuses observed at laparotomy			% Implantation [c]
		Alive	Resorbed	Total (Mean±SD)	
1	Intact	14.2	0	14.2±1.84	100
2	NS	11	0	11.0±1.2 [a]	77.5
3	200 µg Con A	2.1	1.5	3.6±2.79 [b]	25.4
4	400 µg Con A	0.8	2.2	3.0±1.72 [b]	21.1
5	800 µg Con A	0	2.9	2.9±1.91 [b]	20.4
6	50 µg WGA	0	0	0	0
7	100 µg WGA	0	0	0	0
8	200 µg WGA	0	0	0	0
9	400 µg WGA	0	0	0	0

a vs Intact with $P < 0.001$

b vs NS with $P < 0.001$

c % Implantation $= \frac{\text{Mean} \times 100}{14.2}$; 14.2 = implantation rate in normal pregnancy.

(see appendix I)

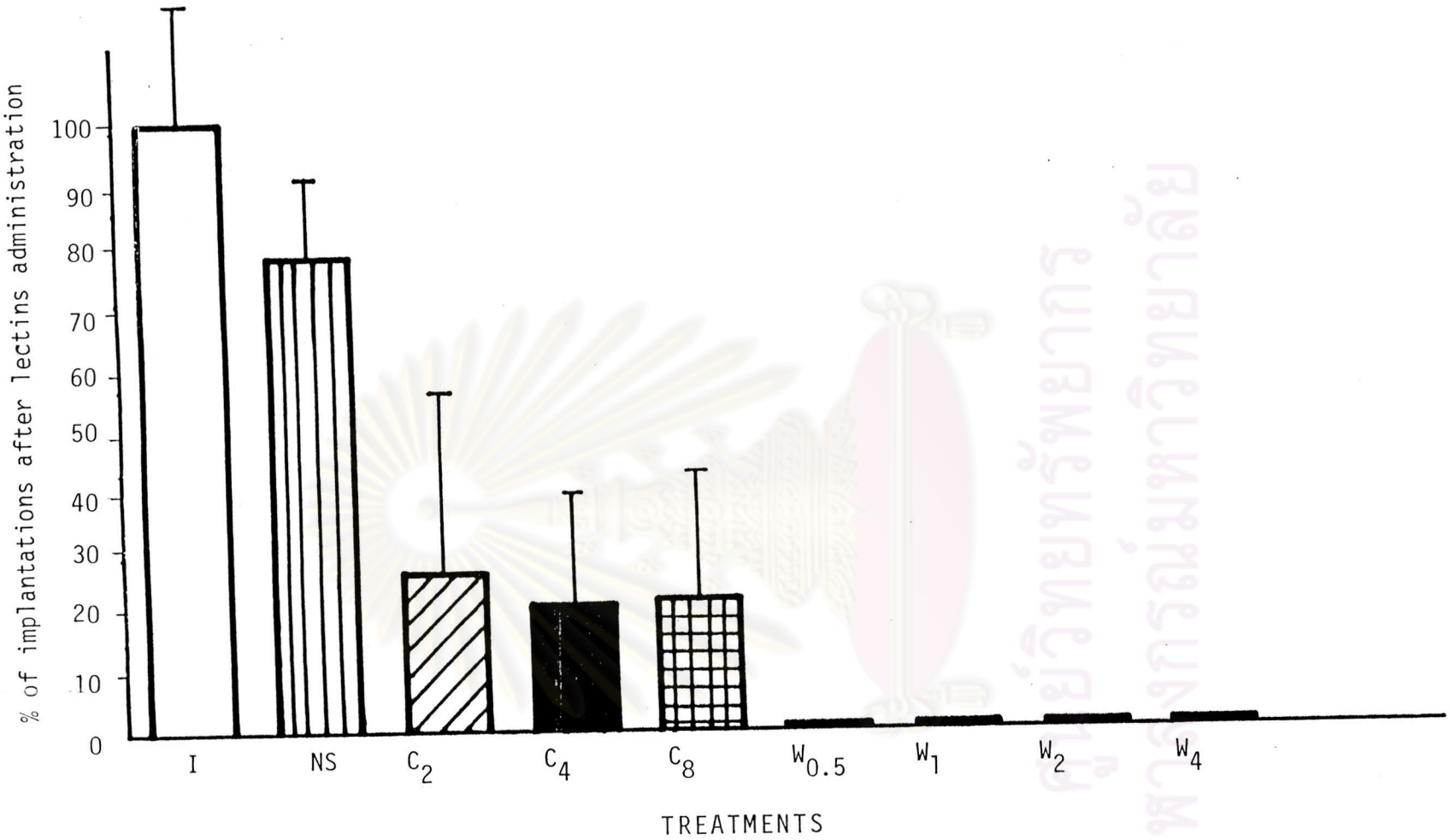

Figure 53 The effect of lectins administration on implantation (I = intact; NS = normal saline; C_2, C_4, C_8 = 200, 400, 800 µg Con A respectively; $W_{0.5}$, W_1, W_2, W_4 = 50, 100, 200, 400 µg WGA respectively).

3.7 Implantation after embryo transfer

A total of 120 embryos were transferred into ten recipients in each group of treatments. Seventy out of 120 embryos (58.3%) incubated in normal saline and transferred into uteri of pseudopregnant recipients were able to implant while the numbers of implantation of embryos treated with 200, 500 and 1000 µg Con A were 67 (55.8%), 60 (50%), and 66 (55%) respectively (Tables 3.7, 3.8; Figure 55). There was no significant difference in the numbers of implantation among various groups of Con A treated and normal saline group. Implantation was dramatically reduced when WGA treated embryos were transferred into uteri of pseudopregnant recipients (Figure 54). Only 10 out of 120 embryos (8.3%) treated with 200 µg WGA/ml NS, but not other higher doses, were able to implant (Table 3.9). All results were summarized in Table 3.10.

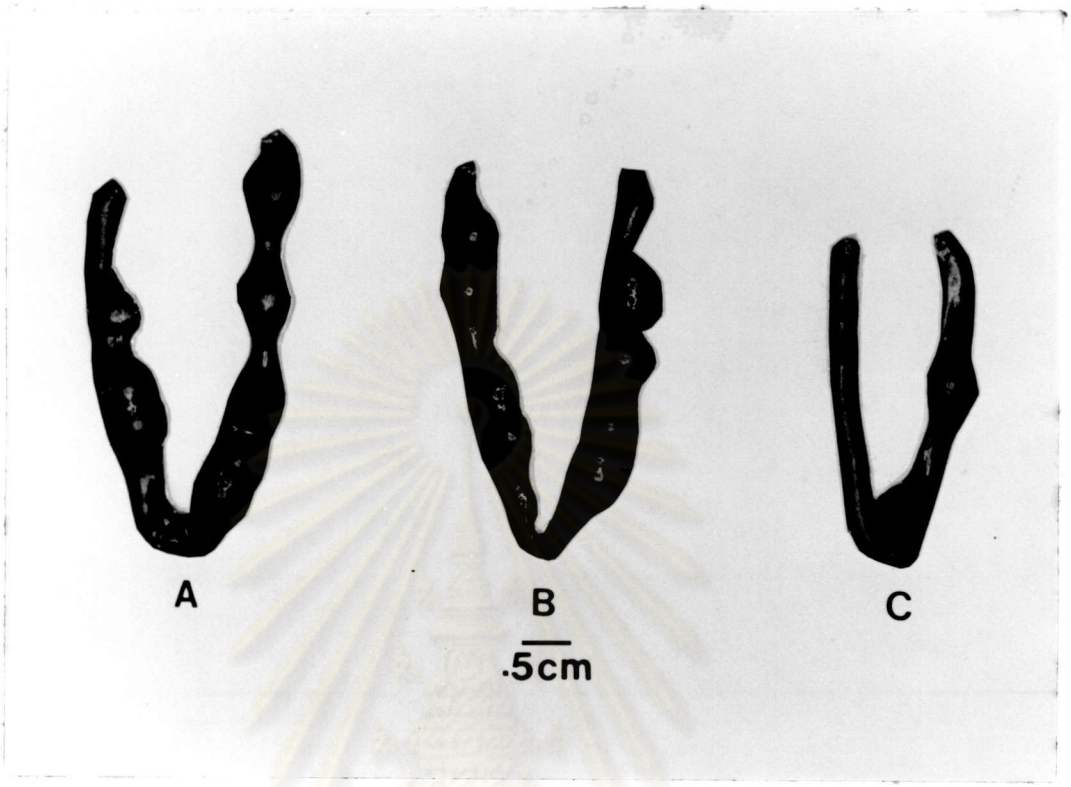

Figure 54 Characteristics of implantation sites from embryo transfers

A : Implantated fetuses in a recipient female from 12 transferred embryos that were pre-incubated in normal saline (NS)

B : Implantated fetuses in a recipient female from 12 transferred embryos that were pre-incubated in Con A. Number of implantation sites was not different from that of NS treated group.

C : Implantated fetuses from 12 transferred embryos that were pre-incubated in 200 µg WGA. Very few number of successful implantation were observed.

Table 3.7 Implantation after transferred of embryos incubated in NS for 10 minutes.

Recipient females(No.)	No. of embryos transferred	No. of implantation sites
1	12	5
2	12	4
3	12	6
4	12	8
5	12	10
6	12	6
7	12	4
8	12	8
9	12	7
10	12	12
Total	120	70
% implantation	$\left(\frac{70 \times 100}{120}\right)$ =	58.3

Table 3.8 Implantation after transferred of embryos treated with various concentrations of Con A for 10 minutes.

Recipient females(No.)	No. of embryos transferred	No. of implantations		
		Con A (μg/ml NS)		
		200	500	1000
1	12	6	6	2
2	12	8	5	6
3	12	5	4	5
4	12	4	4	8
5	12	4	10	4
6	12	6	6	7
7	12	6	2	12
8	12	12	5	6
9	12	8	6	6
10	12	8	12	8
Total	120	67	60	66
% Implantation	=	55.8	50	55

Table 3.9 Implantation after transferred of embryos treated with various concentrations of WGA for 10 minutes.

Recipient Females (No.)	No. of embryos transferred	No. of Implantations		
		WGA (µg/ml NS)		
		200	500	1000
1	12	1	0	0
2	12	0	0	0
3	12	2	0	0
4	12	0	0	0
5	12	2	0	0
6	12	0	0	0
7	12	0	0	0
8	12	2	0	0
9	12	2	0	0
10	12	1	0	0
Total	120	10	0	0
% Implantation	=	8.3	0	0

Table 3.10 Implantation after transferred of embryos treated with lectins (Summary of Table 3.7 - 3.9).

Treatments	Conc. µg/ ml NS	No. of embryos transferred	No. of implantations	% implantation
NS	-	120	70	58.3
Con A	200	120	67	55.8^{ns}
Con A	500	120	60	50 ^{ns}
Con A	1000	120	66	55 ^{ns}
WGA	200	120	10	8.3**
WGA	500	120	0	0
WGA	1000	120	0	0

^{ns} Chi-Square Test vs NS with no significant difference

** vs NS with $P < 0.001$

(see appendix II)

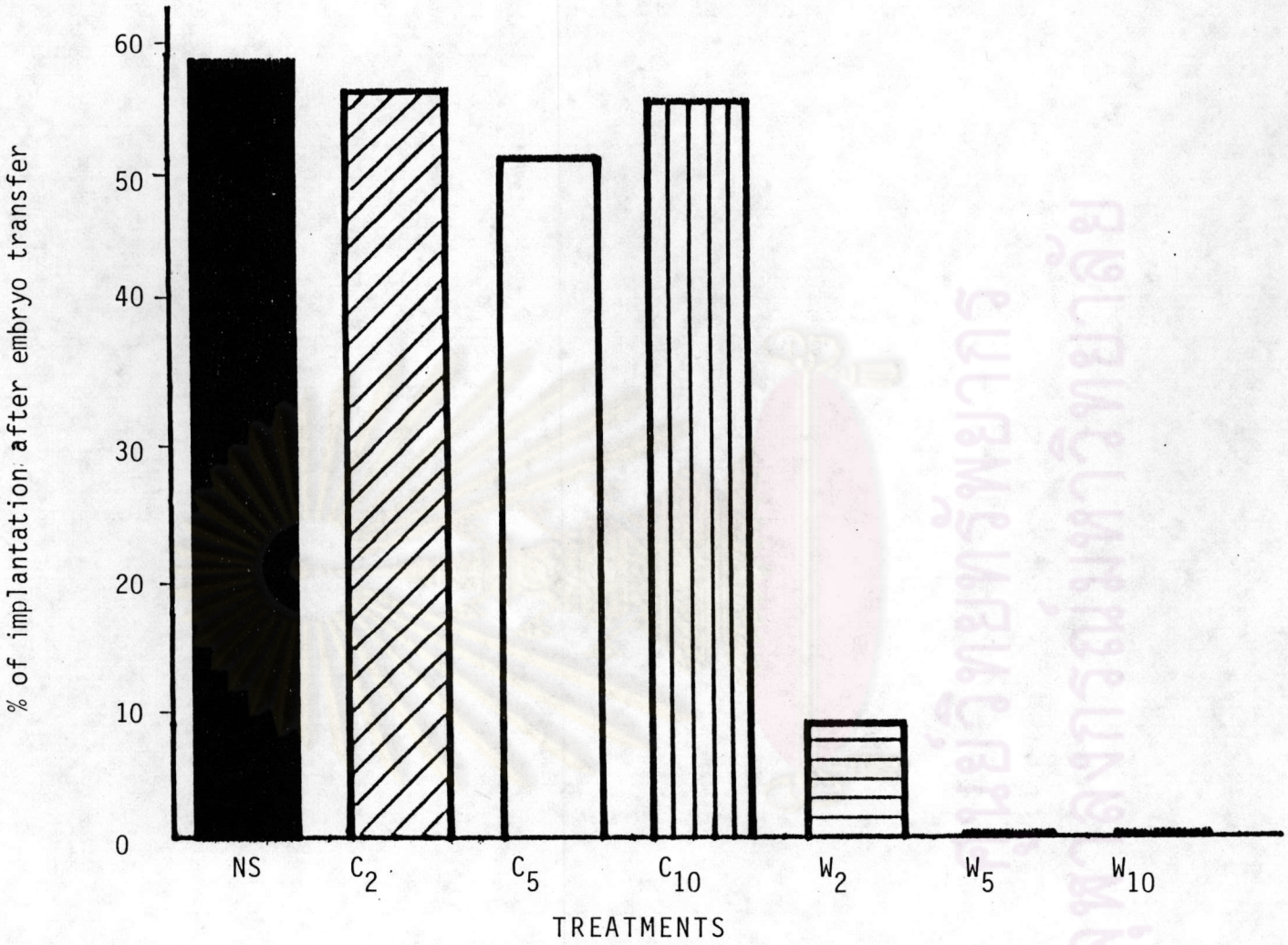

Figure 55 Implantation after transferred of embryos treated with lectins (NS = normal saline; C_2, C_5, C_{10} = 200, 500, 1000 µg Con A, respectively; W_2, W_5, W_{10} = 200, 500, 1000 µg respectively).

3.8 The effect of lectins on uterine morphology

After intraluminal administration of 0.1 ml NS on D_3, on D_4 and D_6, the regions without implantation sites were studied. No change was detected in the structures of both uterine epitelia and stroma layers (Figure 56). Similar features were observed in 200 µg WGA-treated group, on D_4 and D_6 (Figure 57). By contrast, in Con A-treated groups the dramatic change in endometrium was observed on D_4 (Figures 58, 59). Uterine epithelial was vacuolated when treated with 400 µg but not 200 µg Con A. However, at both concentrations as edematous appearance occurred deep in the stromal layer. Stromal cells were widely stretched and separated from each other which resulted in the formation of numerous vacuoles in the ground substance. In 400 µg Con A-treated group, the vacuolation was also observed in deep stromal layer. Endometrium of animals treated with both 200 and 400 µg Con A resumed normal appearance on D_6 (Figure 60) as compared to D_6 endometrium of normal saline-treated group.

Figure 56 Histology of uteri treated with normal saline on D_3, and uterine morphology was observed on D_4 and D_6

A, B : Cross-sections of D_4-uterus, showing normal histological features in both epithelial (EP) and stroma (SL) layers. L = lumen, En = endometrium, My = myometrium. A, x 36; B, x 361.

C, D, E : Cross-sections of D_6-uterus, showing normal histological features in both epithelial (EP) and stroma (SL) layers. C, x36; D, x 181; E, x 361.

Figure
56

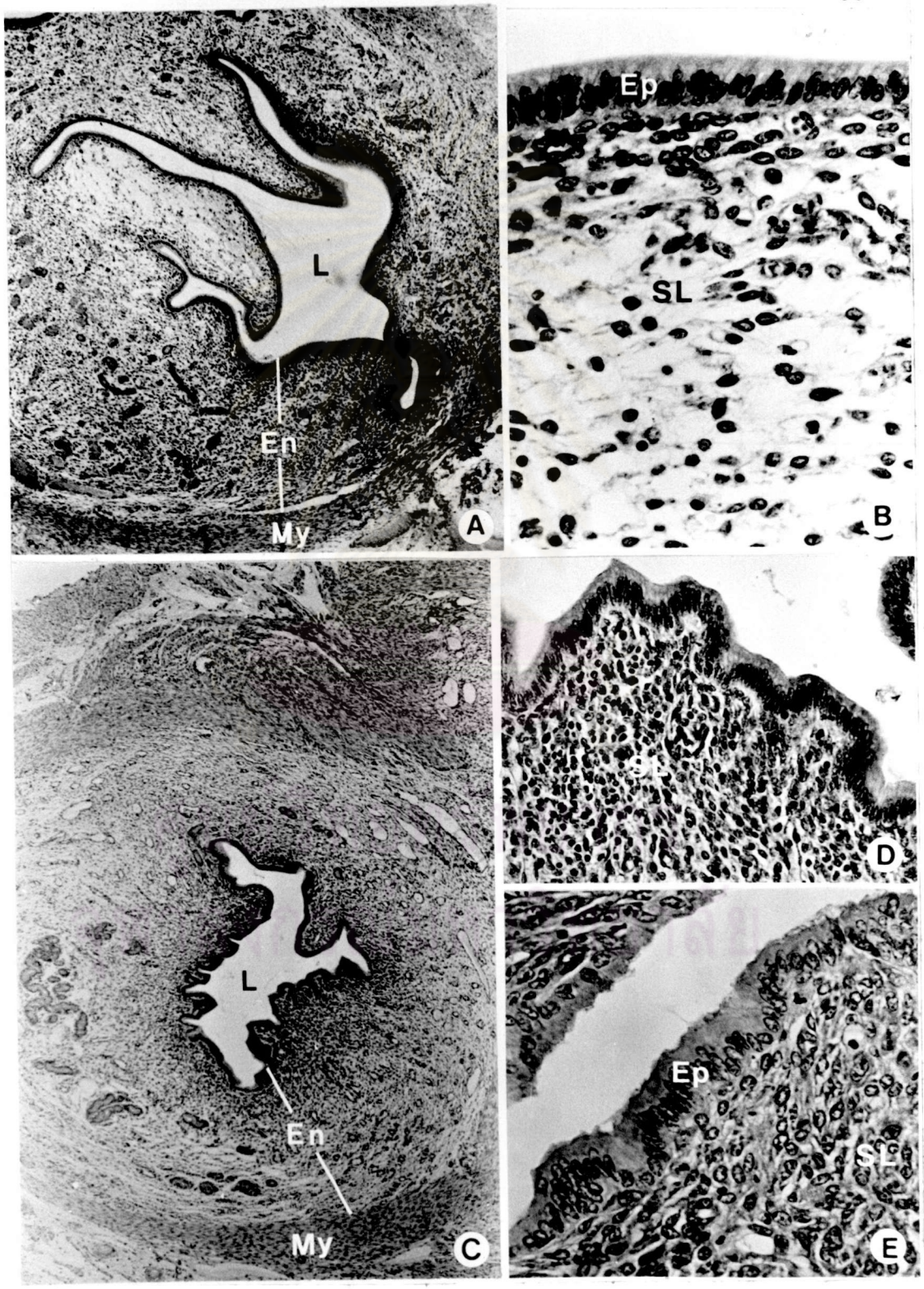

Figure 57 Histology of uteri treated with WGA (200 µg/0.1 ml NS) on D_3, uterine morphology was observed on D_4 and D_6.

A, B : Cross-sections of D_4-uteri. No change was observed in endometrium. A, x 36, B, x 361.

C, D, E : Cross-sections of D_6-uteri. General morphology of endometrium was similar to that of D_6-uteri treated with NS. C, x 36; D, x 181, E, x 361.

Figure 57

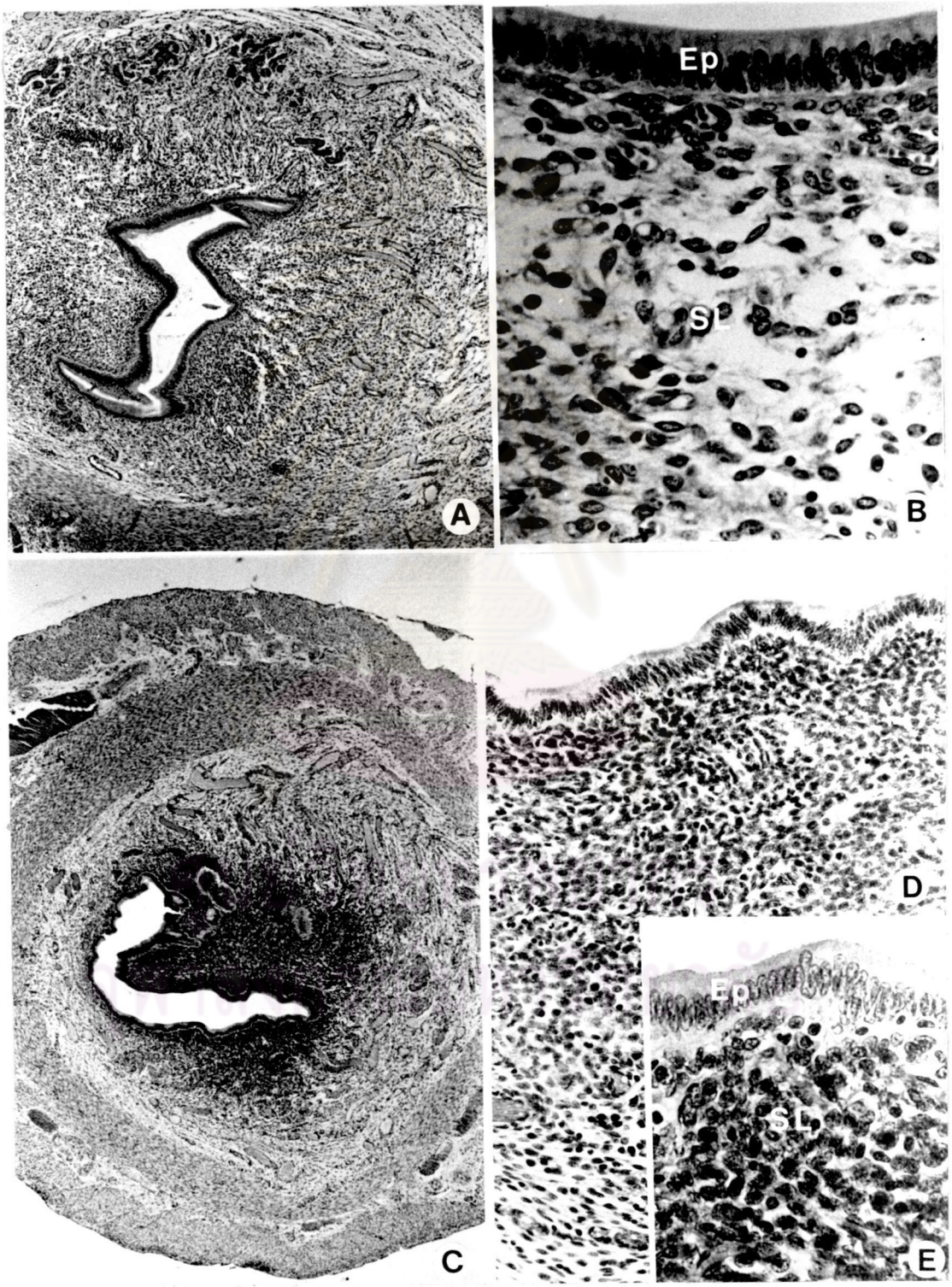

Figure 58 Histology of uteri treated with 200 µg Con A/0.1 ml NS on D_3, uterine morphology was observed on D_4

A : Low magnification of cross-sections of D_4-uteri. x 36.

B : Medium magnification of endometrium. No histological change was found in epithelia and superficial stromal layer (SSL, area 1 in A), while edema and a number of vacuoles(V) were observed in the deep stromal layer (DSL, area 2 in A). x 181.

C : High magnification of SSL morphology of both epithelia and SSL were normal when compared to NS treated uteri. x 361.

D : High magnification of DSL. Numerous vacuoles were found (arrow heads), and intercellular spaces were wider than in SSL. x 361.

Figure 58

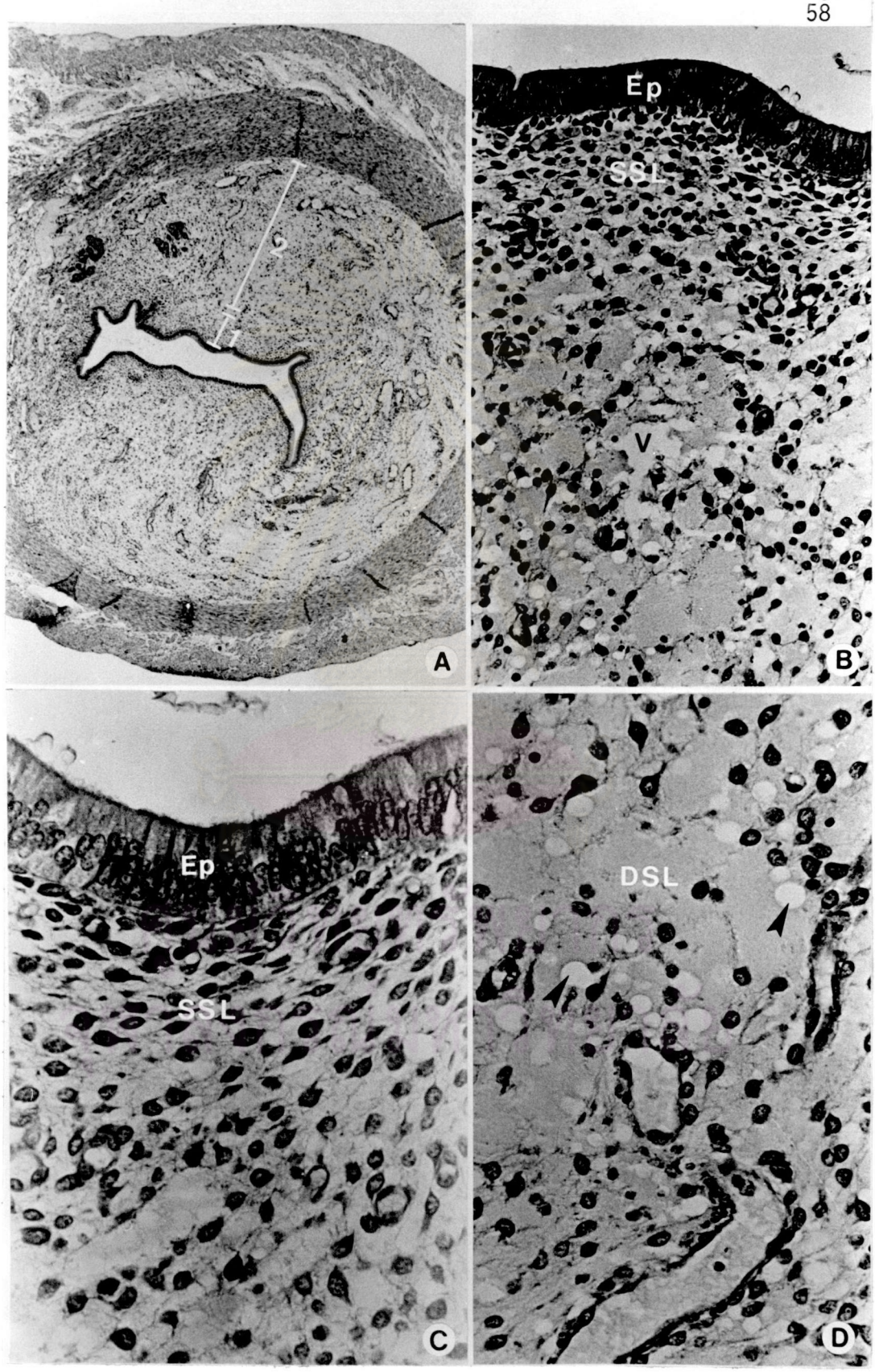

Figure 59 Histology of uteri treated with 400 µg Con A/0.1 ml NS on D_3, uterine morphology was observed on D_4

A : Low magnification of uterus. Severe edema was observed in endometrium (area 1). x 36.

B : High magnification of endometrium (area 1), dramatic changes were noted. Vacuolizations were found in epithelia, SSL and nuclei of stromal cells (SC) (arrow heads). x 361

C : High magnification of area 2, fluid retention (asterisks) was observed in stromal layer. x 361.

Figure 59

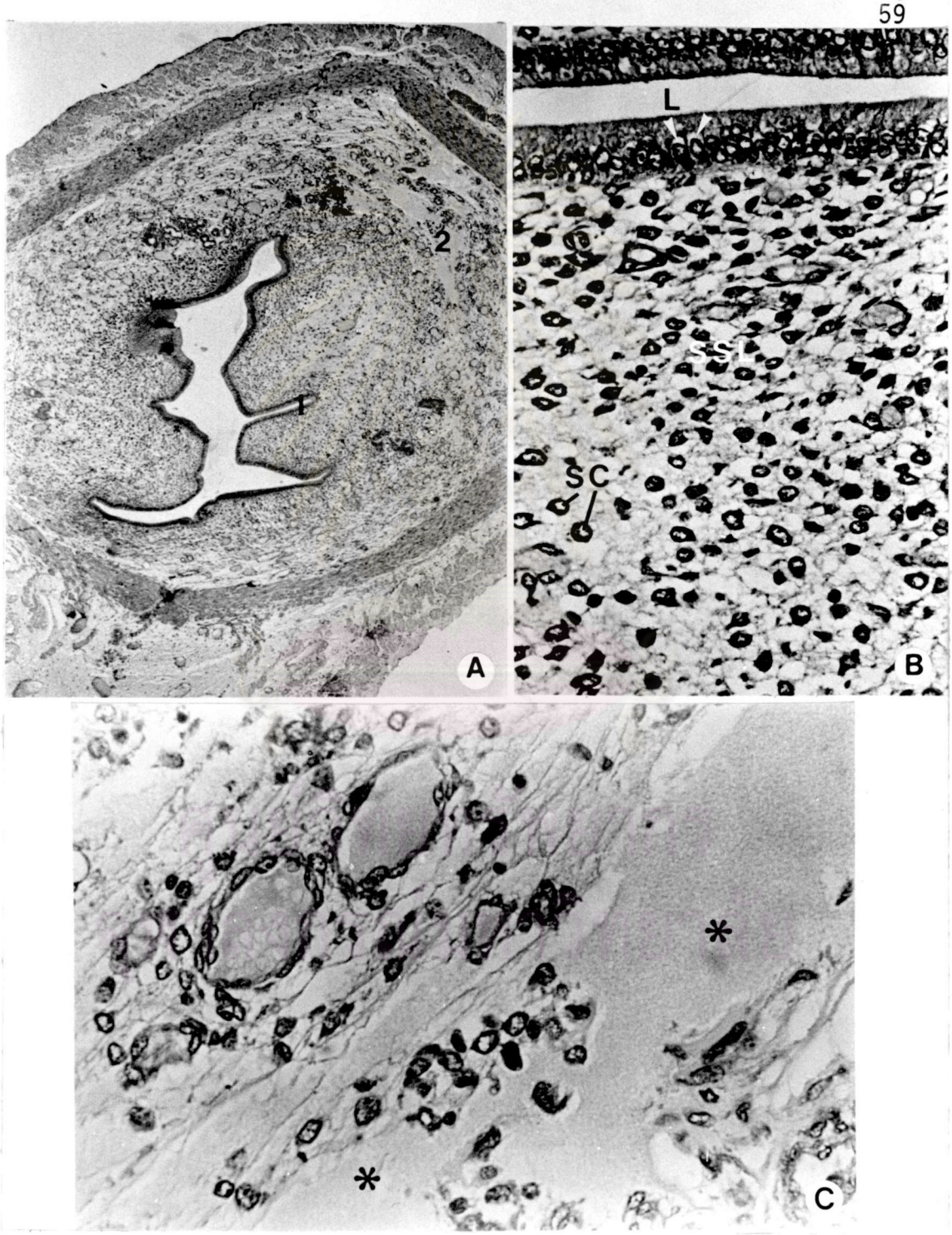

Figure 60 Histology of uteri treated with 200 and 400 µg Con A/ 0.1 ml NS on D_3, uterine morphology was observed on D_6.

A, B, C : Uterine morphology of uterus treated with 200 µg Con A, showing normal structure of endometrium. A, x 36; B, x 181; C, x 361.

D, E, F : Uterine morphology of uterus treated with 400 µg Con A, histological feature of endometrium was also normal. A, x 36; B, x 181; C, x 131.

Figure 60